



Universidade do Estado do Rio de Janeiro

Centro de Tecnologia e Ciências

Instituto de Química

Alice Peccini de Melo

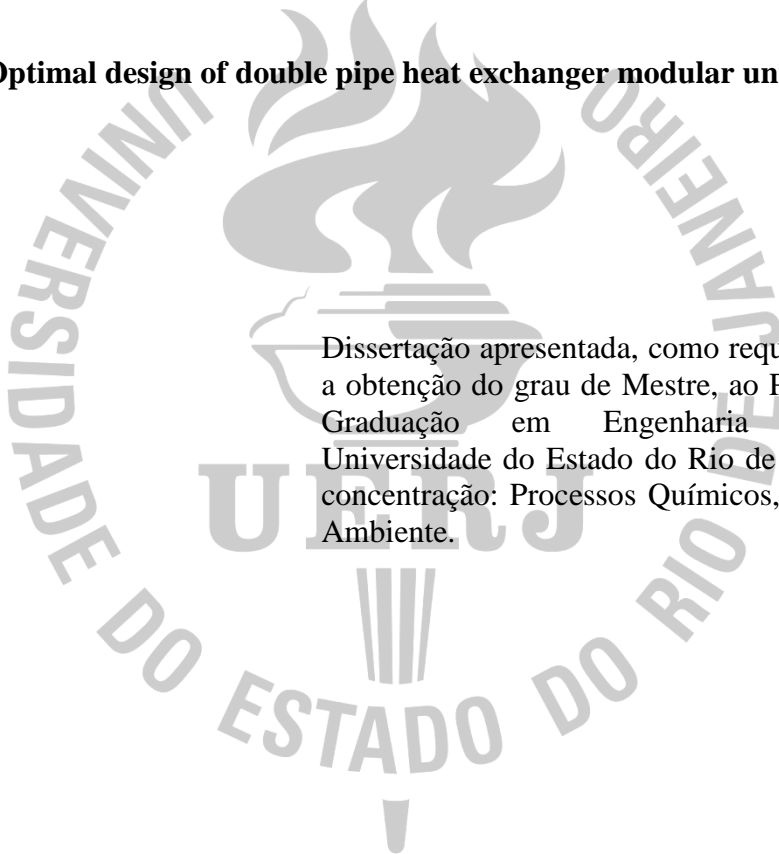
Optimal design of double pipe heat exchanger modular units

Rio de Janeiro

2017

Alice Peccini de Melo

Optimal design of double pipe heat exchanger modular units



Dissertação apresentada, como requisito parcial para a obtenção do grau de Mestre, ao Programa de Pós-Graduação em Engenharia Química, da Universidade do Estado do Rio de Janeiro. Área de concentração: Processos Químicos, Petróleo e Meio Ambiente.

Orientador: Prof. Dr. André Luiz Hemerly Costa

Orientador: Prof. Dr. Miguel Jorge Bagajewicz

Rio de Janeiro

2017

Alice Peccini de Melo

Optimal design of double pipe heat exchanger modular units

Dissertação apresentada, como requisito parcial para a obtenção do grau de Mestre, ao Programa de Pós-Graduação em Engenharia Química, da Universidade do Estado do Rio de Janeiro. Área de concentração: Processos Químicos, Petróleo e Meio Ambiente.

Aprovada em 07 de dezembro de 2017.

Banca Examinadora:

Prof. Dr. André Luiz Hemerly Costa (orientador)

Instituto de Química – UERJ

Prof. Dr. André Luis Alberton

Instituto de Química – UERJ

Prof. Dr. Eduardo Rocha de Almeida Lima

Instituto de Química – UERJ

Prof. Argimiro Resende Secchi

Escola de Química – UFRJ

Rio de Janeiro

2017

DEDICATÓRIA

Dedico esta tese à minha família por todo o amor e incentivo em todos os momentos.

AGRADECIMENTOS

Ao meu orientador, André Hemerly, pelo carinho e dedicação que tem com sua profissão e seus alunos. Sempre fazendo tudo em seu alcance para nos incentivar, ensinar, acalmar e fazer querermos ser profissionais melhores. Tenho grande admiração pelo profissional e pessoa que você é, agradeço muito por toda a ajuda e por estar me ajudando a trilhar meu caminho.

Ao meu co-orientador, que foi uma grande adição ao meu trabalho, criativo e inventivo, sempre trazendo valiosos inputs para melhorar nossos estudos.

Aos meus pais, Gracinda e Sávio, minha gratidão eterna, por toda a dedicação e investimentos que fizeram em mim, sempre com muito carinho, amor, confiança e sem pedir nada em troca a não ser a minha felicidade. E por serem grandes exemplos do tipo de pessoa que quero me tornar. Não tenho palavras para descrever o quanto admiro e agradeço a vocês.

Ao meu irmão, Ugo, que agora está morando longe de mim, e me fazendo sentir uma saudade maior do que eu imaginaria, obrigada, por sempre falar de mim com tanto orgulho, por tentar exigir mais de mim e acreditar no meu potencial e por ser alguém que eu também me encho de orgulho de chamar de irmão.

Ao amor da minha vida, Rafael, a certeza de que você tornou essa jornada muito, mas muito, mais possível e agradável. Me incentivando e alegrando quando eu estava cansada, me ajudando como um colega de profissão quando eu precisava de alguém para discutir alguma questão, me dando aquele empurrãozinho quando eu precisava e mais do que tudo, me fazendo uma pessoa feliz ao longo disso tudo. Um obrigada cheio de amor.

Um agradecimento especial às minhas duas avós, Wanilda e Laudelina (ah, que saudade sua, vovó Deli), mulheres fortes e carinhosas, que me inspiram, me ensinam e me fazem sentir tão especial todo dia, mesmo uma não estando mais entre nós.

À minha amiga de infância, Julia Pinto, que por acaso escolheu a mesma profissão que eu, obrigada por estar presente em tantos momentos da minha vida, por ter sido minha parceira de estudo por tantos anos, por me inspirar e me fazer acreditar que ainda na nossa geração existem pessoas tão lindas e puras como você.

Às minhas outras amigas de infância, Julia Stephan e Thaís, não fiquem com ciúmes, a minha infância e a minha vida não seriam a mesma sem vocês, vocês me fazem uma pessoa mais rica e colorida, vocês são e sempre serão parte de mim.

Às amigas que a engenharia química me deu, e que de mim ninguém tira, Carina, Natália e Vanessa, obrigada por terem feito a minha graduação e agora a minha vida tão, mas tão, mais gostosa, só tenho a agradecer por terem entrado na minha vida.

À Universidade do Estado do Rio de Janeiro, por ter feito parte de toda a minha carreira acadêmica até então, e por morar no meu coração.

E finalmente, ao restante da minha família e amigos, sem quem nada disso faria sentido algum.

RESUMO

MELO, Alice Peccini de. *Projeto ótimo de unidades modulares de trocadores bitubulares*. 145 f. 2017. Dissertação (Mestrado em Engenharia Química) – Instituto de Química, Universidade do estado do Rio de Janeiro, Rio de Janeiro, 2017.

Apesar de trocadores de calor do tipo casco e tubo serem os equipamentos de transferência de calor mais comumente empregados na indústria, diversos outros tipos podem ser mais adequados em determinadas situações. Este trabalho investiga o projeto ótimo de trocadores de calor do tipo bitubulares através de técnicas de programação matemática. A função objetivo é a minimização da área de troca térmica e as restrições envolvem modelagem termofluidodinâmica e especificações de projeto, tais como, perda de carga disponível e área em excesso mínima. O conjunto de variáveis de projeto explora a natureza modular deste tipo de trocador, incluindo a alocação dos fluidos (pelo do tubo interno ou pela região anular), os diâmetros dos tubos interno e externo, o comprimento dos tubos, o número de ramais paralelos e o número de trocadores em série e em paralelo por ramal. Três diferentes formulações matemáticas são propostas, a primeira corresponde a um problema de Programação Não-linear Inteira Mista (MINLP), o segundo é uma formulação MINLP modificada, na qual transformações matemáticas permitem a reorganização do problema, eliminando as não-linearidades associadas a variáveis binárias. Por fim, a terceira formulação, que corresponde a um problema de Programação Linear Inteira Mista (MILP), que permite a identificação do ótimo global. A aplicação da formulação proposta a um problema de projeto da literatura identificou uma redução na área de troca térmica quando comparada a um procedimento tradicional de tentativa e erro. Uma comparação entre as abordagens MINLP evidenciam a importância da identificação do ótimo global, que é encontrado para um conjunto de exemplos com a terceira abordagem. Exemplos adicionais ilustram a flexibilidade do modelo de descrever diferentes regimes, adaptar-se a modificações de vazões e exploram o *trade-off* entre perda de carga disponível e área de troca térmica.

Palavras-chave: Trocador de calor bitubular, otimização, programação matemática, modelo MINLP, modelo MILP

ABSTRACT

MELO, Alice Peccini de. *Optimal design of double pipe heat exchanger modular units*. 145 f. 2017. Dissertação (Mestrado em Engenharia Química) – Instituto de Química, Universidade do Estado do Rio de Janeiro, Rio de Janeiro, 2017.

Although shell-and-tube heat exchangers are the most common heat transfer equipment in the chemical industry, other types may be more suitable in various situations. This work investigates the design optimization of double pipe heat exchangers using mathematical programming. The objective function is the minimization of the heat exchanger area and the constraints encompass the thermo-fluid dynamic model and design specifications, such as, maximum pressure drops and minimum excess area. The set of design variables explores the modular nature of this kind of heat exchanger, encompassing the allocation of the streams (inside the inner tube or in the annulus), the inner and outer tube diameters, the tube length, the number of parallel branches, and the number of units in series or in parallel in each branch. Three different mathematical formulations are proposed, the first corresponds to a mixed-integer nonlinear programming (MINLP), the second is a modified MINLP formulation, where mathematical transformations allow the reorganization of the problem to eliminate the nonlinearities associated to the binary variables. Finally, the third formulation corresponds to a mixed-integer linear programming (MILP), which allows the identification of the global optimum. The application of the proposed optimization to a design task from the literature was able to identify a heat exchanger with smaller area, when compared to a solution obtained through a traditional trial and error procedure. A comparison between both MINLP approaches point out the importance of the identification of the global optimum, which is obtained with the third approach for a set of design problems. Additional examples illustrate the flexibility of the model to describe different flow regimes, adapt to modifications in process throughput and explores the trade-off between available pressure drop and heat transfer area.

Keywords: Double pipe heat exchanger, optimization, mathematical programming, MINLP model, MILP model

LISTA DE FIGURAS

Figure 1: Double pipe heat exchanger.....	24
Figure 2: Cross-section views for double pipe and multi-tube heat exchangers.....	24
Figure 3: Triple tube heat exchangers.....	25
Figure 4: Finned DPHE.....	25
Figure 5: Hairpin structure.....	26
Figure 6: Hairpin structure.....	32
Figure 7: Two hairpins connected in series.....	32
Figure 8: Arrangement I: Tube-side and annulus-side streams aligned in series.....	33
Figure 9: Arrangement II: Tube-side stream aligned in series and annulus-side stream aligned in parallel.....	33
Figure 10: Arrangement III: Tube-side stream aligned in parallel and annulus-side stream aligned in series.....	34
Figure 11: Double pipe heat exchanger structure composed of multiple parallel branches.....	34
Figure 12: Example of a double pipe heat exchanger structure composed of three parallel branches ($y_{B3} = 1$). Each branch has a total of five units and a flow-arrangement as shown in Figure 9(a), where the tube-side stream is aligned in series ($y_{St5} = 1$ and $y_{Pt1} = 1$) and the annulus-side stream is in parallel ($y_{Sa1} = 1$ and $y_{Pa5} = 1$).....	41
Figure 13: Inner tube friction factor profile in all three regimes generated from Eqs. (2.44)-(2.46).....	45
Figure 14: Possible ranges for <i>Ret</i> , <i>Prt</i> , <i>NutS&T</i> and its corresponding binary variables.....	46
Figure 15: Annular friction factor profile in all three regimes generated from Eqs. (2.67)-(2.69).....	49
Figure 16: Possible ranges for <i>Rea</i> , <i>Pra</i> , <i>NuaS&T</i> and its corresponding binary variables...	50
Figure 17: Example 1 - Heat exchanger structure proposed by Serth (2007).....	88
Figure 18: Example 1 - Adaptation of the heat exchanger structure proposed by Serth (2007).....	89
Figure 19: Example 1 – Optimal structures – Original MINLP (a) and Modified MINLP (b).....	96
Figure 20: Example 2 – Optimal structures – Original MINLP (a) and Modified MINLP (b).....	99

Figure 21: Example 3 – Optimal structures – Original MINLP (a) and Modified MINLP (b).	101
Figure 22: Example 4 – Optimal structures – Original MINLP (a) and Modified MINLP (b).	103
Figure 23: Example 5 – Optimal structures – Original MINLP (a) and Modified MINLP (b).	104
Figure 24: Representation of the heat exchangers structures: Trial 1 (a), Trial 2 (b), Trial 3 (c) and Trial 4 (d).	112
Figure 25: Example 6 – Globally optimal solution.	113
Figure 26: Arrangement of the design solutions (a) Example 7 ($\Delta P_{hdisp} = 50$ kPa, $\Delta P_{cdisp} = 50$ kPa); (b) Example 8 ($\Delta P_{hdisp} = 20$ kPa, $\Delta P_{cdisp} = 50$ kPa); (c) Example 9 ($\Delta P_{hdisp} = 20$ kPa, $\Delta P_{cdisp} = 20$ kPa).	117
Figure 27: Example 10 – Arrangement of the design solution.	120
Figure 28: Example 11 – Arrangement of the design solution.	120

LISTA DE TABELAS

Table 1. Reformulation of Eq. (2.60)	56
Table 2. Reformulation of Equation (2.61).	57
Table 3. Reformulation of Eq. (2.83)	59
Table 4. Reformulation of Eq. (2.84)	59
Table 5. Reformulation of Eq. (2.93)	62
Table 6. Initial estimates for key binary variables.....	84
Table 7. Initial estimates for key continuous variables.	85
Table 8. Example 1 - Stream data.....	87
Table 9. Example 1 - Hairpin data (pipe schedule 40)	87
Table 10. Structural discrete options (pipe schedule 40).....	90
Table 11. Example 1 – Design results.	91
Table 12. Examples 2 and 3 – Stream data.....	92
Table 13. Examples 2 and 3 – Design results.....	93
Table 14. Example 4 – Stream data	94
Table 15. Example 5 – Stream data	95
Table 16. Example 1 – Optimization results.	96
Table 17. Example 2 – Optimization results.	98
Table 18. Example 3 – Optimization results.	100
Table 19. Example 4 – Optimization results.	102
Table 20. Example 5 – Optimization results.	104
Table 21. Examples 1 to 5 – Performance comparison of the different MINLP approaches.	106
Table 22. Example 6 - Stream data.....	108
Table 23. Structural discrete options (pipe schedule 40).....	109
Table 24. Fixated design variables for each Trial.	110
Table 25. Trials results.	110
Table 26. Example 6 – Design results.	113
Table 27. Hairpin data (pipe schedule 40) for the structural flexibility analysis.	114
Table 28. Examples 7 to 9 – Stream data.	115
Table 29. Examples 7 to 9 – Design results.	116
Table 30. Examples 10 and 11 – Mass flow rates.	118
Table 31. Examples 10 and 11 (together with Example 7) – Optimization results.	119

LISTA DE ABREVIATURAS E SIGLAS

DPHE	Double Pipe Heat Exchanger
MILP	Mixed-Integer Linear Programming
MINLP	Mixed-Integer Nonlinear Programming

LISTA DE SÍMBOLOS

- Latin letters:

Nu	Nusselt number
h	Convective heat transfer coefficient (W/(m ² °C))
D	Tube diameter (m)
k	Thermal conductivity (W/(m°°C))
Pr	Prandtl number
C_p	Heat capacity (J/(kg °°C))
μ	Viscosity (Pa.s)
L	Total unit tube length (m)
μ_s	Viscosity at surface (m ²)
dh	Hydraulic diameter (m)
Ac	Cross sectional area (m ²)
P_w	Wetted perimeter (m)
D_{ti}	Outer tube internal diameter (m)
d_{te}	Inner tube external diameter (m)
$\widehat{pd_{te}}_{sd}$	Available inside tube external diameters (m)
$y_{d_{sd}}$	Inner tube diameter selection
d_{ti}	Inner tube internal diameter (m)
$\widehat{pd_{ti}}_{sd}$	Available inside tube internal diameters (m)
D_{te}	Outside tube external diameter (m)
$\widehat{pD_{te}}_{sD}$	Available outside tube external diameters (m)
$y_{D_{sD}}$	Outer tube diameter selection

\widehat{pDt}_{sD}	Available outside tube internal diameters (m)
\widehat{pL}_{sL}	Heat exchanger length (m)
yL_{sL}	Tube length selection
NB	Number of parallel branches
\widehat{pNB}_{sB}	Number of available branches
yB_{sB}	Number of branches selection
NSt	Tube-side units in series per branch
\widehat{pNE}_{sE}	Number of available heat exchangers in series by branch
ySt_{sE}	Tube-side number of units in series per branch selection
NSa	Annulus-side units in series per branch
ySa_{sE}	Annulus-side number of units in series per branch selection
NPt	Tube-side units in parallel per branch
yPt_{sE}	Tube-side number of units in parallel per branch selection
NPa	Annulus-side units in parallel per branch
yPa_{sE}	Annulus -side number of units in parallel per branch selection
mt	Inside tube mass flow (kg/s)
\widehat{m}_{sST}	Stream sST mass flow (kg/s)
yT_{sST}	Stream sST allocation (1 = tube-side; 0 = annulus-side)
ma	Annular region mass flow (kg/s)
Cpt	Tube-side stream heat capacity (J/(kg °C))
\widehat{Cp}_{sST}	Stream sST heat capacity (J/(kg °C))
Cpa	Annulus-side stream heat capacity (J/(kg °C))
kt	Tube-side stream thermal conductivity (W/(m °C))
\widehat{k}_{sST}	Stream sST thermal conductivity (W/(m °C))

ka	Annulus-side stream thermal conductivity (W/(m °C))
Rft	Tube-side stream fouling resistance (m ² °C /W)
\widehat{Rf}_{sST}	Stream sST fouling resistance (m ² °C /W)
Rfa	Annulus-side stream fouling resistance (m ² °C /W)
At	Tube-side flow area (m ²)
Aa	Annulus-side flow area (m ²)
Lt	Tube-side hydraulic length (m)
La	Annulus-side hydraulic length (m)
Prt	Tube-side stream Prandtl number
vt	Tube-side velocity (m/s)
Ret	Inner tube Reynolds number
ft	Tube-side friction factor
f_t^{lam}	Tube-side friction factor for laminar flow
f_t^{tran}	Tube-side friction factor for transitional flow
f_t^{turb}	Tube-side friction factor for turbulent flow
Nut^{Gni}	Tube-side Gnielinski Nusselt number
Nut^{Hau}	Tube-side Hausen Nusselt number
$Nut^{S\&T}$	Tube-side Seider & Tate Nusselt number
Nut^{theo}	Tube-side theoretical Nusselt number
$yRet_{sRet}$	Range of inner tube Reynolds number selection
\widehat{URe}	Reynolds number upper limit
$yPrt_{sPrt}$	Range of inner tube Prandtl number selection
\widehat{UPr}	Prandtl number upper limit
$yNut_{sNut}$	Range of inner tube Seider and Tate Nusselt number selection

\widehat{UNu}	Nusselt number upper limit
Nut	Tube-side Nusselt number
Pra	Annulus-side stream Prandtl number
va	Annulus-side velocity (m/s)
Rea	Annulus-side Reynolds number
fa	Annulus-side friction factor
fa^{lam}	Annulus-side friction factor for laminar flow
fa^{tran}	Annulus-side friction factor for transitional flow
fa^{turb}	Annulus-side friction factor for turbulent flow
Nua^{theo}	Annulus-side theoretical Nusselt number
$Nua^{S\&T}$	Annulus-side Seider & Tate Nusselt number
Nua^{Hau}	Annulus-side Hausen Nusselt number
Nua^{Gni}	Annulus-side Gnielinski Nusselt number
$yRea_{sRea}$	Range of annular region Reynolds number selection
$yPra_{sPra}$	Range of annular region Prandtl number selection
$yNua_{sNua}$	Range of annular region Seider and Tate Nusselt number selection
Nua	Annulus-side Nusselt number
ht	Tube-side convective heat transfer coefficient (W/(m ² °C))
ha	Annulus-side convective heat transfer coefficient (W/(m ² °C))
U	Overall heat transfer coefficient (W/(m ² °C))
\bar{Q}	Heat-transfer rate (W)
A_{req}	Required heat transfer area (m ²)
F	Correction factor
\hat{T}_{sST}	Stream sST inlet temperature (°C)

$\widehat{T}_{O_{sST}}$	Stream <i>sST</i> outlet temperature (°C)
$\widehat{pF}_{sST, sE}$	F factor in case <i>sST</i> stream is in series, for $sE \neq 1$
\widehat{pR}_{sST}	R parameter for the calculation of F factor if <i>sST</i> stream is in series
\widehat{pP}_{sST}	P parameter for the calculation of F factor if <i>sST</i> stream is in series
\widehat{A}_{exc}	Minimum area excess (%)
$\widehat{v}t_{min}$	Tube-side minimum velocity (m/s)
$\widehat{v}t_{max}$	Tube-side maximum velocity (m/s)
$\widehat{v}a_{min}$	Annulus-side minimum velocity (m/s)
$\widehat{v}a_{max}$	Annulus-side maximum velocity (m/s)
wft_1	Replacement for the product $ft^{lam}yRet_1$
wft_2	Replacement for the product $ft^{tran}yRet_2$
wft_3	Replacement for the product $ft^{tran}yRet_3$
wft_4	Replacement for the product $ft^{turb}yRet_4$
$wNut_1^{theo}$	Replacement for the product $yRet_1yPrt_1yNut_1$
$wNut_2^{theo}$	Replacement for the product $yRet_2yPrt_1yNut_1$
$wNut_1^{S\&T}$	Replacement for the product $yRet_1yPrt_1yNut_2$
$wNut_2^{S\&T}$	Replacement for the product $yRet_2yPrt_1yNut_2$
$wNut_1^{Hau}$	Replacement for the product $yRet_1yPrt_2$
$wNut_2^{Hau}$	Replacement for the product $yRet_2yPrt_2$
$wNut^{Gni}$	Replacement for the product $Nut^{Gni}(yRet_3 + yRet_4)$
wfa_1	Replacement for the product $fa^{lam}yRea_1$
wfa_2	Replacement for the product $fa^{tran}yRea_2$
wfa_3	Replacement for the product $fa^{tran}yRea_3$
wfa_4	Replacement for the product $fa^{turb}yRea_4$

$wNua_1^{theo}$	Replacement for the product $yRea_1 yPra_1 yNua_1$
$wNua_2^{theo}$	Replacement for the product $yRea_2 yPra_1 yNua$
$wNua_1^{S\&T}$	Replacement for the product $yRea_1 yPra_1 yNua_2$
$wNua_2^{S\&T}$	Replacement for the product $yRea_2 yPra_1 yNua_2$
$wNua_1^{Hau}$	Replacement for the product $yRea_1 yPra_2$
$wNua_2^{Hau}$	Replacement for the product $yRea_2 yPra_2$
$wNua^{Gni}$	Replacement for the product $Nua^{Gni} (yRea_3 + yRea_4)$
$wPtT_{sE,sST}$	Replacement for the product $yPt_{sE} yT_{sST}$
$wPaT_{sE,sST}$	Replacement for the product $yPa_{sE} yT_{sST}$
$wyPtSt_{sE,sE'}$	Replacement for $yPt_{sE} ySt_{sE'}$
$wyPaSa_{sE,sE'}$	Replacement for $yPa_{sE} ySa_{sE'}$
$wvt_{sd,sB,sE,sST}$	Replacement for $yd_{sd} yB_{sB} yPt_{sE} yT_{sST}$
$wNut_{sB,sE,sL,sST}$	Replacement for $yB_{sB} yPt_{sE} yL_{sL} yT_{sST}$
$\widehat{pNut}_{sB,sE,sL,sST}^{S\&T}$	Auxiliary parameter S&T correlation
$wdPt_{sd,sB,sE,sL,sE',sST,sRet}$	Replacement for $yd_{sd} yB_{sB} yPt_{sE} yL_{sL} ySt_{sE'} yT_{sST} yRet_{sRet}$
$\widehat{pdPt1}_{sd,sB,sE,sL,sE',sST}$	Auxiliary parameter pressure drop calculation
$\widehat{pdPt23}_{sd,sB,sE,sL,sE',sST}$	Auxiliary parameter pressure drop calculation
$\widehat{pdPt4}_{sd,sB,sE,sL,sE',sST}$	Auxiliary parameter pressure drop calculation
$wva_{sd,sD,sB,sE,sST}$	Replacement for $yd_{sd} yD_{sD} yB_{sB} yPa_{sE} yT_{sST}$
$wNua_{sd,sD,sB,sE,sL,sST}$	Replacement for $yd_{sd} yD_{sD} yB_{sB} yPa_{sE} yL_{sL} yT_{sST}$
$\widehat{pNua}_{sd,sD,sB,sE,sL,sST}^{S\&T}$	Auxiliary parameter S&T correlation
$wdPa_{sd,sD,sB,sE,sL,sE',sST,sRea}$	Replacement for $yd_{sd} yD_{sD} yB_{sB} yPa_{sE} yL_{sL} ySa_{sE'} yT_{sST} yRea_{sRea}$
$\widehat{pdPa1}_{sd,sD,sB,sE,sL,sE',sST}$	Auxiliary parameter pressure drop calculation
$\widehat{pdPa23}_{sd,sD,sB,sE,sL,sE',sST}$	Auxiliary parameter pressure drop calculation

$\widehat{pdPa}4_{sd,sD,sB,sE,sL,sE',sST}$	Auxiliary parameter pressure drop calculation
$wA_{sd,sB,sE,sL,sE'}$	Replacement for $yd_{sd}yB_{sB}yPt_{sE}yL_{sL}ySt_{sE'}$
$\widehat{pA}_{sd,sB,sE,sL,sE'}$	Auxiliary parameter area calculation
$wht_{sd,sST,sRet,sPrt,sNut}^{theo}$	Replacement for $yd_{sd}yT_{sST}yRet_{sRet}yPrt_{sPrt}yNut_{sNut}$
$wht_{sd,sB,sE,sL,sST,sRet,sPrt,sNut}^{S\&T}$	Replacement for $yd_{sd}yB_{sB}yPt_{sE}yL_{sL}yT_{sST}yRet_{sRet}yPrt_{sPrt}yNut_{sNut}$
$wht_{sd,sB,sE,sL,sST,sRet,sPrt}^{Hau}$	Replacement for $yd_{sd}yB_{sB}yPt_{sE}yL_{sL}yT_{sST}yRet_{sRet}yPrt_{sPrt}$
$wht_{sd,sB,sE,sST,sRet}^{Gni}$	Replacement for $yd_{sd}yB_{sB}yPt_{sE}yT_{sST}yRet_{sRet}$
$wydT_{sd,sST}$	Replacement for $yd_{sd}yT_{sST}$
$wha_{sd,sD,sST,sRea,sPra,sNua}^{theo}$	Replacement for $yd_{sd}yD_{sD}yT_{sST}yRea_{sRea}yPra_{sPra}yNua_{sNua}$
$wha_{sd,sD,sB,sE',sL,sST,sRea,sPra,sNua}^{S\&T}$	Replacement for $yd_{sd}yD_{sD}yB_{sB}yPa_{sE}yL_{sL}yT_{sST}yRea_{sRea}yPra_{sPra}yNua_{sNua}$
$wha_{sd,sD,sB,sE',sL,sST,sRea,sPra}^{Hau}$	Replacement for $yd_{sd}yD_{sD}yB_{sB}yPa_{sE}yL_{sL}yT_{sST}yRea_{sRea}yPra_{sPra}$
$wha_{sd,sD,sB,sE',sL,sST,sRea}^{Gni}$	Replacement for $yd_{sd}yD_{sD}yB_{sB}yPa_{sE}yL_{sL}yT_{sST}yRea_{sRea}$
$wAF1_{sd,sB,sE,sL,sE'',sST}$	Replacement for $wA_{sd,sB,sE,sL,sE''}yT_{sST}$
$wAF2_{sd,sB,sE,sE',sL,sE'',sST}$	Replacement for $wAF1_{sd,sB,sE,sL,sE'',sST}yPa_{sE'}$

- Greek letters:

ρ_t Tube-side stream density (kg/m³)

$\hat{\rho}_{sST}$ Stream *sST* density (kg/m³)

μ_t Tube-side stream viscosity (Pa·s)

$\hat{\mu}_{sST}$ Stream *sST* viscosity (Pa·s)

μ_a Annulus-side stream viscosity (Pa·s)

ΔPt Tube-side pressure drop (Pa)

ΔPa Annulus-side pressure drop (Pa)

$\widehat{\Delta T_{lm}}$ Logarithmic mean temperature (°C)

$\widehat{\Delta P_{ss}}$ Stream *sST* available pressure drop (Pa)

$\widehat{\Phi}$ Nonlinear continuous functions upper limit

- Subscripts:

sd Index of inner tube diameters

sD Index of outer tube diameters

sL Index of tube length

sB Index of number of branches

sE Index of number of units per branch

sST Index of streams

sRet Index of ranges of inner tube Reynolds number

sPrt Index of ranges of inner tube Prandtl number

sNut Index of ranges of inner tube Seider and Tate Nusselt number

sRea Index of ranges of annular region Reynolds number

sPra Index of ranges of annular region Prandtl number

sNua Index of ranges of annular region Seider and Tate Nusselt number

- Superscripts:

lam Laminar flow

tran Transitional flow

turb Turbulent flow

Gni Gnielinski correlation

Hau Hausen correlation

S&T Sieder and Tate correlation

theo Theoretical value

SUMÁRIO

	INTRODUCTION	22
1	REVIEW OF LITERATURE	24
1.1	Double pipe heat exchangers overview	24
1.2	Heat transfer correlations	26
1.2.1	<u>Circular tubes</u>	26
1.2.1.1	Laminar flow	27
1.2.1.2	Turbulent flow	28
1.2.1.3	Annular region	29
1.3	DPHE optimal design	30
1.4	Literature overview and proposed contribution	31
2	MIXED-INTEGER NONLINEAR PROGRAMMING	32
2.1	System Structure	32
2.2	Design Problem	35
2.3	Problem formulation – MINLP 1	36
2.3.1	<u>Constraints</u>	36
2.3.1.1	Representation of the geometric variables	36
2.3.1.2	Stream allocation	42
2.3.1.3	Structural constraints	43
2.3.1.4	Thermal and Hydraulic modeling – Tube-side flow	43
2.3.1.5	Thermal and Hydraulic modeling – Tube-side flow	47
2.3.1.6	Heat transfer coefficients	51
2.3.1.7	Heat transfer rate equation	51
2.3.1.8	Pressure drops and velocity bounds	53
2.3.2	<u>Objective function</u>	54
2.4	Problem Reformulation – MINLP 2	54
2.4.1	<u>Reformulation Techniques</u>	54
2.4.2	<u>Thermal and hydraulic modeling – Tube-side flow</u>	56
2.4.3	<u>Thermal and hydraulic modeling – Annulus-side flow</u>	59
2.4.4	<u>Heat transfer rate equation</u>	62
3	MIXED-INTEGER LINEAR PROGRAMMING	63
3.1	Reformulation Techniques	63
3.2	Reformulation example	64

3.3	MILP formulation	67
3.3.1	<u>Constraints</u>	67
3.3.1.1	Selection of the geometric variables	67
3.3.1.2	Stream allocations	68
3.3.1.3	Structural constraints	68
3.3.1.4	Thermal and hydraulic modeling – Tube-side flow	69
3.3.1.5	Thermal and hydraulic modeling – Annulus-side flow	72
3.3.1.6	Heat transfer rate equation.....	75
3.3.1.7	Pressure drop and velocity bounds	82
3.3.2	<u>Objective function</u>	82
4	RESULTS	83
4.1	MINLP Results	83
4.1.1	<u>Initial Estimates</u>	Erro! Indicador não definido.
4.1.2	<u>Comparison with the literature</u>	87
4.1.3	<u>Analysis of the modeling of different flow regimes</u>	91
4.1.4	<u>Comparison of the MINLP approaches</u>	94
4.2	MILP Results	106
4.2.1	<u>Trial and Error Procedure</u>	108
4.2.2	<u>Global optimum analysis</u>	112
4.2.3	<u>Structural flexibility</u>	114
4.2.3.1	Variation of the hydraulic bounds	114
4.2.3.2	Modifications in the process throughput	118
	CONCLUSIONS AND SUGESTIONS	121
	Conclusions	121
	Sugestions	122
	REFERÊNCIAS	123
	APPENDIX A – Description of correlations correction factor	126
	APPENDIX B – List of symbols in alphabetic order divided by type	133
	APPENDIX C – Scientific production	141

INTRODUCTION

The chemical industry is one of the prime cores of the modern world and in every industrial process there are streams that need to be at a specific temperature and/or physical state and therefore must be heated or cooled down to reach the corresponding target. Thus, heat exchangers, responsible for these tasks, are primordial equipment in the chemical industry. Dealing with a highly competitive environment, the search for cost reduction becomes intense and there are a vast number of works related to the optimization of heat exchanger design, particularly the shell-and-tube type.

Although shell-and-tube heat exchangers are the most common heat transfer equipment in chemical process plants (Towler and Sinnott, 2008), there is a lack of robust works when it comes to the study of optimal design of some other heat exchanger types. For instance, double pipe heat exchangers (DPHE) can be an economically more advantageous option when smaller services are in place (e.g. heat transfer area lower than 50 m²) (Kakaç and Liu, 2002). If the stream contains solids in suspension, double pipe heat exchangers may also be a better alternative, because they can be built with an inner tube with larger diameter to avoid plugging. The smaller diameters of the outer tube in double pipe heat exchangers when compared to large shell diameters are a particular advantage in high-pressure services, because it implies a smaller wall thickness. In addition, double pipe heat exchangers are easily cleaned and the longitudinal flow avoids the existence of stagnation regions prone to fouling (Butterworth et al, 2008). Double pipe heat exchangers also have the benefit of flexibility due to its modular structure, which allows an easier adaptation to process modifications.

Aiming to contribute for filling the gap in the literature about the optimal DPHE design problem, this work presents the economic optimization of the design of double pipe heat exchangers using mathematical programming. Our optimization procedure explores the modular structure of double pipe heat exchangers, considering multiple units in series and in parallel. The corresponding thermo-fluid dynamic model can describe different flow regimes (laminar, transitional and turbulent).

In addition, our set of design variables is broader than the one in previous literature papers, encompassing the allocation of the streams (inside the inner tube or in the annulus), the inner and outer tube diameters, the tube length, the number of parallel branches, the number of units in series and in parallel in each branch, which determine the arrangement of the existent units.

Initially, the problem is formulated using the thermo-fluid dynamic model equations in their original form, thus yielding a mixed-integer nonlinear programming (MINLP) problem. In this model, we also make use of the fact that the geometric variables (diameters, lengths, etc.) can be expressed in a form of discrete choices. Then, a modified MINLP model, where mathematical transformations are applied to exclude nonlinearities involving binary variables is also presented, so that methods requiring linearity in binary variables like Outer Approximation (Duran and Grossmann, 1986) can be employed to solve it.

However, the solution of nonconvex MINLP problems may present convergence limitations and be trapped in poor local optima (which demands more specialized solvers based on global optimization algorithms). These problems in the MINLP design formulations are even more pronounced when considering the potential use of heat exchanger models in process synthesis, such as heat exchanger networks (HEN synthesis).

Thus, in a third approach, we eliminate these drawbacks through applying the same mathematical transformations used to generate the second MINLP problem to reformulate all constraints yielding a mixed-integer linear programming (MILP) problem. Linear problems are immune to nonconvergence issues and the global optimum can be always attained using conventional algorithms. The reformulation proposed does not imply any simplification of the original model, i.e. the feasible regions of the original MINLP problem and the new MILP problem are identical. This third formulation is the only one that can guarantee global optimality when the non-convex MINLP models are solved using local solvers.

This dissertation is organized as follows: Chapter 1 presents the review of literature; Chapter 2 encompasses the description of the system structure, the corresponding design problem and present both MINLP problem formulations; Chapter 3 exhibits the MILP problem formulation; Chapter 4 contains the numerical results; Chapter 5 discusses the conclusions and brings suggestions for improvement of this work.

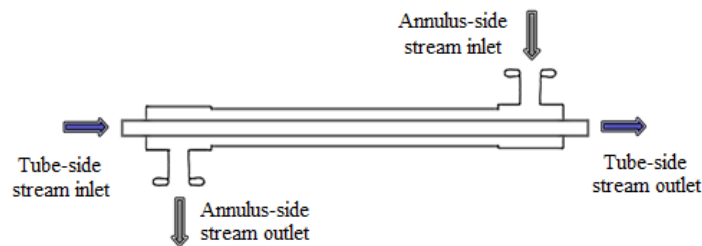
1 REVIEW OF LITERATURE

The review of literature is divided in four main aspects: (i) Double pipe heat exchangers overview; (ii) Heat transfer correlations; (iii) DPHE optimal design; (iv) Literature overview and Proposed contribution.

1.1 Double pipe heat exchangers overview

The basic structure of a double pipe heat exchanger consists in two concentric tubes, as shown in Figure 1 for a countercurrent configuration.

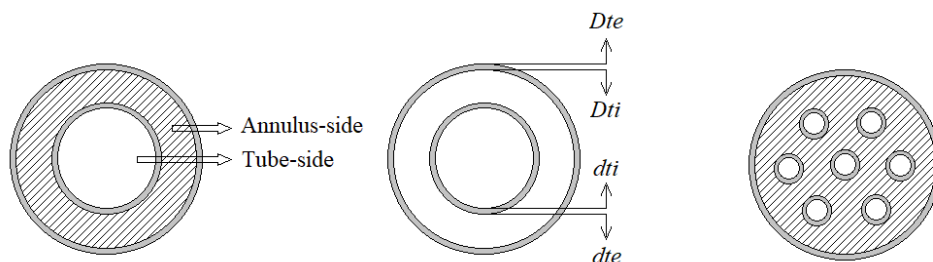
Figure 1: Double pipe heat exchanger.



Source: The autor.

There are two flow paths, inside the inner tube or in the annular region formed between both tubes. There are yet a few variations of this type of heat exchanger. One of them is the multi-tube heat exchanger, where there is a tube bundle inside the outer tube instead of just one concentric tube (Serth, 2007). The cross-section views for both types are illustrated in Figure 2.

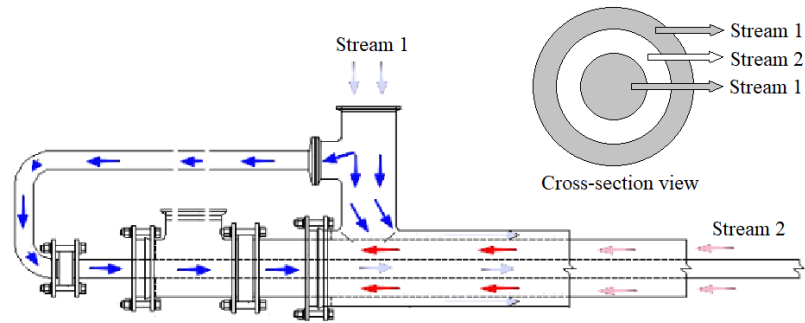
Figure 2: Cross-section views for double pipe and multi-tube heat exchangers.



Source: The autor.

There are still the triple tube heat exchangers, mostly used in the food industry, which consists in three concentric tubes, as shown in Figure 3.

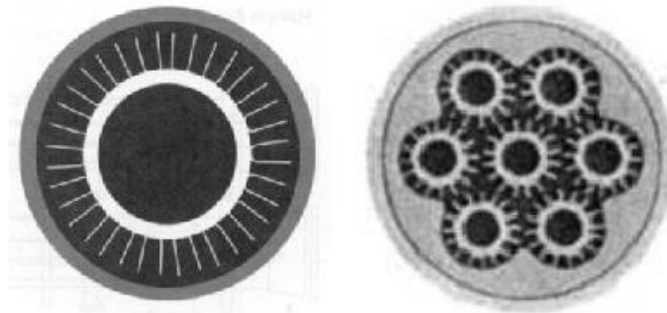
Figure 3: Triple tube heat exchangers.



Source: Adapted from (GENEMCO, 2017).

Double pipe heat exchangers can also be constituted of plain tubes, as the ones showed so far, or equipped with longitudinal fins (Serth, 2007), as shown in Figure 4.

Figure 4: Finned DPHE.



Source: Serth (2017).

Double pipe heat exchangers are most commonly commercialized in the form of hairpins, as illustrated in Figure 5

Figure 5: Hairpin structure.



Source: (KOCH Heat Transfer, 2017).

1.2 Heat transfer correlations

Heat transfer in pipes has been widely approached in literature and there are many correlations to the calculation of the convection heat transfer coefficient for different flow regimes. This section will do a brief essay on the most important and applied correlations.

For all correlations that follow, the physical properties are considered constant and evaluated at the mean temperature between the stream inlet and outlet temperatures.

1.2.1 Circular tubes

The dimensionless representation of the convection heat transfer coefficient corresponds to the Nusselt number, which for internal flow in circular tubes is represented by Equation (1.1):

$$Nu = \frac{h D}{k} \quad (1.1)$$

where Nu is the Nusselt number, h is the convection heat transfer coefficient, D is the inner diameter and k is the tube thermal conductivity.

1.2.1.1 Laminar flow

For fully developed laminar flow and constant surface temperatures, the assumption of negligible axial conduction is often reasonable and it is possible to algebraically demonstrate that the theoretical Nusselt number for this case is (KAYS, 1993):

$$Nu = 3.66 \quad (1.2)$$

For the entrance region, however, the energy equation becomes a little more complex due to the presence of radial advection and some simplifications may not be done. There are two approaches for the entrance length, the thermal entrance length and the combined entrance length. The first one, and the simpler one, assumes that the velocity profile is fully developed while the thermal conditions are still in developing process. The second one assumes that both temperature and velocity profiles develop simultaneously (Incropera et al., 2008).

Since, in the combined entrance length, the results depend on how the velocity distribution develops, it is sensitive to the fluid viscosity, and to the Prandtl number, which is the dimensionless ratio between the diffusions of momentum and heat:

$$Pr = \frac{C_p \mu}{k} \quad (1.3)$$

where Pr is the Prandtl number, C_p is the fluid heat capacity, μ is the fluid viscosity and k is the fluid thermal conductivity.

For Pr higher than 5, where the fluid dynamic conditions develop faster than the thermal ones, the assumption made by the thermal entrance length approach is quite reasonable and the correlation proposed by Hausen (1943) is appropriate:

$$Nu = 3.66 + \frac{0.0668(D/L)Re Pr}{1 + 0.04[(D/L)Re Pr]^{2/3}} \quad (1.4)$$

where L is the tube length and Re is the Reynolds number.

For moderated Prandtl numbers ($0.6 \leq Pr \leq 5$), associated to the combined entrance length approach, Sieder and Tate (1936) proposed the following correlation:

$$Nu = 1.86 \left(\frac{Re Pr}{L/D} \right)^{1/3} \left(\frac{\mu}{\mu_s} \right)^{0.14} \quad (1.5)$$

where μ_s is the surface viscosity.

According to the suggestion of Incropera et al. (2008), if the value predicted by the Sieder and Tate correlation is smaller than the theoretical value showed on (1.2) it would mean that fully developed conditions cover most of the tube length, and the theoretical value, $Nu = 3.66$, should be applied.

1.2.1.2 Turbulent flow

The description of turbulent flow conditions is considerably more complex. Thus, there is a bigger focus on empirical correlations when compared to laminar flow. A classic correlation for fully developed turbulent flow inside circular tubes was proposed by Colburn (1933):

$$Nu = 0.023 Re^{4/5} Pr^{1/3} \quad (1.6)$$

A small modification, and more accurate correlation was proposed in the same decade by Dittus and Boelter (Winterton, 1998) and it is shown below:

$$Nu = 0.023 Re^{4/5} Pr^n \quad (1.7)$$

where $n = 0.4$ for heating and $n = 0.3$ for cooling.

Both correlations were tested for a given range of Prandtl number ($0.7 \leq Pr \leq 160$), Reynolds number ($Re \geq 10\,000$) and L/D ratio (≥ 10) and may be used for small to moderate temperature differences. For scenarios where there is a more significant change in physical properties Sieder and Tate (1936) proposed this correlation:

$$Nu = 0.027 Re^{4/5} Pr^{1/3} \left(\frac{\mu}{\mu_s} \right)^{0.14} \quad (1.8)$$

which is valid for the same ranges of Reynolds number and L/D ratio as the previous correlations and for a different Prandtl number range ($0.7 \leq Pr \leq 16\,700$).

Although the previous correlations are easily applied, they may result in errors up to 25%, which may be reduced down to less than 10% by the use of more recent correlations (Incropera et al., 2008). One of which was proposed by Gnielinski (1976):

$$Nu = \frac{(f/8)(Re - 1000)Pr}{1 + 12.7(f/8)^{1/2}(Pr^{2/3} - 1)} \quad (1.9)$$

where f is the Darcy friction factor.

Gnielinski correlation is valid for a wider range of Reynolds number ($3000 \leq Re \leq 5 \cdot 10^6$) and Prandtl number ($0.5 \leq Pr \leq 2\,000$) and it is the correlation to be used in this work which, despite the higher complexity, should bring better results.

1.2.1.3 Annular region

The correlations presented in this section for flow inside circular tubes may be applied to the annular region through the concept of a hydraulic diameter (dh), which is defined as four times the cross-sectional flow area divided by the wetted perimeter (Incropera et al., 2008):

$$dh = \frac{4A_c}{P_w} \quad (1.10)$$

The hydraulic diameter should be used for the calculation of both Reynolds and Nusselt numbers in replacement of the inner tube diameter. In addition, for two concentric tubes, as illustrated in Figure 1, it can be simplified as the difference between the inner diameter of the outer tube (Di) and the outer diameter of the inner tube (dte), as shown below:

$$dh = \frac{4(\pi/4)(Dti^2 - dte^2)}{\pi Dti + \pi dte} = \frac{(Dti + dte)(Dti - dte)}{(Dti + dte)} = Dti - dte \quad (1.11)$$

1.3 DPHE optimal design

Several papers address the design of double pipe heat exchangers, but a large number of them are focused on heat transfer enhancement devices rather than on the general optimization of the equipment design (for example, diameter and length of the tubes are usually considered fixed parameters) (Omidi et al., 2017). For example, Sahiti et al. (2008) investigated the optimization of the pin fins in the heat exchanger annulus aiming at the minimization of the entropy generation. Their heat exchanger model was based on experimental data and the optimal set of variables was determined through a sensitivity analysis study.

In turn, using genetic algorithms and a trust region method, Syed et al. (2011) investigated the optimal configuration of the annulus with trapezoidal fins through the selection of the number of fins, fin height, fin thickness, and the radius ratio of the inner and outer tubes. A similar investigation was also proposed by the same authors using parabolic fins (Iqbal et al., 2011) and using a generalized optimization of the fin shape (Iqbal et al., 2013).

Later, Han et al. (2015) investigated the design of the outer surface corrugation of the inner tube using multi-objective optimization for the determination of the optimal values of the pitch, height, and radius of the corrugation, and the Reynolds number (the objective functions involved the Nusselt number, the friction factor, and the overall heat transfer coefficient). Their optimization was based on a response surface methodology (RSM) using simulation data generated through computational fluid dynamics (CFD).

Finally, Dastmalchi et al. (2017) employed a particle swarm algorithm (PSO) associated to a CFD model for the optimization of the inner micro-finned tube surface, contemplating the selection of the number of micro-fins, the micro-fin height, and the micro-fin helix angle.

The aforementioned studies do not account for the operational and capital costs in their objective functions and are focused on enhancing the heat transfer variables such as

Nusselt number and heat transfer coefficient, sometimes the minimization of entropy generation but never discussing a complete design.

Reducing costs is, after all, the main motivation for design optimization in practice. The literature involving the solution of the least-cost design problem of double pipe heat exchangers is scarce and the available papers are based on limited search spaces of the geometric variables. First, Söylemez (2004) investigated the optimization of double pipe heat exchangers for waste heat recovery, aiming at identifying the inner tube diameter, with a fixed ratio of the outer and inner tube diameters, for the minimization of capital and operating costs. Later, Swamee et al. (2008) presented the optimization of double pipe heat exchangers focusing on operational costs, encompassing the heat load, the pumping power, and the utility consumption. The decision variables are the inner and outer tube diameters and the utility flow rate, but the tube length is assumed known.

1.4 Literature overview and proposed contribution

In this review of literature, the double pipe heat exchanger and its variations were discussed, as well as available correlations for the calculation of the convection heat transfer coefficients. In addition, what has been addressed in the literature in terms of DPHE design has also been discussed.

In this work, aiming to bring an applicable yet robust formulation we assume the classical double-pipe heat exchanger structure, where two concentric tubes are the components. One unit will be associated with the hairpin structure showed in Figure 5, and the unit length (L) will be interpreted as the total tube length comprised in the unit (e.g. a 5 ft hairpin has a total of 10 ft of tube length). The most recent correlations, associated with smaller errors will be applied.

In comparison to the studies mentioned in the previous section we bring a more robust design formulation, including the description of different flow regimes (laminar, transitional and turbulent) and a broader set of design variables, encompassing the allocation of the streams (inside the inner tube or in the annulus), the inner and outer tube diameters, the tube length, the number of parallel branches, the number of units in series and in parallel in each branch, which determine the arrangement of the existent units.

In addition, three formulations are proposed where the third one, the MILP formulation, is able to achieve global optimality.

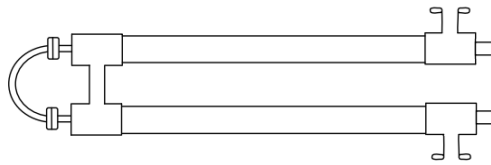
2 MIXED-INTEGER NONLINEAR PROGRAMMING

This chapter is divided in four sections: (i) the system structure is further explained; (ii) the design problem to be studied is approached; (iii) the first mixed-integer nonlinear programming approach is presented (MINLP 1); and (iv) the second approach (MINLP 2) is explored, where mathematical transformations are applied yielding a formulation with nonlinearities restricted to continuous variables, aiming to ameliorate convergence and to provide a more robust formulation.

2.1 System Structure

For a simpler understanding of the modular feature of the double pipe heat exchanger and of the possible arrangements considered in this work, this section will give a more detailed description of the system structure. In a more simplified illustration a hairpin as the one showed in Figure 5 for two concentric tubes is presented in Figure 6.

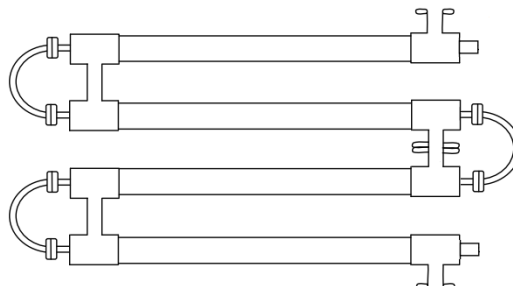
Figure 6: Hairpin structure.



Source: The autor.

In this work, the term unit will be associated with one hairpin. If the thermal service demands a higher heat transfer area, several units can be interconnected. For example, Figure 7 illustrates two hairpins connected in series.

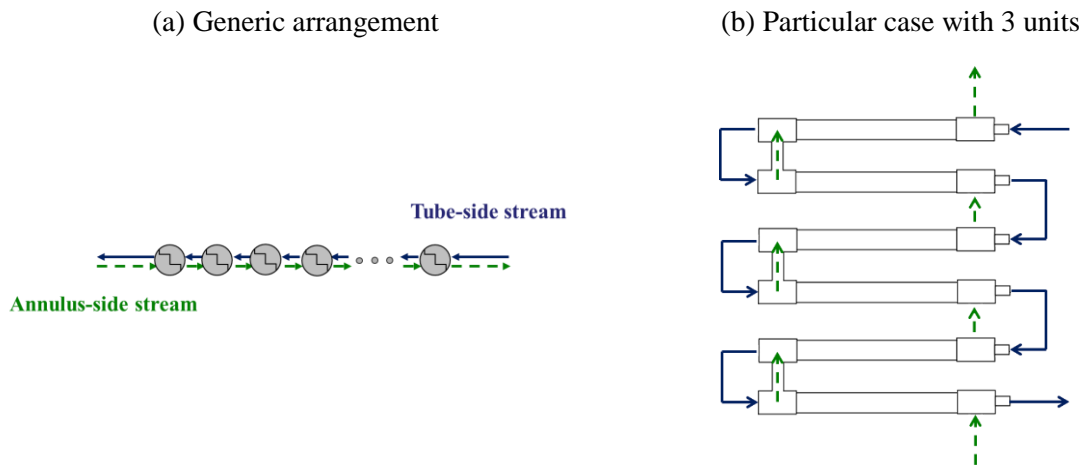
Figure 7: Two hairpins connected in series.



Source: The autor.

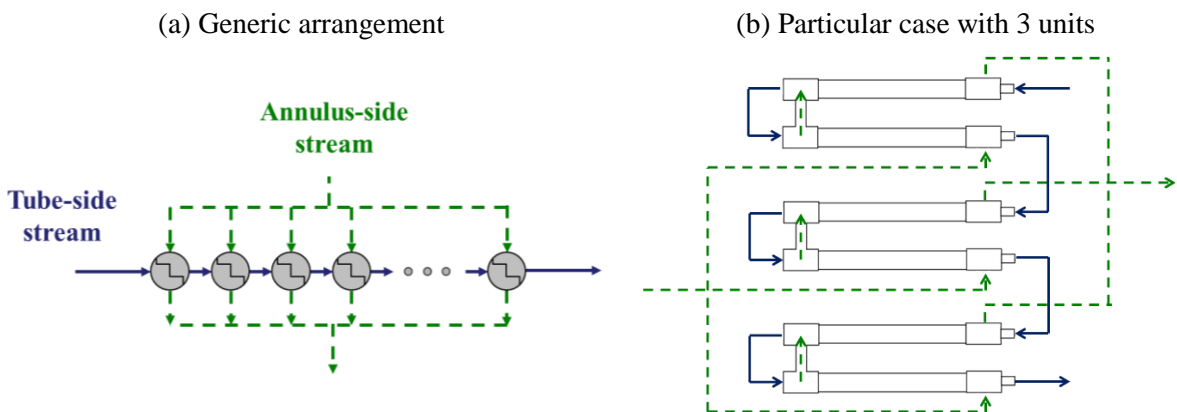
Different interconnection patterns among the heat exchanger units provide flexible design alternatives better suited to attain the heat load and maximum pressure drop specifications of the service. The mathematical formulation proposed here explores three main arrangements: tube-side and annulus-side streams aligned in series (Figure 8), tube-side stream aligned in series and annulus-side stream aligned in parallel (Figure 9), and tube-side stream aligned in parallel and annulus-side stream in series (Figure 10).

Figure 8: Arrangement I: Tube-side and annulus-side streams aligned in series.



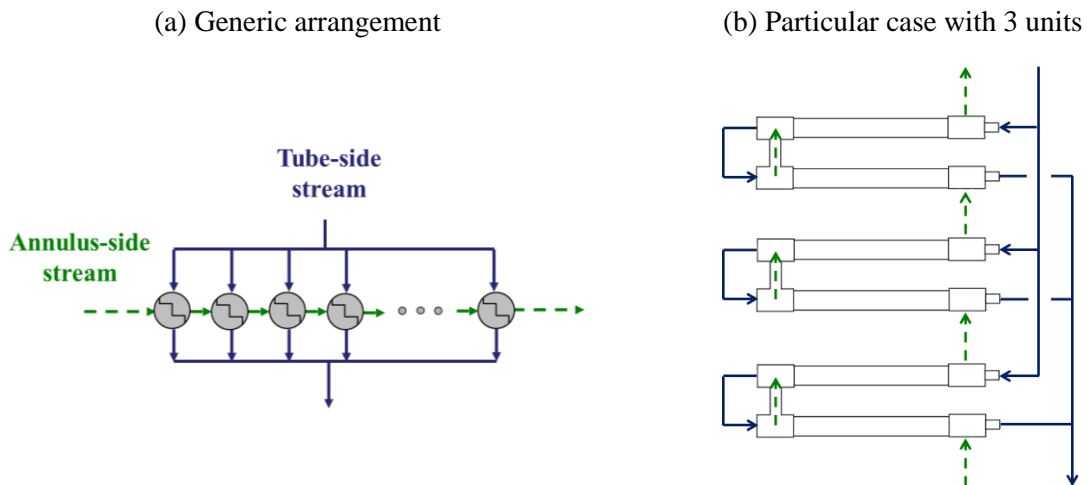
Source: The autor.

Figure 9: Arrangement II: Tube-side stream aligned in series and annulus-side stream aligned in parallel.



Source: The autor.

Figure 10: Arrangement III: Tube-side stream aligned in parallel and annulus-side stream aligned in series.



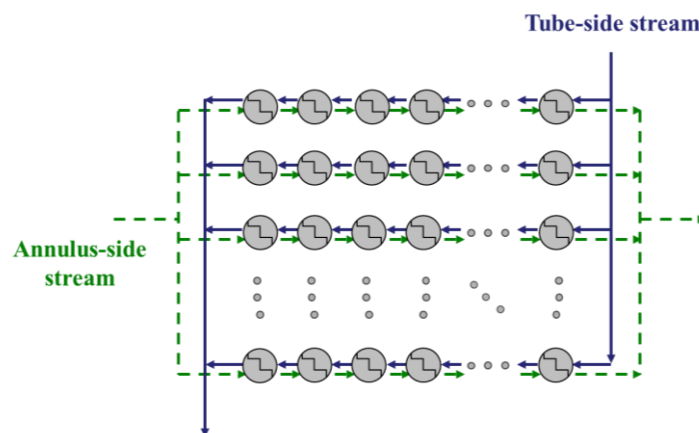
Source: The autor.

Figure 8(b), Figure 9(b) and Figure 10(b) are but a particular case of each main arrangement, when the number of units is equal to 3. Their representation was executed with hairpins to easier the reader understanding, however, from now on the units will be illustrated as the more generic representation from figures (a).

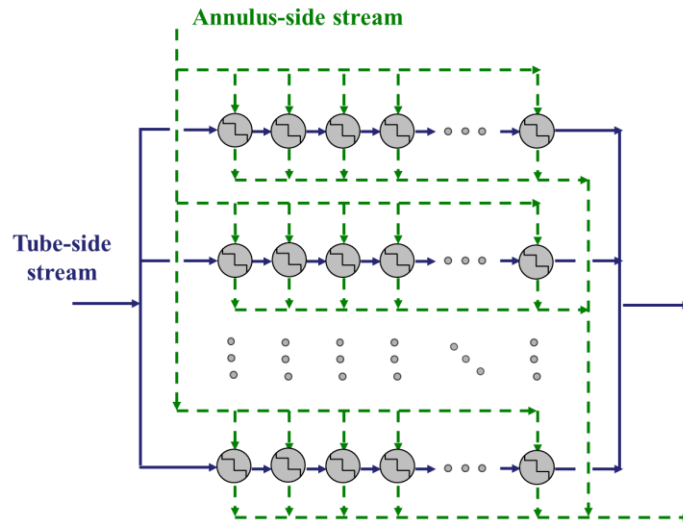
These three types of arrangements are the possibilities for what is here called a branch. The complete heat exchanger structure can also be composed of a set of parallel branches, which is illustrated by Figure 11 for each type of arrangement.

Figure 11: Double pipe heat exchanger structure composed of multiple parallel branches.

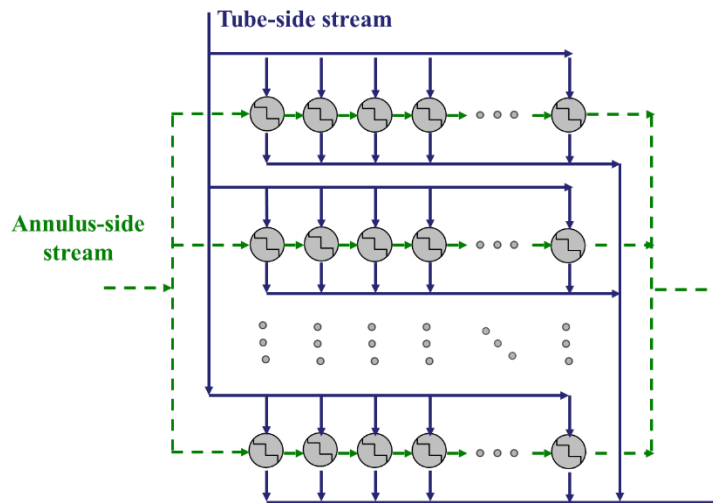
(a) Arrangement I: Tube-side and annulus-side streams aligned in series



(b) Arrangement II: Tube-side stream aligned in series and annulus-side stream aligned in parallel.



(c) Arrangement III: Tube-side stream aligned in parallel and annulus-side stream aligned in series.



Source: The autor.

2.2 Design Problem

The design problem involves the determination of the following data:

- Stream allocation of the hot and cold streams (tube-side or annulus-side).
- Diameter and length of the tubes of the heat exchanger units. All units are considered identical (i.e. same diameter and length).

- Structure layout (number of units in parallel and series per branch and the number of branches).

The goal is to identify an optimal solution, according to the usual heat exchanger design equations and thermal hydraulic modelling (LMTD method and Darcy-Weisbach equation), associated to the minimization of the total heat transfer area, restricted by a maximum allowed pressure drop and a minimum excess area.

Finally, we only consider streams without phase change and constant physical properties (representing average values), but considering any flow regime (laminar, transitional, and turbulent), which is associated to a particular formulation applying binary variables that will be further explored in the next section.

2.3 Problem formulation – MINLP 1

2.3.1 Constraints

The problem constraints are composed of the representation of the geometric variables, stream allocation equations, structural constraints, thermal and hydraulic modelling, and pressure drop and velocity bounds. The parameters in the constraints are identified with a symbol ^ on top.

2.3.1.1 Representation of the geometric variables

The diameter and length of the tubes employed in the construction of the heat exchanger must be selected among the set of discrete values according to the available standard options. This design feature imposes the following relations involving the sets of binary variables that represent the available options:

$$dte = \sum_{sd=1}^{sdmax} \widehat{pdte}_{sd} y_{sd} \quad (2.1)$$

$$dti = \sum_{sd=1}^{sdmax} \widehat{pd}ti_{sd} yd_{sd} \quad (2.2)$$

$$Dte = \sum_{sD=1}^{sDmax} \widehat{pD}te_{sD} yD_{sD} \quad (2.3)$$

$$Dti = \sum_{sD=1}^{sDmax} \widehat{pD}ti_{sD} yD_{sD} \quad (2.4)$$

$$L = \sum_{sL=1}^{sLmax} \widehat{pL}_{sL} yL_{sL} \quad (2.5)$$

$$\sum_{sd=1}^{sdmax} yd_{sd} = 1 \quad (2.6)$$

$$\sum_{sD=1}^{sDmax} yD_{sD} = 1 \quad (2.7)$$

$$\sum_{sL=1}^{sLmax} yL_{sL} = 1 \quad (2.8)$$

where dte and dti are the outer and inner diameters of the inner tube, Dte and Dti are the outer and inner diameters of the outer tube, and L is the tube length of each unit. The corresponding binary variables which indicate the discrete options selected are yd_{sd} for the inner tube diameter (discrete values: $\widehat{pd}te_{sd}$ and $\widehat{pd}ti_{sd}$), yD_{sD} for the outer tube diameter (discrete values: $\widehat{pD}te_{sD}$ and $\widehat{pD}ti_{sD}$), and yL_{sL} for the tube length (discrete values: \widehat{pL}_{sL}).

The constraints in Eq. (2.6) to (2.8) ensure that only one discrete option will be selected for each variable.

The selection of the number of parallel branches present in the heat exchanger design is represented by the binary variables yB_{sB} :

$$NB = \sum_{sB=1}^{sBmax} \widehat{pNB}_{sB} yB_{sB} \quad (2.9)$$

$$\sum_{sB=1}^{sBmax} yB_{sB} = 1 \quad (2.10)$$

where \widehat{pNB}_{sB} is the set of discrete values of the possible number of parallel branches (1, 2, ..., $sBmax$).

The number of units aligned in series and aligned in parallel in each branch for the tube-side stream and for the annulus-side stream are also represented using binary variables according to their integer nature:

$$NSt = \sum_{sE=1}^{sEmax} \widehat{pNE}_{sE} ySt_{sE} \quad (2.11)$$

$$NSa = \sum_{sE=1}^{sEmax} \widehat{pNE}_{sE} ySa_{sE} \quad (2.12)$$

$$NPt = \sum_{sE=1}^{sEmax} \widehat{pNE}_{sE} yPt_{sE} \quad (2.13)$$

$$NPa = \sum_{sE=1}^{sEmax} \widehat{pNE}_{sE} yPa_{sE} \quad (2.14)$$

$$\sum_{sE=1}^{sEmax} ySt_{sE} = 1 \quad (2.15)$$

$$\sum_{sE=1}^{sEmax} ySa_{sE} = 1 \quad (2.16)$$

$$\sum_{sE=1}^{sEmax} yPt_{sE} = 1 \quad (2.17)$$

$$\sum_{sE=1}^{sE_{max}} yPa_{sE} = 1 \quad (2.18)$$

where ySt_{sE} and ySa_{sE} are the binary variables which represent the integer options of the number of units in series per branch for the tube-side and the annulus-side streams, yPt_{sE} and yPa_{sE} are the equivalent variables related to the number of units in parallel per branch, and \overline{pNE}_{sE} is the sequence of integer numbers which represents the number of units that can be interconnected along a branch (1, 2, ..., sE_{max}).

According to the possible structural options for a single branch shown in Figure 8 to Figure 10, four additional constraints must be included:

$$yPt_{sE=1} + yPa_{sE=1} \geq 1 \quad (2.19)$$

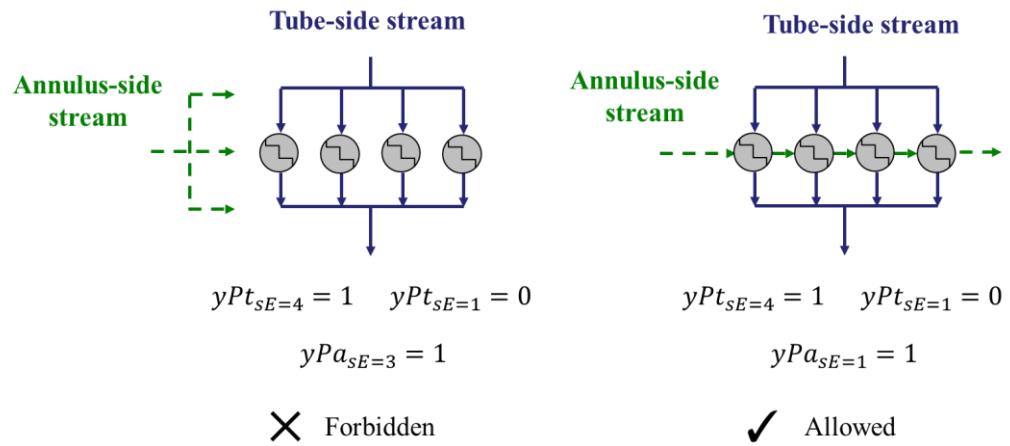
$$yPt_{sE=1} + ySt_{sE=1} \geq 1 \quad (2.20)$$

$$yPa_{sE=1} + ySa_{sE=1} \geq 1 \quad (2.21)$$

$$NPt NSt = NPa NSa \quad (2.22)$$

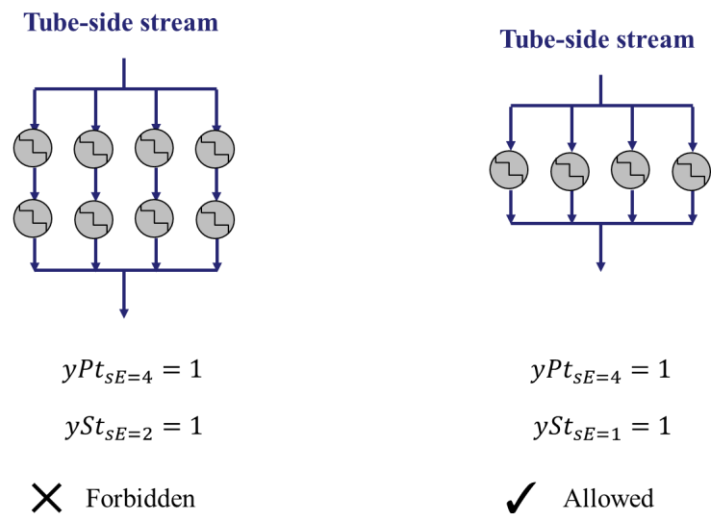
Eq. (2.19) ensures that if the tube-side has already more than one parallel passage, the annular side can be only arranged in series and vice-versa (e.g. Figure 12). Eqs. (2.20) and (2.21) guarantee that if a given side has multiple parallel passages it can only have one unit in series (). Finally, the constraint in Eq. (2.22) must be included to avoid alternatives without physical meaning related to the arrangement of the flow distribution among the set of units of the tube-side and annulus-side streams.

Figure 12: Violation example for Eq. (2.19).



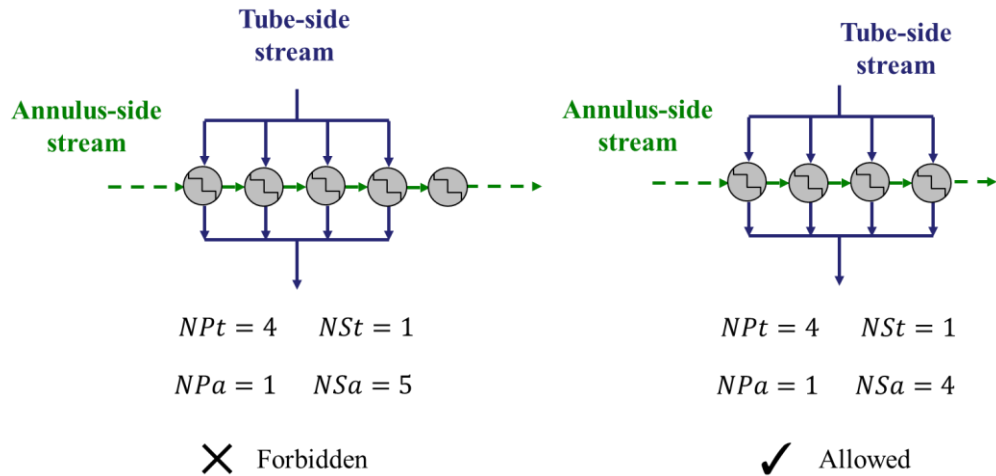
Source: The autor.

Figure 13: Violation example for Eq. (2.20).



Source: The autor.

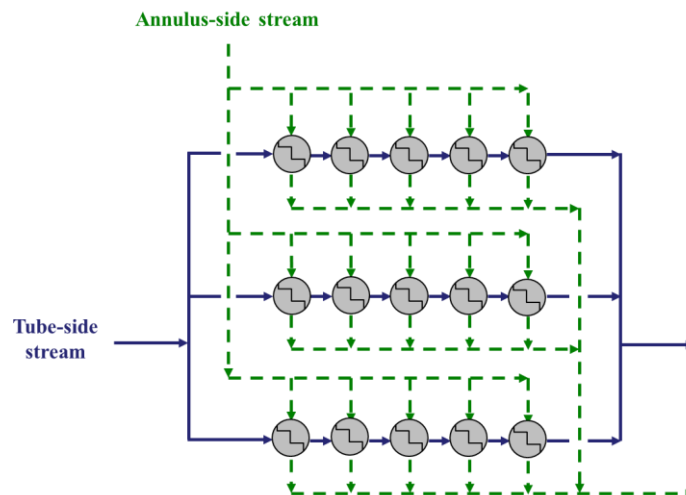
Figure 14: Violation example for Eq. (2.22).



Source: The autor.

The utilization of the proposed set of binary variables and constraints, shown in this subsection, to describe the interconnection structure of double pipe heat exchanger units is illustrated by the example depicted in Figure 15. According to the proposed approach, the nonzero binary variables that describe the structure present in this figure are: $y_{B_3} = 1$ (three parallel branches), $y_{St_5} = 1$ and $y_{Pt_1} = 1$ (five units aligned in series for the tube-side flow), $y_{Sa_1} = 1$ and $y_{Pa_5} = 1$ (five units aligned in parallel for the annulus-side flow).

Figure 15: Example of a double pipe heat exchanger structure composed of three parallel branches ($y_{B_3} = 1$). Each branch has a total of five units and a flow-arrangement as shown in Figure 9(a), where the tube-side stream is aligned in series ($y_{St_5} = 1$ and $y_{Pt_1} = 1$) and the annulus-side stream is in parallel ($y_{Sa_1} = 1$ and $y_{Pa_5} = 1$).



Source: The autor.

An important observation is that the proposed structure contemplates rectangular arrangements, in which the discrete options \widehat{pNE}_{sE} for the number of units per branch necessarily begins at $sE = 1$.

2.3.1.2 Stream allocation

The stream allocation is controlled by the binary variables yT_{sST} , where sST is the set of streams $sST = \{c, h\}$, c being the cold stream and h the hot stream. If $yT_c = 1$, then the cold stream flows inside the inner tube and the hot stream flows in the annulus; if $yT_h = 1$, then the hot stream flows inside the inner tube and the cold stream flows in the annulus.

The following equations relate the mass flow rates, physical properties and fouling factors of the hot and cold streams to the corresponding values of the tube-side and annulus-side flows:

$$mt = \widehat{m}_c yT_c + \widehat{m}_h yT_h \quad (2.23)$$

$$ma = \widehat{m}_c yT_h + \widehat{m}_h yT_c \quad (2.24)$$

$$\rho t = \widehat{\rho}_c yT_c + \widehat{\rho}_h yT_h \quad (2.25)$$

$$\rho a = \widehat{\rho}_c yT_h + \widehat{\rho}_h yT_c \quad (2.26)$$

$$C_{pt} = \widehat{Cp}_c yT_c + \widehat{Cp}_h yT_h \quad (2.27)$$

$$C_{pa} = \widehat{Cp}_c yT_h + \widehat{Cp}_h yT_c \quad (2.28)$$

$$\mu t = \widehat{\mu}_c yT_c + \widehat{\mu}_h yT_h \quad (2.29)$$

$$\mu a = \widehat{\mu}_c yT_h + \widehat{\mu}_h yT_c \quad (2.30)$$

$$kt = \widehat{k}_c yT_c + \widehat{k}_h yT_h \quad (2.31)$$

$$ka = \widehat{k}_c yT_h + \widehat{k}_h yT_c \quad (2.32)$$

$$Rft = \widehat{Rf}_c yT_c + \widehat{Rf}_h yT_h \quad (2.33)$$

$$Rfa = \widehat{Rf}_c yT_h + \widehat{Rf}_h yT_c \quad (2.34)$$

$$yT_c + yT_h = 1 \quad (2.35)$$

where m is the mass flow rate, ρ is the density, C_p is the heat capacity, μ is the viscosity, k is the thermal conductivity, R_f is the fouling factor, and the subscripts c and h indicate the cold and hot streams, respectively.

2.3.1.3 Structural constraints

The flow area and length of the hydraulic path of the streams considering the complete double pipe heat exchanger structure depend on the selection of the tube diameters and length, the number of units in series and in parallel in each branch, and the number of parallel branches:

$$A_t = \left(\frac{\pi d t_i^2}{4} \right) N_B N_{P_t} \quad (2.36)$$

$$A_a = \left(\frac{\pi D t_i^2}{4} - \frac{\pi d t_e^2}{4} \right) N_B N_{P_a} \quad (2.37)$$

$$L_t = L N_{S_t} \quad (2.38)$$

$$L_a = L N_{S_a} \quad (2.39)$$

where A_t and A_a are the tube-side and annulus-side flow area, and L_t and L_a are the corresponding flow path lengths.

2.3.1.4 Thermal and Hydraulic modeling – Tube-side flow

The Prandtl number of the stream that flows inside the inner tube is stated as:

$$Pr_t = \frac{C_{p_t} \mu_t}{k_t} \quad (2.40)$$

The flow velocity inside the inner tube and the corresponding Reynolds number are given by:

$$v_t = \frac{(m_t/\rho_t)}{A_t} \quad (2.41)$$

$$Re_t = \frac{d_{ti} v_t \rho_t}{\mu_t} \quad (2.42)$$

The pressure drop of the flow in the inner tube is calculated by the Darcy-Weisbach equation (omitting the viscosity correction factor) (Saunders, 1988):

$$\Delta P_t = \rho_t f_t \frac{L_t v_t^2}{d_{ti} 2} \quad (2.43)$$

where f_t is the Darcy friction factor.

The friction factor depends on the flow regime according to the following equations (Saunders, 1988):

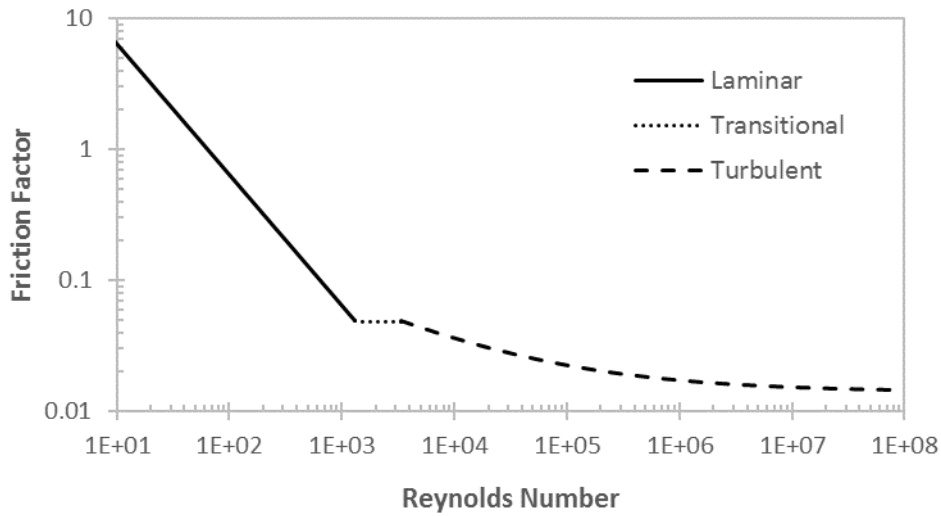
$$f_t^{lam} = \frac{64}{Re_t} \quad \text{for } Re_t \leq 1311 \quad (2.44)$$

$$f_t^{tran} = 0.0488 \quad \text{for } 1311 < Re_t \leq 3380 \quad (2.45)$$

$$f_t^{turb} = 0.014 + \frac{1.056}{Re_t^{0.42}} \quad \text{for } Re_t > 3380 \quad (2.46)$$

The values of the intervals of the different flow regimes in Eqs. (2.44)-(2.46) guarantee a continuous profile of the friction factor, as shown in Figure 16.

Figure 16: Inner tube friction factor profile in all three regimes generated from Eqs. (2.44)-(2.46).



Source: The autor.

Regarding the Nusselt number; laminar, transitional, and turbulent flows are considered, with the threshold of $Ret = 2300$ between the laminar and the transitional/turbulent flow. For the transitional and turbulent flow, the Gnielinski correlation is applied (Incropera et al., 2009):

$$Nut^{Gni} = \frac{(ft/8) (Ret - 1000) Prt}{1 + 12.7 (ft/8)^{1/2} (Prt^{2/3} - 1)} \quad \text{for } Ret > 2300 \quad (2.47)$$

Since the laminar flow is more affected by the entry region, more than one equation is utilized, according to the proposal of Incropera et al., (2009). For $Prt > 5$, Hausen correlation is applied:

$$Nut^{Hau} = 3.66 + \frac{0,0668 (dti/L) Ret Prt}{1 + 0,04((dti/L)Ret Prt)^{2/3}} \quad \text{for } Ret \leq 2300 \text{ and } Prt > 5 \quad (2.48)$$

For $Prt \leq 5$, the Nusselt number is specified by the Seider & Tate correlation unless its given value is lower than the theoretical Nusselt number for fully developed flow (3.66), in which case the latter is applied:

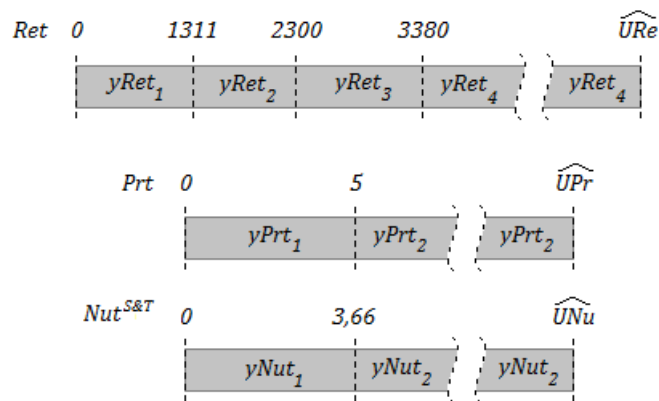
$$Nut^{S\&T} = 1.86 \left(\frac{Ret Prt dti}{L} \right)^{\frac{1}{3}} \quad \text{for } Ret \leq 2300, Prt \leq 5, Nut^{S\&T} \geq 3.66 \quad (2.49)$$

$$Nut^{thso} = 3.66 \quad \text{for } Ret \leq 2300, Prt \leq 5, Nut^{S\&T} < 3.66 \quad (2.50)$$

The viscosity correction factor in the Seider & Tate correlation in Equation (2.49) has also been omitted (i.e. the ratio between bulk and wall viscosities were considered equal to one).

In order to formulate a set of constraints able to represent the friction factor and Nusselt number evaluation for all possible conditions described in Eqs. (2.44) to (2.50), binary variables are included associated to the possible ranges of *Ret*, *Prt* and *Nut*, as indicated in Figure 17, where \widehat{URe} , \widehat{UPr} , and \widehat{UNu} are maximum values of *Re*, *Pr*, and *Nu*, respectively. In each interval, the corresponding binary variable is equal to 1 and the others are 0.

Figure 17: Possible ranges for *Ret*, *Prt*, $Nut^{S\&T}$ and its corresponding binary variables.



Source: The autor.

The following equations relates the binary variables and its corresponding ranges:

$$Ret \leq 1311 yRet_1 + 2300 yRet_2 + 3380 yRet_3 + \widehat{URe} yRet_4 \quad (2.51)$$

$$Ret \geq 1311 yRet_2 + 2300 yRet_3 + 3380 yRet_4 + \varepsilon \quad (2.52)$$

$$Prt \leq 5 yPrt_1 + \widehat{UPr} yPrt_2 \quad (2.53)$$

$$Prt \geq 5 yPrt_2 + \varepsilon \quad (2.54)$$

$$Nut^{S\&T} \leq 3.66yNut_1 + \widehat{UNu} yNut_2 - \varepsilon \quad (2.55)$$

$$Nut^{S\&T} \geq 3.66yNut_2 \quad (2.56)$$

where ε is a small positive number.

Since only one binary variable must be selected for each set of intervals, it yields:

$$\sum_{sRet=1}^{sRetmax} yRet_{sRet} = 1 \quad (2.57)$$

$$yPrt_1 + yPrt_2 = 1 \quad (2.58)$$

$$yNut_1 + yNut_2 = 1 \quad (2.59)$$

Therefore, the evaluation of the friction factor and the Nusselt number are represented by:

$$ft = ft^{lam}yRet_1 + ft^{tran} (yRet_2 + yRet_3) + ft^{turb}yRet_4 \quad (2.60)$$

$$Nut = Nut^{theo} (yRet_1 + yRet_2)yPrt_1yNut_1 + Nut^{S\&T} (yRet_1 + yRet_2)yPrt_1yNut_2 \\ + Nut^{Hau} (yRet_1 + yRet_2)yPrt_2 + Nut^{Gni} (yRet_3 + yRet_4) \quad (2.61)$$

2.3.1.5 Thermal and Hydraulic modeling – Annular flow

The Prandtl number of the stream flowing in the annular region is stated as:

$$Pra = \frac{Cpa \mu a}{ka} \quad (2.62)$$

The flow velocity inside the annular region is given by:

$$va = \frac{(ma/\rho a)}{Aa} \quad (2.63)$$

The hydraulic diameter is here calculated as four times the flow cross-sectional area divided by the wetted perimeter, which in the case of only one concentric tube can be simplified to (Incropera et al., 2009):

$$dh = D_{ti} - d_{te} \quad (2.64)$$

The Reynolds number can then be calculated by:

$$Re_a = \frac{dh \ v_a \ \rho_a}{\mu_a} \quad (2.65)$$

The pressure drop of the flow in the annulus is given by the Darcy-Weisbach equation using the hydraulic diameter (also omitting the viscosity correction factor) (Saunders, 1988):

$$\Delta P_a = \rho_a \ f_a \ \frac{L_t \ v_a^2}{dh \ 2} \quad (2.66)$$

where f_a is the Darcy friction factor for the annular flow.

The annular region friction factor, analogously to the inner tube, depends on the flow regime according to the following equations (Saunders, 1988):

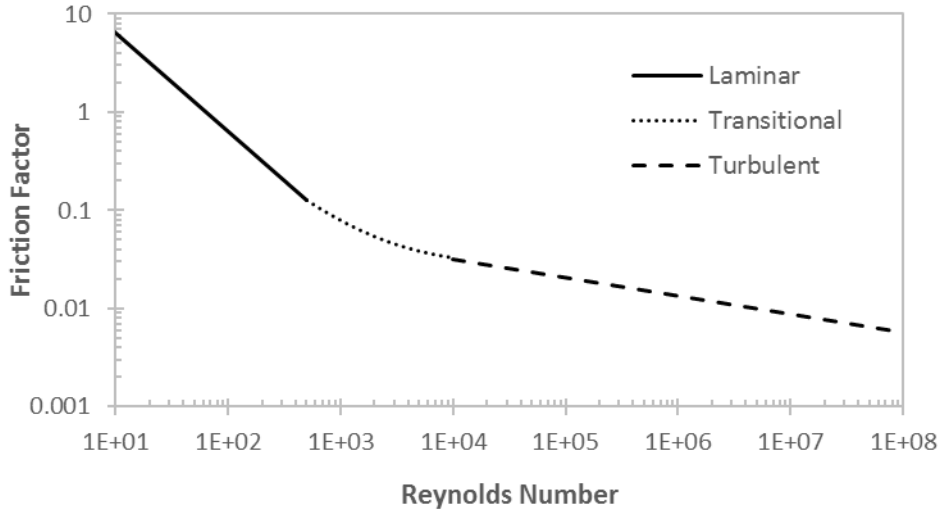
$$f_a^{lam} = \frac{64}{Re_a} \quad \text{for } Re_a \leq 500 \quad (2.67)$$

$$f_a^{tran} = 0.02696 + \frac{32.656}{Re_a^{0.93}} \quad \text{for } 500 < Re_a \leq 10000 \quad (2.68)$$

$$f_a^{turb} = \frac{0.178}{Re_a^{0.1865}} \quad \text{for } Re_a > 10000 \quad (2.69)$$

The threshold Reynolds number values in this case are 500 and 10000 and it also forms a continuous profile for calculation of the friction factor, as shown in Figure 18.

Figure 18: Annular friction factor profile in all three regimes generated from Eqs. (2.67)-(2.69).



Source: The autor.

Regarding the Nusselt number, the same ranges and correlations used for the tube-side are applied, replacing the inner tube diameter by the hydraulic diameter:

$$Nua^{theo} = 3.66 \quad \text{for } Rea \leq 2300, Pra \leq 5 \text{ and } Nua^{S\&T} < 3.66 \quad (2.70)$$

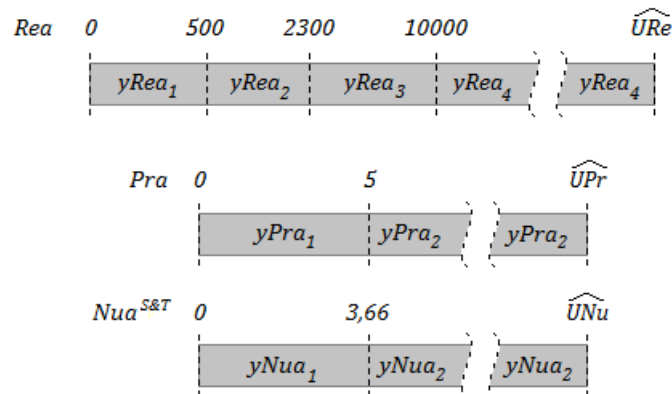
$$Nua^{S\&T} = 1.86 \left(\frac{Rea Pra dh}{L} \right)^{\frac{1}{3}} \quad \text{for } Rea \leq 2300, Pra \leq 5 \text{ and } Nua^{S\&T} \geq 3.66 \quad (2.71)$$

$$Nua^{Hau} = 3.66 + \frac{0.0668 (dh/L) Rea Pra}{1 + 0.04 \left((dh/L) Rea Pra \right)^{\frac{2}{3}}} \quad \text{for } Rea \leq 2300 \text{ and } Pra > 5 \quad (2.72)$$

$$Nua^{Gni} = \frac{(fa/8)(Rea - 1000)Pra}{1 + 12.7 (fa/8)^{\frac{1}{2}} (Pra^{\frac{2}{3}} - 1)} \quad \text{for } Rea > 2300 \quad (2.73)$$

Binary variables are then included to describe each interval of Rea , Pra and $Nua^{S\&T}$, as depicted in Figure 19.

Figure 19: Possible ranges for Rea , Pra , $Nua^{S\&T}$ and its corresponding binary variables.



Source: The autor.

The same approach used for the tube-side flow for the evaluation of the Nusselt number is implemented here:

$$Rea \leq 500 yRea_1 + 2300 yRea_2 + 10000 yRea_3 + \widehat{URe} yRea_4 \quad (2.74)$$

$$Rea \geq 500yRea_2 + 2300yRea_3 + 10000 yRea_4 + \varepsilon \quad (2.75)$$

$$Pra \leq 5yPra_1 + \widehat{UPr} yPra_2 \quad (2.76)$$

$$Pra \geq 5yPra_2 + \varepsilon \quad (2.77)$$

$$Nua^{S\&T} \leq 3.66yNua_1 + \widehat{UNu} yNua_2 - \varepsilon \quad (2.78)$$

$$Nua^{S\&T} \geq 3.66yNua_2 \quad (2.79)$$

$$\sum_{sRea=1}^{sReamax} yRea_{sRea} = 1 \quad (2.80)$$

$$yPra_1 + yPra_2 = 1 \quad (2.81)$$

$$yNua_1 + yNua_2 = 1 \quad (2.82)$$

$$fa = fa^{lam} yRea_1 + fa^{tran} (yRea_2 + yRea_3) + fa^{turb} yRea_4 \quad (2.83)$$

$$Nua = Nua^{theo} (yRea_1 + yRea_2) yPra_1 yNua_1 + Nua^{S\&T} (yRea_1 + yRea_2) yPra_1 yNua_2 + Nua^{Hau} (yRea_1 + yRea_2) yPra_2 + Nua^{Gni} (yRea_3 + yRea_4) \quad (2.84)$$

2.3.1.6 Heat transfer coefficients

The convective heat transfer coefficient for the tube-side and annulus-side flows are given by:

$$h_t = \frac{N_{ut} k_t}{d_{ti}} \quad (2.85)$$

$$h_a = \frac{N_{ua} k_a}{d_h} \quad (2.86)$$

The overall heat transfer coefficient is then determined by:

$$U = \frac{1}{\frac{1}{h_t} \frac{d_{te}}{d_{ti}} + R_{ft} \frac{d_{te}}{d_{ti}} + \frac{d_{te} \ln\left(\frac{d_{te}}{d_{ti}}\right)}{2k_{tube}} + R_{fa} + \frac{1}{h_a}} \quad (2.87)$$

where k_{tube} is the thermal conductivity of the inner tube.

2.3.1.7 Heat transfer rate equation

According to the LMTD method, the heat transfer rate is given by:

$$\hat{Q} = U A_{req} \widehat{\Delta T}_{lm} F \quad (2.88)$$

where A_{req} is the required heat transfer area, $\widehat{\Delta T}_{lm}$ is the logarithmic mean temperature, and F is the correction factor.

The logarithmic mean temperature is defined as:

$$\widehat{\Delta T}_{lm} = \frac{(\widehat{T}_{i_h} - \widehat{T}_{o_c}) - (\widehat{T}_{o_h} - \widehat{T}_{i_c})}{\ln\left(\frac{(\widehat{T}_{i_h} - \widehat{T}_{o_c})}{(\widehat{T}_{o_h} - \widehat{T}_{i_c})}\right)} \quad (2.89)$$

The correction factor depends on the structure of the arrangement of the double pipe heat exchanger units. If the structure is based on an arrangement where both streams are aligned in series, as shown in Figure 8, the correction factor is equal to unity. If the structure has one of the streams in parallel, as shown in Figure 9 and Figure 10, its value depends on which stream is in parallel and on the number of existing units per branch (Serth, 2007). Those correction factor options are calculated as parameters prior to the optimization. For stream sSt (cold, $sSt = c$, or hot, $sSt = h$) aligned in series and the other stream in parallel, the correction factor is given by (Serth, 2007):

$$\bar{p}F_{sSt,sE} = \frac{(\bar{p}R_{sSt} - \bar{p}NE_{sE})}{\bar{p}NE_{sE}(\bar{p}R_{sSt} - 1)} \frac{\ln\left(\frac{1 - \bar{p}P_{sSt}}{1 - \bar{p}P_{sSt}\bar{p}R_{sSt}}\right)}{\ln\left(\frac{\bar{p}R_{sSt} - \bar{p}NE_{sE}}{\bar{p}R_{sSt}(1 - \bar{p}P_{sSt}\bar{p}R_{sSt})^{1/\bar{p}NE_{sE}} + \frac{\bar{p}NE_{sE}}{\bar{p}R_{sSt}}}\right)} \quad \text{for } sE \quad (2.90)$$

$\neq 1$

where the factors $\bar{p}R_{sSt}$ and $\bar{p}P_{sSt}$ are specified as:

$$\bar{p}R_{sSt} = \begin{cases} \frac{(\bar{T}O_c - \bar{T}I_c)}{(\bar{T}I_h - \bar{T}O_h)} & \text{for } sSt = c \\ \frac{(\bar{T}I_h - \bar{T}O_h)}{(\bar{T}O_c - \bar{T}I_c)} & \text{for } sSt = h \end{cases} \quad (2.91)$$

$$\bar{p}P_c = \begin{cases} \frac{(\bar{T}I_h - \bar{T}O_h)}{(\bar{T}I_h - \bar{T}I_c)} & \text{for } sSt = c \\ \frac{(\bar{T}O_c - \bar{T}I_c)}{(\bar{T}I_h - \bar{T}I_c)} & \text{for } sSt = h \end{cases} \quad (2.92)$$

Based on these expressions, the constraint that represents the correction factor (F) evaluation becomes:

$$F = 1 + \sum_{sE=2}^{sE_{max}} \sum_{sE'=2}^{sE'_{max}} \left[(\widehat{pF}_{c,sE} - 1) y P t_{sE} y T_c + (\widehat{pF}_{h,sE} - 1) y P t_{sE} y T_h \right. \\ \left. + (\widehat{pF}_{h,sE'} - 1) y P a_{sE'} y T_c + (\widehat{pF}_{c,sE'} - 1) y P a_{sE'} y T_h \right] \quad (2.93)$$

Aiming at guaranteeing a design margin, a minimum area excess (\widehat{A}_{exc}) is imposed:

$$A \geq \left(1 + \frac{\widehat{A}_{exc}}{100} \right) A_{req} \quad (2.94)$$

where the equipment heat transfer area is given by:

$$A = \pi d t e L N B N P t N S t \quad (2.95)$$

Therefore, the heat transfer rate shown in Eq. (2.88) can be reorganized as:

$$UA \geq \frac{\widehat{Q} \left(\frac{\widehat{A}_{exc}}{100} + 1 \right)}{\Delta T \widehat{lm} F} \quad (2.96)$$

2.3.1.8 Pressure drops and velocity bounds

The lower and upper bounds on the velocities of the tube-side flow and annulus-side flow are given by:

$$v_t \geq \widehat{v}_{t_{min}} \quad (2.97)$$

$$v_t \leq \widehat{v}_{t_{max}} \quad (2.98)$$

$$v_a \geq \widehat{v}_{a_{min}} \quad (2.99)$$

$$v_a \leq \widehat{v}_{a_{max}} \quad (2.100)$$

While the pressure drop bounds are represented by:

$$\Delta Pt \leq \widehat{\Delta P}_{c\,disp} yT_c + \widehat{\Delta P}_{h\,disp} yT_h \quad (2.101)$$

$$\Delta Pa \leq \widehat{\Delta P}_{c\,disp} yT_h + \widehat{\Delta P}_{h\,disp} yT_c \quad (2.102)$$

2.3.2 Objective function

The objective function is given by the minimization of the heat transfer area:

$$\min A \quad (2.103)$$

The above model may present difficulties for certain MINLP algorithms as it contains products of binary variables and products of continuous and binary variables. Trying to make the model more amenable to be solved, we present a reformulation to obtain an MINLP model that is linear in binaries.

2.4 **Problem Reformulation – MINLP 2**

This section presents the reformulation of some constraints to eliminate the nonlinearities involving binary variables. The linear constraints or the constraints with continuous-only nonlinearities remain the same.

2.4.1 Reformulation Techniques

In the original optimization problem, there are two types of nonlinear terms involving binaries: the product of two or more binary variables and the product of a binary variable and a function of continuous variables (Williams, 2013).

The product of binary variables can be substituted by a continuous variable and a set of linear inequalities, as follows.

Let yz_i, yz_j, \dots , and yz_k be a set of binary variables. The product of these variables can be substituted by a continuous nonnegative variable $w_{i,j,\dots,k}$:

$$w_{i,j,\dots,k} = yp_i yq_j \dots yz_k \quad (2.104)$$

$$w_{i,j,\dots,k} \geq 0 \quad (2.105)$$

where the equality shown in Eq. (2.104) is guaranteed by the inclusion of these constraints:

$$w_{i,j,\dots,k} \leq yp_i \quad (2.106)$$

$$w_{i,j,\dots,k} \leq yq_j \quad (2.107)$$

....

$$w_{i,j,\dots,k} \leq yz_k \quad (2.108)$$

$$w_{i,j,\dots,k} \geq yp_i + yq_j + \dots + yz_k - (m - 1) \quad (2.109)$$

where m is the number of binary variables in the product.

The reformulation of the product between a binary variable and a function of continuous variables also involves the introduction of an additional continuous variable and a set of inequality constraints.

Let $f(x_1, x_2, \dots)$ be a function of continuous variables such that $0 \leq f \leq \widehat{\Phi}$ in the problem domain and y be a binary variable. The product of this function and the binary variable can be substituted by a continuous nonnegative variable w together with the inclusion of these constraints:

$$w - \widehat{\Phi}y \leq 0 \quad (2.110)$$

$$f(x_1, x_2, \dots) - w - \widehat{\Phi}(1 - y) \leq 0 \quad (2.111)$$

$$f(x_1, x_2, \dots) - w \geq 0 \quad (2.112)$$

2.4.2 Thermal and hydraulic modeling – Tube-side flow

The reformulation of the tube-side flow friction factor constraint (Eq. (2.60)) involves the substitutions depicted in Table 1.

Table 1. Reformulation of Eq. (2.60)

Original term	Variable
$ft^{lam}yRet_1$	wft_1
$ft^{tran}yRet_2$	wft_2
$ft^{tran}yRet_3$	wft_3
$ft^{turb}yRet_4$	wft_4

Source: The autor.

The reformulated expression of the friction factor constraint and the corresponding additional linear inequality constraints are:

$$ft = wft_1 + wft_2 + wft_3 + wft_4 \quad (2.113)$$

$$wft_1 - \tilde{\Phi}_{ft1}yRet_1 \leq 0 \quad (2.114)$$

$$[ft^{lam} - wft_1] - \tilde{\Phi}_{ft1}(1 - yRet_1) \leq 0 \quad (2.115)$$

$$ft^{lam} - wft_1 \geq 0 \quad (2.116)$$

$$wft_2 - \tilde{\Phi}_{ft2}yRet_2 \leq 0 \quad (2.117)$$

$$[ft^{tran} - wft_2] - \tilde{\Phi}_{ft2}(1 - yRet_2) \leq 0 \quad (2.118)$$

$$ft^{tran} - wft_2 \geq 0 \quad (2.119)$$

$$wft_3 - \tilde{\Phi}_{ft3}yRet_3 \leq 0 \quad (2.120)$$

$$[ft^{tran} - wft_3] - \tilde{\Phi}_{ft3}(1 - yRet_3) \leq 0 \quad (2.121)$$

$$ft^{tran} - wft_3 \geq 0 \quad (2.122)$$

$$wft_4 - \tilde{\Phi}_{ft4}yRet_4 \leq 0 \quad (2.123)$$

$$[ft^{turb} - wft_4] - \widehat{\Phi}_{ft_4}(1 - yRet_4) \leq 0 \quad (2.124)$$

$$ft^{turb} - wft_4 \geq 0 \quad (2.125)$$

The modifications of the Nusselt number constraint (Eq. (2.61)) are illustrated in Table 2.

Table 2. Reformulation of Equation (2.61).

Original term	Variable
$yRet_1 yPrt_1 yNut_1$	$wNut_1^{theo}$
$yRet_2 yPrt_1 yNut_1$	$wNut_2^{theo}$
$yRet_1 yPrt_1 yNut_2$	$wNut_1^{S\&T}$
$yRet_2 yPrt_1 yNut_2$	$wNut_2^{S\&T}$
$yRet_1 yPrt_2$	$wNut_1^{Hau}$
$yRet_2 yPrt_2$	$wNut_2^{Hau}$
$Nut^{Gni} (yRet_3 + yRet_4)$	$wNut^{Gni}$

Source: The autor.

The reformulated tube-side Nusselt number constraints and the additional inequality constraints are:

$$Nut = Nut^{theo} (wNut_1^{theo} + wNut_2^{theo}) + Nut^{S\&T} (wNut_1^{S\&T} + wNut_2^{S\&T}) + Nut^{Hau} (wNut_1^{Hau} + wNut_2^{Hau}) + wNut^{Gni} \quad (2.126)$$

$$wNut_1^{theo} \leq yRet_1 \quad (2.127)$$

$$wNut_1^{theo} \leq yPrt_1 \quad (2.128)$$

$$wNut_1^{theo} \leq yNut_1 \quad (2.129)$$

$$wNut_1^{theo} \geq yRet_1 + yPrt_1 + yNut_1 - 2 \quad (2.130)$$

$$wNut_2^{theo} \leq yRet_2 \quad (2.131)$$

$$wNut_2^{theo} \leq yPrt_1 \quad (2.132)$$

$$wNut_2^{theo} \leq yNut_1 \quad (2.133)$$

$$wNut_2^{theo} \geq yRet_2 + yPrt_1 + yNut_1 - 2 \quad (2.134)$$

$$wNut_1^{S\&T} \leq yRet_1 \quad (2.135)$$

$$wNut_1^{S\&T} \leq yPrt_1 \quad (2.136)$$

$$wNut_1^{S\&T} \leq yNut_2 \quad (2.137)$$

$$wNut_1^{S\&T} \geq yRet_1 + yPrt_1 + yNut_2 - 2 \quad (2.138)$$

$$wNut_2^{S\&T} \leq yRet_2 \quad (2.139)$$

$$wNut_2^{S\&T} \leq yPrt_1 \quad (2.140)$$

$$wNut_2^{S\&T} \leq yNut_2 \quad (2.141)$$

$$wNut_2^{S\&T} \geq yRet_2 + yPrt_1 + yNut_2 - 2 \quad (2.142)$$

$$wNut_1^{Hau} \leq yRet_1 \quad (2.143)$$

$$wNut_1^{Hau} \leq yPrt_2 \quad (2.144)$$

$$wNut_1^{Hau} \geq yRet_1 + yPrt_2 - 1 \quad (2.145)$$

$$wNut_2^{Hau} \leq yRet_2 \quad (2.146)$$

$$wNut_2^{Hau} \leq yPrt_2 \quad (2.147)$$

$$wNut_2^{Hau} \geq yRet_2 + yPrt_2 - 1 \quad (2.148)$$

$$wNut^{Gni} - \widehat{\Phi}_{Nut}(yRet_3 + yRet_4) \leq 0 \quad (2.149)$$

$$[Nut^{Gni} - wNut^{Gni}] - \widehat{\Phi}_{Nut}(1 - yRet_3 - yRet_4) \leq 0 \quad (2.150)$$

$$Nut^{Gni} - wNut^{Gni} \geq 0 \quad (2.151)$$

2.4.3 Thermal and hydraulic modeling – Annulus-side flow

Analogously to the tube-side flow, the constraints related to the friction factor (Eq. (2.83)) and Nusselt number (Eq. (2.84)) in the annulus are modified according to Table 3 and Table 4:

Table 3. Reformulation of Eq. (2.83)

Original term	Variable
$f a^{lam} yRea_1$	wfa_1
$f a^{tran} yRea_2$	wfa_2
$f a^{tran} yRea_3$	wfa_3
$f a^{turb} yRea_4$	wfa_4

Source: The autor.

Table 4. Reformulation of Eq. (2.84)

Original term	Variable
$yRea_1 yPra_1 yNua_1$	$wNua_1^{theo}$
$yRea_2 yPra_1 yNua$	$wNua_2^{theo}$
$yRea_1 yPra_1 yNua_2$	$wNua_1^{S\&T}$
$yRea_2 yPra_1 yNua_2$	$wNua_2^{S\&T}$
$yRea_1 yPra_2$	$wNua_1^{Hau}$
$yRea_2 yPra_2$	$wNua_2^{Hau}$
$Nua^{Gni} (yRea_3 + yRea_4)$	$wNua^{Gni}$

Source: The autor.

The constraints of the friction factor of the annulus-side flow are:

$$fa = wfa_1 + wfa_2 + wfa_3 + wfa_4 \quad (2.152)$$

$$wfa_1 - \tilde{\Phi}_{fa1} yRea_1 \leq 0 \quad (2.153)$$

$$[fa^{lam} - wfa_1] - \tilde{\Phi}_{fa1}(1 - yRea_1) \leq 0 \quad (2.154)$$

$$fa^{lam} - wfa_1 \geq 0 \quad (2.155)$$

$$wfa_2 - \tilde{\Phi}_{fa2}yRea_2 \leq 0 \quad (2.156)$$

$$[fa^{tran} - wfa_2] - \tilde{\Phi}_{fa2}(1 - yRea_2) \leq 0 \quad (2.157)$$

$$fa^{tran} - wfa_2 \geq 0 \quad (2.158)$$

$$wfa_3 - \tilde{\Phi}_{fa3}yRea_3 \leq 0 \quad (2.159)$$

$$[fa^{tran} - wfa_3] - \tilde{\Phi}_{fa3}(1 - yRea_3) \leq 0 \quad (2.160)$$

$$fa^{tran} - wfa_3 \geq 0 \quad (2.161)$$

$$wfa_4 - \tilde{\Phi}_{fa4}yRea_4 \leq 0 \quad (2.162)$$

$$[fa^{turb} - wfa_4] - \tilde{\Phi}_{fa4}(1 - yRea_4) \leq 0 \quad (2.163)$$

$$fa^{turb} - wfa_4 \geq 0 \quad (2.164)$$

The Nusselt number constraints for the annular flow become:

$$Nua = Nua^{theo}(wNua_1^{theo} + wNua_2^{theo}) + Nua^{S\&T}(wNua_1^{S\&T} + wNua_2^{S\&T}) \\ + Nut^{Hau}(wNua_1^{Hau} + wNua_2^{Hau}) + wNua^{Gni} \quad (2.165)$$

$$wNua_1^{theo} \leq yRea_1 \quad (2.166)$$

$$wNua_1^{theo} \leq yPra_1 \quad (2.167)$$

$$wNua_1^{theo} \leq yNua_1 \quad (2.168)$$

$$wNua_1^{theo} \geq yRea_1 + yPra_1 + yNua_1 - 2 \quad (2.169)$$

$$wNua_2^{theo} \leq yRea_2 \quad (2.170)$$

$$wNua_2^{theo} \leq yPra_1 \quad (2.171)$$

$$wNua_2^{theo} \leq yNua_1 \quad (2.172)$$

$$wNua_2^{thso} \geq yRea_2 + yPra_1 + yNua_1 - 2 \quad (2.173)$$

$$wNua_1^{S\&T} \leq yRea_1 \quad (2.174)$$

$$wNua_1^{S\&T} \leq yPra_1 \quad (2.175)$$

$$wNua_1^{S\&T} \leq yNua_2 \quad (2.176)$$

$$wNua_1^{S\&T} \geq yRea_1 + yPra_1 + yNua_2 - 2 \quad (2.177)$$

$$wNua_2^{S\&T} \leq yRea_2 \quad (2.178)$$

$$wNua_2^{S\&T} \leq yPra_1 \quad (2.179)$$

$$wNua_2^{S\&T} \leq yNua_2 \quad (2.180)$$

$$wNua_2^{S\&T} \geq yRea_2 + yPra_1 + yNua_2 - 2 \quad (2.181)$$

$$wNua_1^{Hau} \leq yRea_1 \quad (2.182)$$

$$wNua_1^{Hau} \leq yPra_2 \quad (2.183)$$

$$wNua_1^{Hau} \geq yRea_1 + yPra_2 - 1 \quad (2.184)$$

$$wNua_2^{Hau} \leq yRea_2 \quad (2.185)$$

$$wNua_2^{Hau} \leq yPra_2 \quad (2.186)$$

$$wNua_2^{Hau} \geq yRea_2 + yPra_2 - 1 \quad (2.187)$$

$$wNua^{Gni} - \widehat{\Phi}_{Nua}(yRea_3 + yRea_4) \leq 0 \quad (2.188)$$

$$[Nua^{Gni} - wNua^{Gni}] - \widehat{\Phi}_{Nua}(1 - yRea_3 - yRea_4) \leq 0 \quad (2.189)$$

$$Nua^{Gni} - wNua^{Gni} \geq 0 \quad (2.190)$$

2.4.4 Heat transfer rate equation

The correction factor constraint (Eq. (2.93)) is modified according to Table 5.

Table 5. Reformulation of Eq. (2.93)

Original term	Reformulated term
$yPt_{sE}yT_{sST}$	$wPtT_{sE,sST}$
$yPa_{sE}yT_{sST}$	$wPaT_{sE,sST}$

Source: The autor.

The reformulated constraints of the correction factor are:

$$F = 1 + \sum_{sE=2}^{sE_{max}} \sum_{sE'=2}^{sE'_{max}} [(\bar{pF}_{c,sE} - 1)wPtT_{sE,c} + (\bar{pF}_{h,sE} - 1)wPtT_{sE,h} + (\bar{pF}_{h,sE'} - 1)wPaT_{sE',c} + (\bar{pF}_{c,sE'} - 1)wPaT_{sE',h}] \quad (2.191)$$

$$wPtT_{sE,sST} \leq yPt_{sE} \quad (2.192)$$

$$wPtT_{sE,sST} \leq yT_{sST} \quad (2.193)$$

$$wPtT_{sE,sST} \geq yPt_{sE} + yT_{sST} - 1 \quad (2.194)$$

$$wPaT_{sE,sST} \leq yPa_{sE} \quad (2.195)$$

$$wPaT_{sE,sST} \leq yT_{sST} \quad (2.196)$$

$$wPaT_{sE,sST} \geq yPa_{sE} + yT_{sST} - 1 \quad (2.197)$$

3 MIXED-INTEGER LINEAR PROGRAMMING

This chapter presents the generation of a MILP formulation. Mathematical transformations are applied in the original MINLP model, which does not imply any simplification of the original model (i.e. the feasible regions of the original MINLP problem and the new MILP problem are identical).

3.1 Reformulation Techniques

The first step towards the linear model is to substitute all the continuous variables in the MINLP problem by the corresponding binary representations of the design variables using the procedure described below (recursive substitutions may be necessary to represent all the variables in relation to the fundamental design variables).

Let p, q, \dots, z be variables that are related to available discrete values, $\widehat{pd}_i, \widehat{qd}_j, \dots, \widehat{zd}_k$. Because of their discrete nature, these variables can be represented by sets of binaries.

The corresponding mathematical relation is presented here, for instance, for the variable p :

$$p = \sum_i \widehat{pd}_i y_{p_i} \quad (3.1)$$

where y_{p_i} is the binary variable for the selection among the available discrete options. Additionally, since only one option must be selected, then:

$$\sum_i y_{p_i} = 1 \quad (3.2)$$

The heat exchanger model constraints correspond to mathematical relations involving products of powers. Let $f(p, q, \dots, z)$ be a typical constraint composed of a function of the design variables:

$$f(p, q, \dots, z) = \widehat{K} p^{n_p} q^{n_q} \dots z^{n_z} \quad (3.3)$$

where \bar{K} is a model parameter. The substitution of these variables by their corresponding binary expressions yields:

$$f(p, q, \dots, z) = f(y_{p_i}, y_{q_j}, \dots, y_{z_k}) = \bar{K} \left(\sum_i \bar{p}d_i y_{p_i} \right)^{np} \left(\sum_j \bar{q}d_j y_{q_j} \right)^{nq} \dots \left(\sum_k \bar{z}d_k y_{z_k} \right)^{nz} \quad (3.4)$$

Since all binary variables are equal to one only once in each corresponding set (Eq. (3.2)), the constraint becomes equivalent to:

$$f(y_{p_i}, y_{q_j}, \dots, y_{z_k}) = \bar{K} \sum_i \sum_j \dots \sum_k \bar{p}d_i^{np} \bar{q}d_j^{nq} \dots \bar{z}d_k^{nz} y_{p_i} y_{q_j} \dots y_{z_k} \quad (3.5)$$

After this rearrangement, there are only binary variables and the existing nonlinearity corresponds to product of binaries. The elimination of this nonlinear term can be conducted using the same technique already explained in subsection 2.4.1 for binary products.

3.2 Reformulation example

The application of the reformulation techniques presented in the previous section will be detailed for one of the model constraints from start to finish. The selected constraint is the tube-side Reynolds number calculation, which in the original MINLP model is given by:

$$Ret = \frac{dt_i vt \rho t}{\mu t} \quad (3.6)$$

We have a function of continuous variables ($Re(dt_i, vt, \rho t, \mu t)$) and the first step is to substitute them for their binary representations. However, the tube-side velocity (vt) is itself a function of continuous variables ($vt(mt, \rho t, At)$), as well as the tube-side flow area ($At(dt_i, NB, NPt)$), as shown by the following original constraints:

$$vt = \frac{(mt/\rho t)}{At} \quad (3.7)$$

$$At = \left(\frac{\pi dti^2}{4} \right) NB NPt \quad (3.8)$$

For the remaining variables (dti , mt , ρt , μt , NB , NPt), we can apply the following binary representations:

$$dti = \sum_{sd=1}^{sdmax} \widehat{pd}ti_{sd} yd_{sd} \quad (3.9)$$

$$mt = \sum_{sST} \widehat{m}_{sST} yT_{sST} \quad (3.10)$$

$$\rho t = \sum_{sST} \widehat{\rho}_{sST} yT_{sST} \quad (3.11)$$

$$\mu t = \sum_{sST} \widehat{\mu}_{sST} yT_{sST} \quad (3.12)$$

$$NB = \sum_{sB=1}^{sBmax} \widehat{pNB}_{sB} yB_{sB} \quad (3.13)$$

$$NPt = \sum_{sE=1}^{sEmax} \widehat{pNE}_{sE} yPt_{sE} \quad (3.14)$$

Applying all the proposed substitutions, the tube-side flow area becomes:

$$\begin{aligned} At(yd_{sd}, yB_{sB}, yPt_{sE}) &= \left(\frac{\pi \left(\sum_{sd=1}^{sdmax} \widehat{pd}ti_{sd} yd_{sd} \right)^2}{4} \right) \left(\sum_{sB=1}^{sBmax} \widehat{pNB}_{sB} yB_{sB} \right) \left(\sum_{sE=1}^{sEmax} \widehat{pNE}_{sE} yPt_{sE} \right) \\ &= \sum_{sd=1}^{sdmax} \sum_{sB=1}^{sBmax} \sum_{sE=1}^{sEmax} \frac{\pi}{4} \widehat{pd}ti_{sd}^2 \widehat{pNB}_{sB} \widehat{pNE}_{sE} yd_{sd} yB_{sB} yPt_{sE} \end{aligned} \quad (3.15)$$

which render, for the tube-side velocity constraint, the following equation:

$$\begin{aligned}
& vt(yd_{sd}, yB_{sB}, yPt_{sE}, yT_{sST}) \\
&= \frac{\left(\sum_{sST} \hat{m}_{sST} yT_{sST} \right)}{\sum_{sd=1}^{sdmax} \sum_{sB=1}^{sBmax} \sum_{sE=1}^{sEmax} \frac{\pi}{4} \widehat{pdti}_{sd}^2 \widehat{pNB}_{sB} \widehat{pNE}_{sE} yd_{sd} yB_{sB} yPt_{sE}} \\
&= \sum_{sd=1}^{sdmax} \sum_{sB=1}^{sBmax} \sum_{sE=1}^{sEmax} \sum_{sST} \frac{4 \hat{m}_{sST}}{\pi \hat{\rho}_{sST} \widehat{pdti}_{sd}^2 \widehat{pNB}_{sB} \widehat{pNE}_{sE}} yd_{sd} yB_{sB} yPt_{sE} yT_{sST}
\end{aligned} \tag{3.16}$$

Finally, for the tube-side Reynolds number, we have:

$$\begin{aligned}
& Ret(yd_{sd}, yB_{sB}, yPt_{sE}, yT_{sST}) \\
&= \sum_{sd=1}^{sdmax} \sum_{sB=1}^{sBmax} \sum_{sE=1}^{sEmax} \sum_{sST} \frac{4 \hat{m}_{sST}}{\pi \hat{\rho}_{sST} \widehat{pdti}_{sd}^2 \widehat{pNB}_{sB} \widehat{pNE}_{sE}} yd_{sd} yB_{sB} yPt_{sE} yT_{sST}
\end{aligned} \tag{3.17}$$

In Eq. (3.17) **Erro! Fonte de referência não encontrada.**, after all the proper substitutions, the second step, shown in subsection 2.4.1, can be applied. Thus, the existing binary product $(yd_{sd} yB_{sB} yPt_{sE} yT_{sST})$ is replaced by a continuous variable $(wvt_{sd,sB,sE,sST})$ and the linear inequalities are added, yielding the following constraints:

$$Ret = \sum_{sd=1}^{sdmax} \sum_{sB=1}^{sBmax} \sum_{sE=1}^{sEmax} \sum_{sST} \frac{4 \hat{m}_{sST}}{\pi \hat{\rho}_{sST} \widehat{pdti}_{sd}^2 \widehat{pNB}_{sB} \widehat{pNE}_{sE}} wvt_{sd,sB,sE,sST} \tag{3.18}$$

$$wvt_{sd,sB,sE,sST} \leq yd_{sd} \tag{3.19}$$

$$wvt_{sd,sB,sE,sST} \leq yB_{sB} \tag{3.20}$$

$$wvt_{sd,sB,sE,sST} \leq yPt_{sE} \tag{3.21}$$

$$wvt_{sd,sB,sE,sST} \leq yT_{sST} \tag{3.22}$$

$$wvt_{sd,sB,sE,sST} \geq yd_{sd} + yB_{sB} + yPt_{sE} + yT_{sST} - 3 \tag{3.23}$$

Therefore, the constraint from the original MINLP model (Eq. (3.6)) is replaced in the new MILP model by Eqs. (3.18) to (3.23).

The next section shows the result of the application of the proposed procedure for the entire optimization problem.

3.3 MILP formulation

3.3.1 Constraints

The problem constraints are composed of the selection of geometric variables, stream allocation equations, structural constraints, thermal and hydraulic modelling, and pressure drop and velocity bounds.

3.3.1.1 Selection of the geometric variables

According to the discrete nature of the original geometric variables, the selection of their corresponding values for the description of each solution candidate employs the following set of binaries: y_{sd} for the inner tube diameter (discrete values of the outer and inner values: \widehat{pdte}_{sd} and \widehat{pdti}_{sd}), y_{sD} for the outer tube diameter (discrete values of the outer and inner values: \widehat{pDte}_{sd} and \widehat{pDti}_{sd}), y_{sL} for the tube length (discrete values: \widehat{pL}_{sL}), y_{sB} for the number of parallel branches present in the heat exchanger design (discrete values: \widehat{pNB}_{sB}), $y_{Pt_{sE}}$ and $y_{Pa_{sE}}$ for the number of parallel units per branch in the tube-side and annulus-side, respectively (discrete values: \widehat{pNE}_{sE}), and $y_{St_{sE}}$ and $y_{Sa_{sE}}$ for the number of units in series per branch for the tube-side and annulus-side, respectively (discrete values: \widehat{pNE}_{sE}).

This set of binary variables must be associated to constraints to ensure that only one of the available options will be selected:

$$\sum_{sd=1}^{sdmax} y_{sd} = 1 \quad (3.24)$$

$$\sum_{sD=1}^{sDmax} y_{sD} = 1 \quad (3.25)$$

$$\sum_{sL=1}^{sLmax} yL_{sL} = 1 \quad (3.26)$$

$$\sum_{sB=1}^{sBmax} yB_{sB} = 1 \quad (3.27)$$

$$\sum_{sE=1}^{sEmax} yPt_{sE} = 1 \quad (3.28)$$

$$\sum_{sE=1}^{sEmax} yPa_{sE} = 1 \quad (3.29)$$

$$\sum_{sE=1}^{sEmax} ySt_{sE} = 1 \quad (3.30)$$

$$\sum_{sE=1}^{sEmax} ySa_{sE} = 1 \quad (3.31)$$

3.3.1.2 Stream allocations

The stream allocation is controlled by the binary variables yTc and yTh . If $yTc = 1$, then the cold stream flows inside the inner tube and the hot stream flows in the annulus; if $yTh = 1$, then the hot stream flows inside the inner tube and the cold stream flows in the annulus, which is guaranteed by the following constraint:

$$yT_c + yT_h = 1 \quad (3.32)$$

3.3.1.3 Structural constraints

The following constraint ensures that if one flow-side has already more than one parallel unit per branch then the only possibility for the other side is to be aligned in series. It

also guarantees that for the same side if there are multiple parallel passages there can only be one unit in series, respecting the structural options presented in Figure 8:

$$yPt_{sE=1} + yPa_{sE=1} \geq 1 \quad (3.33)$$

$$yPt_{sE=1} + ySt_{sE=1} \geq 1 \quad (3.34)$$

$$yPa_{sE=1} + ySa_{sE=1} \geq 1 \quad (3.35)$$

The last structural constraint guarantees that alternatives without physical meaning related to the arrangement of the flow distribution among the set of units of the tube-side and annulus-side streams are discarded:

$$\sum_{sE=1}^{sEmax} \sum_{sE'=1}^{sEmax'} \widehat{pNE}_{sE} \widehat{pNE}_{sE'} wyPtSt_{sE,sE'} = \sum_{sE=1}^{sEmax} \sum_{sE'=1}^{sEmax'} \widehat{pNE}_{sE} \widehat{pNE}_{sE'} wyPaSa_{sE,sE'} \quad (3.36)$$

$$wyPtSt_{sE,sE'} \leq yPt_{sE} \quad (3.37)$$

$$wyPtSt_{sE,sE'} \leq ySt_{sE'} \quad (3.38)$$

$$wyPtSt_{sE,sE'} \geq yPt_{sE} + ySt_{sE'} - 1 \quad (3.39)$$

$$wyPaSa_{sE,sE'} \leq yPa_{sE} \quad (3.40)$$

$$wyPaSa_{sE,sE'} \leq ySa_{sE'} \quad (3.41)$$

$$wyPaSa_{sE,sE'} \geq yPa_{sE} + ySa_{sE'} - 1 \quad (3.42)$$

3.3.1.4 Thermal and hydraulic modeling – Tube-side flow

The flow velocity inside the inner tube, its corresponding Reynolds number and additional linear inequalities are:

$$vt = \sum_{sd=1}^{sdmax} \sum_{sB=1}^{sBmax} \sum_{sE=1}^{sEmax} \sum_{sST} \frac{4 \widehat{m}_{sST}}{\pi \widehat{\rho}_{sST} \widehat{pdt}_{sd}^2 \widehat{pNB}_{sB} \widehat{pNE}_{sE}} wvt_{sd,sB,sE,sST} \quad (3.43)$$

$$Ret = \sum_{sd=1}^{sdmax} \sum_{sB=1}^{sBmax} \sum_{sE=1}^{sEmax} \sum_{sST} \frac{4 \hat{m}_{sST}}{\pi \hat{\mu}_{sST} \widehat{pdti}_{sd} \widehat{pNB}_{sB} \widehat{pNE}_{sE}} wvt_{sd,sB,sE,sST} \quad (3.44)$$

$$wvt_{sd,sB,sE,sST} \leq yd_{sd} \quad (3.45)$$

$$wvt_{sd,sB,sE,sST} \leq yB_{sB} \quad (3.46)$$

$$wvt_{sd,sB,sE,sST} \leq yPt_{sE} \quad (3.47)$$

$$wvt_{sd,sB,sE,sST} \leq yT_{sST} \quad (3.48)$$

$$wvt_{sd,sB,sE,sST} \geq yd_{sd} + yB_{sB} + yPt_{sE} + yT_{sST} - 3 \quad (3.49)$$

The Prandtl number of the inner tube stream becomes:

$$Prt = \frac{\widehat{Cp}_c \hat{\mu}_c}{\widehat{k}_c} yT_c + \frac{\widehat{Cp}_h \hat{\mu}_h}{\widehat{k}_h} yT_h \quad (3.50)$$

The evaluation of the Nusselt number by the Seider & Tate correlation and its additional linear inequalities are:

$$Nut^{S\&T} = \sum_{sB=1}^{sBmax} \sum_{sE=1}^{sEmax} \sum_{sL=1}^{sLmax} \sum_{sST} \widehat{pNut}_{sB,sE,sL,sST}^{S\&T} wNut_{sB,sE,sL,sST} \quad (3.51)$$

$$wNut_{sB,sE,sL,sST} \leq yB_{sB} \quad (3.52)$$

$$wNut_{sB,sE,sL,sST} \leq yPt_{sE} \quad (3.53)$$

$$wNut_{sB,sE,sL,sST} \leq yL_{sL} \quad (3.54)$$

$$wNut_{sB,sE,sL,sST} \leq yT_{sST} \quad (3.55)$$

$$wNut_{sB,sE,sL,sST} \geq yB_{sB} + yPt_{sE} + yL_{sL} + yT_{sST} - 3 \quad (3.56)$$

where the parameter $\widehat{pNut}_{sB,sE,sL,sST}^{S\&T}$, is given by:

$$\widehat{pNut}_{sB,sE,sL,sST}^{S\&T} = 1.86 \left(\frac{4 \widehat{Cp}_{sST} \widehat{m}_{sST}}{\pi \widehat{k}_{sST} \widehat{pNB}_{sB} \widehat{pNE}_{sE} \widehat{pL}_{sL}} \right)^{1/3} \quad (3.57)$$

The scheme to describe the activation of different flow regime calculations was explained in Chapter 1.42 and will not be repeated here. The constraints that relates the binary variables to its corresponding ranges remain the same:

$$Ret \leq 1311 yRet_1 + 2300 yRet_2 + 3380 yRet_3 + \widehat{URe} yRet_4 \quad (3.58)$$

$$Ret \geq 1311 yRet_2 + 2300 yRet_3 + 3380 yRet_4 + \varepsilon \quad (3.59)$$

$$Prt \leq 5 yPrt_1 + \widehat{UPr} yPrt_2 \quad (3.60)$$

$$Prt \geq 5 yPrt_2 + \varepsilon \quad (3.61)$$

$$Nut^{S\&T} \leq 3,66 yNut_1 + \widehat{UNu} yNut_2 - \varepsilon \quad (3.62)$$

$$Nut^{S\&T} \geq 3,66 yNut_2 \quad (3.63)$$

$$\sum_{sRet=1}^{sRetmax} yRet_{sRet} = 1 \quad (3.64)$$

$$yPrt_1 + yPrt_2 = 1 \quad (3.65)$$

$$yNut_1 + yNut_2 = 1 \quad (3.66)$$

The pressure drop evaluation of the flow in the inner tube is based on the Darcy-Weisbach equation (omitting the viscosity correction factor) (Saunders, 1988), which after the reformulation proposed becomes:

$$\begin{aligned} \Delta Pt = & \sum_{sd=1}^{sdmax} \sum_{sB=1}^{sBmax} \sum_{sE=1}^{sEmax} \sum_{sL=1}^{sLmax} \sum_{sE'=1}^{sEmax} \sum_{sST} [\widehat{pdPt1}_{sd,sB,sE,sL,sE',sST} \widehat{wdPt}_{sd,sB,sE,sL,sE',sST,1} \\ & + \widehat{pdPt23}_{sd,sB,sE,sL,sE',sST} (\widehat{wdPt}_{sd,sB,sE,sL,sE',sST,2} + \widehat{wdPt}_{sd,sB,sE,sL,sE',sST,3}) \\ & + \widehat{pdPt4}_{sd,sB,sE,sL,sE',sST} \widehat{wdPt}_{sd,sB,sE,sL,sE',sST,4}] \end{aligned} \quad (3.67)$$

$$\widehat{wdPt}_{sd,sB,sE,sL,sE',sST,sRet} \leq wvt_{sd,sB,sE,sST} \quad (3.68)$$

$$wdPt_{sd,sB,sE,sL,sE',sST,sRet} \leq yL_{sL} \quad (3.69)$$

$$wdPt_{sd,sB,sE,sL,sE',sST,sRet} \leq ySt_{sE'} \quad (3.70)$$

$$wdPt_{sd,sB,sE,sL,sE',sST,sRet} \leq yRet_{sRet} \quad (3.71)$$

$$wdPt_{sd,sB,sE,sL,sE',sST,sRet} \geq wvt_{sd,sB,sE,sST} + yL_{sL} + ySt_{sE'} + yRet_{sRet} - 3 \quad (3.72)$$

The additional parameters inserted for simplification purposes in Eq. (3.67) are given by:

$$\widehat{pdPt1}_{sd,sB,sE,sL,sE',sST} = \frac{128 \widehat{m}_{sST} \widehat{\mu}_{sST} \widehat{pL}_{sL} \widehat{pNE}_{sE'}}{\pi \widehat{\rho}_{sST} \widehat{pdti}_{sd}^4 \widehat{pNB}_{sB} \widehat{pNE}_{sE}} \quad (3.73)$$

$$\widehat{pdPt23}_{sd,sB,sE,sL,sE',sST} = \frac{0.3904 \widehat{m}_{sST}^2 \widehat{pL}_{sL} \widehat{pNE}_{sE'}}{\pi^2 \widehat{\rho}_{sST} \widehat{pdti}_{sd}^5 \widehat{pNB}_{sB}^2 \widehat{pNE}_{sE}^2} \quad (3.74)$$

$$\begin{aligned} \widehat{pdPt4}_{sd,sB,sE,sL,sE',sST} \\ = \frac{0.112 \widehat{m}_{sST}^2 \widehat{pL}_{sL} \widehat{pNE}_{sE'}}{\pi^2 \widehat{\rho}_{sST} \widehat{pdti}_{sd}^5 \widehat{pNB}_{sB}^2 \widehat{pNE}_{sE}^2} + \frac{8.448 \widehat{m}_{sST}^{1.58} \widehat{\mu}_{sST}^{0.42} \widehat{pL}_{sL} \widehat{pNE}_{sE'}}{4^{0.42} \pi^{1.58} \widehat{\rho}_{sST} \widehat{pdti}_{sd}^{4.58} \widehat{pNB}_{sB}^{1.58} \widehat{pNE}_{sE}^{1.58}} \end{aligned} \quad (3.75)$$

3.3.1.5 Thermal and hydraulic modeling – Annulus-side flow

The annulus-side stream velocity, its corresponding Reynolds number and additional linear inequalities are given by:

$$va = \sum_{sd=1}^{sdmax} \sum_{sD=1}^{sDmax} \sum_{sB=1}^{sBmax} \sum_{sE=1}^{sEmax} \sum_{sST} \frac{\widehat{m}_{sST}^*}{\widehat{\rho}_{sST}^* \widehat{pAa}_{sd,sD} \widehat{pNB}_{sB} \widehat{pNE}_{sE}} wva_{sd,sD,sB,sE,sST} \quad (3.76)$$

$$Rea = \sum_{sd=1}^{sdmax} \sum_{sD=1}^{sDmax} \sum_{sB=1}^{sBmax} \sum_{sE=1}^{sEmax} \sum_{sST} \frac{\widehat{m}_{sST}^* \widehat{pdh}_{sd,sD}}{\widehat{\mu}_{sST}^* \widehat{pAa}_{sd,sD} \widehat{pNB}_{sB} \widehat{pNE}_{sE}} wva_{sd,sD,sB,sE,sST} \quad (3.77)$$

$$wva_{sd,sD,sB,sE,sST} \leq yd_{sd} \quad (3.78)$$

$$wva_{sd,sD,sB,sE,sST} \leq yD_{sD} \quad (3.79)$$

$$wva_{sd,sD,sB,sE,sST} \leq yB_{sB} \quad (3.80)$$

$$wva_{sd,sD,sB,sE,sST} \leq yPa_{sE} \quad (3.81)$$

$$wva_{sd,sD,sB,sE,sST} \leq yT_{sST}$$

$$wva_{sd,sD,sB,sE,sST} \geq yd_{sd} + yD_{sD} + yB_{sB} + yPa_{sE} + yT_{sST} - 4 \quad (3.82)$$

where if $sST = h$, then $sST^* = c$ and vice-versa.

The Prandtl number of the annulus-side stream becomes:

$$Pra = \frac{\widehat{Cp}_c \widehat{\mu}_c}{\widehat{k}_c} yT_h + \frac{\widehat{Cp}_h \widehat{\mu}_h}{\widehat{k}_h} yT_c \quad (3.83)$$

The Nusselt number given by Seider & Tate correlation and its additional linear inequalities are:

$$Nua^{S\&T} = \sum_{sd=1}^{sdmax} \sum_{sD=1}^{sDmax} \sum_{sB=1}^{sBmax} \sum_{sE=1}^{sEmax} \sum_{sL=1}^{sLmax} \sum_{sST} p\widehat{Nua}_{sd,sD,sB,sE,sL,sST}^{S\&T} wNua_{sd,sD,sB,sE,sL,sST} \quad (3.84)$$

$$wNua_{sd,sD,sB,sE,sL,sST} \leq wva_{sd,sD,sB,sE,sST} \quad (3.85)$$

$$wNua_{sd,sD,sB,sE,sL,sST} \leq yL_{sL} \quad (3.86)$$

$$wNua_{sd,sD,sB,sE,sL,sST} \geq wva_{sd,sD,sB,sE,sST} + yL_{sL} - 1 \quad (3.87)$$

where the parameter $p\widehat{Nut}_{sB,sE,sL,sST}^{S\&T}$ is given by:

$$p\widehat{Nua}_{sd,sD,sB,sE,sL,sST}^{S\&T} = 1.86 \left(\frac{\widehat{Cp}_{sST^*} \widehat{m}_{sST^*} \widehat{pd}h_{sd,sD}^2}{\widehat{k}_{sST^*} p\widehat{Aa}_{sd,sD} p\widehat{NB}_{sB} p\widehat{NE}_{sE} p\widehat{L}_{sL}} \right)^{\frac{1}{3}} \quad (3.88)$$

where if $sST = h$, then $sST^* = c$ and vice-versa.

The constraints that relate the binary variables to its corresponding ranges, as for the tube-side, remain the same:

$$Rea \leq 500 yRea_1 + 2300 yRea_2 + 10000 yRea_3 + \widehat{URe} yRea_4 \quad (3.89)$$

$$Rea \geq 500yRea_2 + 2300yRea_3 + 10000 yRea_4 + \varepsilon \quad (3.90)$$

$$Pra \leq 5yPra_1 + \widehat{UPr} yPra_2 \quad (3.91)$$

$$Pra \geq 5yPra_2 + \varepsilon \quad (3.92)$$

$$Nua^{S\&T} \leq 3.66yNua_1 + \widehat{UNu} yNua_2 - \varepsilon \quad (3.93)$$

$$Nua^{S\&T} \geq 3.66yNua_2 \quad (3.94)$$

$$\sum_{sRea=1}^{sReamax} yRea_{sRea} = 1 \quad (3.95)$$

$$yPra_1 + yPra_2 = 1 \quad (3.96)$$

$$yNua_1 + yNua_2 = 1 \quad (3.97)$$

The pressure drop of the flow in the annulus is given by the Darcy-Weisbach equation using the hydraulic diameter (also omitting the viscosity correction factor) (Saunders, 1988), which after the reformulation proposed becomes:

$$\begin{aligned} \Delta Pa &= \sum_{sd=1}^{sdmax} \sum_{sD=1}^{sDmax} \sum_{sB=1}^{sBmax} \sum_{sE=1}^{sEmax} \sum_{sL=1}^{sLmax} \sum_{sE'=1}^{sEmax} \sum_{sST} [\widehat{pdPa}1_{sd,sD,sB,sE,sL,sE',sST} wdPa_{sd,sD,sB,sE,sL,sE',sST,1} \\ &+ \widehat{pdPa}23_{sd,sD,sB,sE,sL,sE',sST} (wdPa_{sd,sD,sB,sE,sL,sE',sST,2} + wdPa_{sd,sD,sB,sE,sL,sE',sST,3}) \\ &+ \widehat{pdPa}4_{sd,sD,sB,sE,sL,sE',sST} wdPa_{sd,sD,sB,sE,sL,sE',sST,4}] \end{aligned} \quad (3.98)$$

$$wdPa_{sd,sD,sB,sE,sL,sE',sST,sRea} \leq wNua_{sd,sD,sB,sE,sL,sST} \quad (3.99)$$

$$wdPa_{sd,sD,sB,sE,sL,sE',sST,sRea} \leq ySa_{sE'} \quad (3.100)$$

$$wdPa_{sd,sD,sB,sE,sL,sE',sST,sRea} \leq yRea_{sRea} \quad (3.101)$$

$$wdPa_{sd,sD,sB,sE,sL,sE',sST,sRea} \geq wNua_{sd,sD,sB,sE,sL,sST} + ySa_{sE'} + yRea_{sRea} - 2 \quad (3.102)$$

The additional parameters inserted for simplification purposes in Eq. (3.98) are given by:

$$\widehat{pdPa1}_{sd,sD,sB,sE,sL,sE',sST} = \frac{32 \hat{\mu}_{sST} \hat{m}_{sST} \widehat{pL}_{sL} \widehat{pNE}_{sE'}}{\hat{\rho}_{sST} \widehat{pdh}_{sd,sD}^2 \widehat{pAa}_{sd,sD} \widehat{pNB}_{sB} \widehat{pNE}_{sE}} \quad (3.103)$$

$$\begin{aligned} \widehat{pdPa23}_{sd,sD,sB,sE,sL,sE',sST} &= \frac{0.01348 \hat{m}_{sST}^2 \widehat{pL}_{sL} \widehat{pNE}_{sE'}}{\hat{\rho}_{sST} \widehat{pdh}_{sd,sD} \widehat{pAa}_{sd,sD}^2 \widehat{pNB}_{sB}^2 \widehat{pNE}_{sE}^2} \\ &+ \frac{16.328 \hat{\mu}_{sST}^{0.93} \hat{m}_{sST}^{1.07} \widehat{pL}_{sL} \widehat{pNE}_{sE'}}{\hat{\rho}_{sST} \widehat{pdh}_{sd,sD}^{1.93} \widehat{pAa}_{sd,sD}^{1.07} \widehat{pNB}_{sB}^{1.07} \widehat{pNE}_{sE}^{1.07}} \end{aligned} \quad (3.104)$$

$$\widehat{pdPa4}_{sd,sD,sB,sE,sL,sE',sST} = \frac{0.089 \hat{\mu}_{sST}^{0.1865} \hat{m}_{sST}^{1.8135} \widehat{pL}_{sL} \widehat{pNE}_{sE'}}{\hat{\rho}_{sST} \widehat{pdh}_{sd,sD}^{1.1865} \widehat{pAa}_{sd,sD}^{1.8135} \widehat{pNB}_{sB}^{1.8135} \widehat{pNE}_{sE}^{1.8135}} \quad (3.105)$$

where if $sST = h$, then $sST^* = c$ and vice-versa.

3.3.1.6 Heat transfer rate equation

The heat exchanger area evaluation and its additional inequalities are given by:

$$A = \sum_{sd=1}^{sdmax} \sum_{sL=1}^{sLmax} \sum_{sB=1}^{sBmax} \sum_{sE=1}^{sEmax} \sum_{sE'=1}^{sEmax} \widehat{pA}_{sd,sB,sE,sL,sE'} wA_{sd,sB,sE,sL,sE'} \quad (3.106)$$

$$wA_{sd,sB,sE,sL,sE'} \leq wyPtSt_{sE,sE'} \quad (3.107)$$

$$wA_{sd,sB,sE,sL,sE'} \leq yd_{sd} \quad (3.108)$$

$$wA_{sd,sB,sE,sL,sE'} \leq yB_{sB} \quad (3.109)$$

$$wA_{sd,sB,sE,sL,sE'} \leq yL_{sL} \quad (3.110)$$

$$wA_{sd,sB,sE,sL,sE'} \geq wyPtSt_{sE,sE'} + yd_{sd} + yB_{sB} + yL_{sL} - 3 \quad (3.111)$$

where the parameter $\widehat{pA}_{sd,sL,sB,sE,sE'}$ is given by:

$$\widehat{pA}_{sd,sB,sE,sL,sE'} = \pi \widehat{pdte}_{sd} \widehat{pNB}_{sB} \widehat{pNE}_{sE} \widehat{pL}_{sL} \widehat{pNE}_{sE'} \quad (3.112)$$

The heat transfer rate, based on the LMTD method, after reformulation becomes:

$$\begin{aligned}
\hat{Q} & \sum_{sd=1}^{sdmax} \sum_{sD=1}^{sDmax} \sum_{sB=1}^{sBmax} \sum_{sE=1}^{sEmax} \sum_{sE'=1}^{sEmax} \sum_{sL=1}^{sLmax} \sum_{sST} \left[\sum_{sRet=1}^2 \left(\frac{\widehat{pdte}_{sd}}{3.66 \widehat{k}_{sST}} wht_{sd,sST,sRet,1,1}^{theo} \right. \right. \\
& + \frac{\widehat{pdte}_{sd}}{\widehat{k}_{sST} \widehat{pNua}_{sB,sE,sL,sST}^{S\&T}} wht_{sd,sB,sE,sL,sST,sRet,1,2}^{S\&T} \\
& + \left. \frac{\widehat{pdte}_{sd}}{\widehat{k}_{sST} \widehat{pNua}_{sB,sE,sL,sST}^{Hau}} wht_{sd,sB,sE,sL,sST,sRet,2}^{Hau} \right) + \frac{\widehat{pdte}_{sd}}{\widehat{k}_{sST} \widehat{pNua}_{tran, sd,sB,sE,sST}^{Gni}} wht_{sd,sB,sE,sST,3}^{Gni} \\
& + \frac{\widehat{pdte}_{sd}}{\widehat{k}_{sST} \widehat{pNua}_{turb, sd,sB,sE,sST}^{Gni}} wht_{sd,sB,sE,sST,4}^{Gni} + \widehat{Rf}_{sST} \frac{\widehat{pdte}_{sd}}{\widehat{pdti}_{sd}} wydT_{sd,sST} \\
& + \frac{\widehat{pdte}_{sd} \ln \left(\frac{\widehat{pdte}_{sd}}{\widehat{pdti}_{sd}} \right)}{2ktube} yd_{sd} + \widehat{Rf}_{sST} yT_{sST} \\
& + \sum_{sRea=1}^2 \left(\frac{\widehat{pdh}_{sd,sD}}{3.66 \widehat{k}_{sST}} w ha_{sd,sD,sST,sRea,1,1}^{theo} \right. \\
& + \frac{\widehat{pdh}_{sd,sD}}{\widehat{k}_{sST} \widehat{pNua}_{sd,sD,sB,sE',sL,sST}^{S\&T}} w ha_{sd,sD,sB,sE',sL,sST,sRea,1,2}^{S\&T} \\
& + \left. \frac{\widehat{pdh}_{sd,sD}}{\widehat{k}_{sST} \widehat{pNua}_{sd,sD,sB,sE',sL,sST}^{Hau}} w ha_{sd,sD,sB,sE',sL,sST,sRea,2}^{Hau} \right) \\
& + \frac{\widehat{pdh}_{sd,sD}}{\widehat{k}_{sST} \widehat{pNua}_{tran, sd,sD,sB,sE',sST}^{Gni}} w ha_{sd,sD,sB,sE',sST,3}^{Gni} \\
& + \left. \frac{\widehat{pdh}_{sd,sD}}{\widehat{k}_{sST} \widehat{pNua}_{turb, sd,sD,sB,sE',sST}^{Gni}} w ha_{sd,sD,sB,sE',sST,4}^{Gni} \right] \\
& \leq \frac{\Delta Tlm}{\left(\frac{Aexc}{100} + 1 \right)} \sum_{sd=1}^{sdmax} \sum_{sB=1}^{sBmax} \sum_{sE=1}^{sEmax} \sum_{sE'=1}^{sEmax} \sum_{sL=1}^{sLmax} \sum_{sE''=1}^{sEmax} \sum_{sST} \left(\widehat{pA}_{sd,sB,sE,sL,sE''} w A_{sd,sB,sE,sL,sE''} \right. \\
& + \widehat{pA}_{sd,sB,sE,sL,sE''} \left(\widehat{pF}_{sST,sE} - 1 \right) w AF1_{sd,sB,sE,sL,sE'',sST} \\
& + \left. \widehat{pA}_{sd,sB,sE,sL,sE''} \left(\widehat{pF}_{sST,sE'} - 1 \right) w AF2_{sd,sB,sE,sE',sL,sE'',sST} \right)
\end{aligned} \tag{3.113}$$

$$wydT_{sd,sST} \leq yd_{sd} \quad (3.114)$$

$$wydT_{sd,sST} \leq yT_{sST} \quad (3.115)$$

$$wydT_{sd,sST} \geq yd_{sd} + yT_{sST} - 1 \quad (3.116)$$

$$wht_{sd,sST,sRet,1,1}^{theo} \leq wydT_{sd,sST} \quad \text{for } sRet = \{1,2\} \quad (3.117)$$

$$wht_{sd,sST,sRet,1,1}^{theo} \leq yRet_{sRet} \quad \text{for } sRet = \{1,2\} \quad (3.118)$$

$$wht_{sd,sST,sRet,1,1}^{theo} \leq yPrt_1 \quad \text{for } sRet = \{1,2\} \quad (3.119)$$

$$wht_{sd,sST,sRet,1,1}^{theo} \leq yNut_1 \quad \text{for } sRet = \{1,2\} \quad (3.120)$$

$$wht_{sd,sST,sRet,1,1}^{theo} \geq wydT_{sd,sST} + yRet_{sRet} + yPrt_1 + yNut_1 - 3 \quad \text{for } sRet = \{1,2\} \quad (3.121)$$

$$wht_{sd,sB,sE,sL,sST,sRet,1,2}^{S\&T} \leq wydT_{sd,sST} \quad \text{for } sRet = \{1,2\} \quad (3.122)$$

$$wht_{sd,sB,sE,sL,sST,sRet,1,2}^{S\&T} \leq yB_{sB} \quad \text{for } sRet = \{1,2\} \quad (3.123)$$

$$wht_{sd,sB,sE,sL,sST,sRet,1,2}^{S\&T} \leq yPt_{sE} \quad \text{for } sRet = \{1,2\} \quad (3.124)$$

$$wht_{sd,sB,sE,sL,sST,sRet,1,2}^{S\&T} \leq yL_{sL} \quad \text{for } sRet = \{1,2\} \quad (3.125)$$

$$wht_{sd,sB,sE,sL,sST,sRet,1,2}^{S\&T} \leq yRet_{sRet} \quad \text{for } sRet = \{1,2\} \quad (3.126)$$

$$wht_{sd,sB,sE,sL,sST,sRet,1,2}^{S\&T} \leq yPrt_1 \quad \text{for } sRet = \{1,2\} \quad (3.127)$$

$$wht_{sd,sB,sE,sL,sST,sRet,1,2}^{S\&T} \leq yNut_2 \quad \text{for } sRet = \{1,2\} \quad (3.128)$$

$$wht_{sd,sB,sE,sL,sST,sRet,1,2}^{S\&T} \geq wydT_{sd,sST} + yB_{sB} + yPt_{sE} + yL_{sL} + yRet_{sRet} + yPrt_1 + yNut_2 \quad (3.129)$$

$$- 6 \quad \text{for } sRet = \{1,2\}$$

$$wht_{sd,sB,sE,sL,sST,sRet,2}^{Hau} \leq wydT_{sd,sST} \quad \text{for } sRet = \{1,2\} \quad (3.130)$$

$$wht_{sd,sB,sE,sL,sST,sRet,2}^{Hau} \leq yB_{sB} \quad \text{for } sRet = \{1,2\} \quad (3.131)$$

$$wht_{sd,sB,sE,sL,sST,sRet,2}^{Hau} \leq yPt_{sE} \quad \text{for } sRet = \{1,2\} \quad (3.132)$$

$$wht_{sd,sB,sE,sL,sST,sRet,2}^{Hau} \leq yL_{sL} \quad \text{for } sRet = \{1,2\} \quad (3.133)$$

$$wht_{sd,sB,sE,sL,sST,sRet,2}^{Hau} \leq yRet_{sRet} \quad \text{for } sRet = \{1,2\} \quad (3.134)$$

$$wht_{sd,sB,sE,sL,sST,sRet,2}^{Hau} \leq yPrt_2 \quad \text{for } sRet = \{1,2\} \quad (3.135)$$

$$wht_{sd,sB,sE,sL,sST,sRet,2}^{Hau} \quad (3.136)$$

$$\begin{aligned} &\geq wydT_{sd,sST} + yB_{sB} + yPt_{sE} + yL_{sL} + yRet_{sRet} + yPrt_2 \\ &- 5 \quad \text{for } sRet = \{1,2\} \end{aligned}$$

$$wht_{sd,sB,sE,sST,sRet}^{Gni} \leq wydT_{sd,sST} \quad \text{for } sRet = \{3,4\} \quad (3.137)$$

$$wht_{sd,sB,sE,sST,sRet}^{Gni} \leq yB_{sB} \quad \text{for } sRet = \{3,4\} \quad (3.138)$$

$$wht_{sd,sB,sE,sST,sRet}^{Gni} \leq yPt_{sE} \quad \text{for } sRet = \{3,4\} \quad (3.139)$$

$$wht_{sd,sB,sE,sST,sRet}^{Gni} \leq yRet_{sRet} \quad \text{for } sRet = \{3,4\} \quad (3.140)$$

$$wht_{sd,sB,sE,sST,sRet}^{Gni} \geq wydT_{sd,sST} + yB_{sB} + yPt_{sE} + yRet_{sRet} - 3 \quad \text{for } sRet = \{3,4\} \quad (3.141)$$

$$wha_{sd,sD,sST,sRea,1,1}^{theo} \leq wydT_{sd,sST} \quad \text{for } sRea = \{1,2\} \quad (3.142)$$

$$wha_{sd,sD,sST,sRea,1,1}^{theo} \leq yD_{sD} \quad \text{for } sRea = \{1,2\} \quad (3.143)$$

$$wha_{sd,sD,sST,sRea,1,1}^{theo} \leq yRea_{sRea} \quad \text{for } sRea = \{1,2\} \quad (3.144)$$

$$wha_{sd,sD,sST,sRea,1,1}^{theo} \leq yPra_1 \quad \text{for } sRea = \{1,2\} \quad (3.145)$$

$$wha_{sd,sD,sST,sRea,1,1}^{theo} \leq yNua_1 \quad \text{for } sRea = \{1,2\} \quad (3.146)$$

$$wha_{sd,sD,sST,sRea,1,1}^{theo} \quad (3.147)$$

$$\begin{aligned} &\geq wydT_{sd,sST} + yD_{sD} + yRea_{sRea} + yPra_1 + yNua_1 \\ &- 4 \quad \text{for } sRea = \{1,2\} \end{aligned}$$

$$wha_{sd,sD,sB,sE',sL,sST,sRea,1,2}^{S\&T} \leq wydT_{sd,sST} \quad \text{for } sRea = \{1,2\} \quad (3.148)$$

$$wha_{sd,sD,sB,sE',sL,sST,sRea,1,2}^{S\&T} \leq yD_{sD} \quad \text{for } sRea = \{1,2\} \quad (3.149)$$

$$wha_{sd,sD,sB,sE',sL,sST,sRea,1,2}^{S\&T} \leq yB_{sB} \quad \text{for } sRea = \{1,2\} \quad (3.150)$$

$$wha_{sd,sD,sB,sE',sL,sST,sRea,1,2}^{S\&T} \leq yPa_{sE'} \quad \text{for } sRea = \{1,2\} \quad (3.151)$$

$$wha_{sd,sD,sB,sE',sL,sST,sRea,1,2}^{S\&T} \leq yL_{sL} \quad \text{for } sRea = \{1,2\} \quad (3.152)$$

$$wha_{sd,sD,sB,sE',sL,sST,sRea,1,2}^{S\&T} \leq yRea_{sRea} \quad \text{for } sRea = \{1,2\} \quad (3.153)$$

$$wha_{sd,sD,sB,sE',sL,sST,sRea,1,2}^{S\&T} \leq yPra_1 \quad \text{for } sRea = \{1,2\} \quad (3.154)$$

$$wha_{sd,sD,sB,sE',sL,sST,sRea,1,2}^{S\&T} \leq yNua_2 \quad \text{for } sRea = \{1,2\} \quad (3.155)$$

$$\begin{aligned} wha_{sd,sD,sB,sE',sL,sST,sRea,1,2}^{S\&T} &\geq wydT_{sd,sST} + yD_{sD} + yB_{sB} + yPa_{sE'} + yL_{sL} + yRea_{sRea} + yPra_1 \\ &+ yNua_2 \\ &- 7 \quad \text{for } sRea \\ &= \{1,2\} \end{aligned} \quad (3.156)$$

$$wha_{sd,sD,sB,sE',sL,sST,sRea,2}^{Hau} \leq wydT_{sd,sST} \quad \text{for } sRea = \{1,2\} \quad (3.157)$$

$$wha_{sd,sD,sB,sE',sL,sST,sRea,2}^{Hau} \leq yD_{sD} \quad \text{for } sRea = \{1,2\} \quad (3.158)$$

$$wha_{sd,sD,sB,sE',sL,sST,sRea,2}^{Hau} \leq yB_{sB} \quad \text{for } sRea = \{1,2\} \quad (3.159)$$

$$wha_{sd,sD,sB,sE',sL,sST,sRea,2}^{Hau} \leq yPa_{sE'} \quad \text{for } sRea = \{1,2\} \quad (3.160)$$

$$wha_{sd,sD,sB,sE',sL,sST,sRea,2}^{Hau} \leq yL_{sL} \quad \text{for } sRea = \{1,2\} \quad (3.161)$$

$$wha_{sd,sD,sB,sE',sL,sST,sRea,2}^{Hau} \leq yRea_{sRea} \quad \text{for } sRea = \{1,2\} \quad (3.162)$$

$$wha_{sd,sD,sB,sE',sL,sST,sRea,2}^{Hau} \leq yPra_2 \quad \text{for } sRea = \{1,2\} \quad (3.163)$$

$$\begin{aligned} wha_{sd,sD,sB,sE',sL,sST,sRea,2}^{Hau} &\geq wydT_{sd,sST} + yD_{sD} + yB_{sB} + yPa_{sE'} + yL_{sL} + yRea_{sRea} + yPra_2 \\ &- 6 \quad \text{for } sRea \\ &= \{1,2\} \end{aligned} \quad (3.164)$$

$$wha_{sd,sD,sB,sE',sST,sRea}^{Gni} \leq wydT_{sd,sST} \quad \text{for } sRea = \{3,4\} \quad (3.165)$$

$$wha_{sd,sD,sB,sE',sST,sRea}^{Gni} \leq yD_{sD} \quad \text{for } sRea = \{3,4\} \quad (3.166)$$

$$wha_{sd,sD,sB,sE',sST,sRea}^{Gni} \leq yB_{sB} \quad \text{for } sRea = \{3,4\} \quad (3.167)$$

$$wha_{sd,sD,sB,sE',sST,sRea}^{Gni} \leq yPa_{sE'} \quad \text{for } sRea = \{3,4\} \quad (3.168)$$

$$wha_{sd,sD,sB,sE',sST,sRea}^{Gni} \leq yRea_{sRea} \quad \text{for } sRea = \{3,4\} \quad (3.169)$$

$$\begin{aligned}
w\hat{h}a_{sd,sD,sB,sE',sST,sRea}^{Gni} &\geq wydT_{sd,sST} + yD_{sD} + yB_{sB} + yPa_{sE'} + yRea_{sRea} \\
- 4 &\quad \text{for } sRea = \{3,4\}
\end{aligned} \tag{3.170}$$

$$wAF1_{sd,sB,sE',sL,sE'',sST} \leq wA_{sd,sB,sE',sL,sE''} \tag{3.171}$$

$$wAF1_{sd,sB,sE',sL,sE'',sST} \leq yT_{sST} \tag{3.172}$$

$$wAF1_{sd,sB,sE',sL,sE'',sST} \geq wA_{sd,sB,sE',sL,sE''} + yT_{sST} - 1 \tag{3.173}$$

$$wAF2_{sd,sB,sE',sL,sE'',sST} \leq wAF1_{sd,sB,sE',sL,sE'',sST} \tag{3.174}$$

$$wAF2_{sd,sB,sE',sL,sE'',sST} \leq yPa_{sE'} \tag{3.175}$$

$$wAF2_{sd,sB,sE',sL,sE'',sST} \geq wAF1_{sd,sB,sE',sL,sE'',sST} + yPa_{sE'} - 1 \tag{3.176}$$

The logarithmic mean temperature is defined as:

$$\Delta\widehat{Tlm} = \frac{(\widehat{T}i_h - \widehat{T}o_c) - (\widehat{T}o_h - \widehat{T}i_c)}{\ln\left(\frac{(\widehat{T}i_h - \widehat{T}o_c)}{(\widehat{T}o_h - \widehat{T}i_c)}\right)} \tag{3.177}$$

The parameters related to the correction factor of the LMTD are given by (Serth, 2007):

$$\begin{aligned}
\widehat{p}\widehat{F}_{sST,sE} &= \frac{(\widehat{p}\widehat{R}_{sST} - \widehat{p}\widehat{N}\widehat{E}_{sE})}{\widehat{p}\widehat{N}\widehat{E}_{sE}(\widehat{p}\widehat{R}_{sST} - 1)} \frac{\ln\left(\frac{1 - \widehat{p}\widehat{P}_{sST}}{1 - \widehat{p}\widehat{P}_{sST}\widehat{p}\widehat{R}_{sST}}\right)}{\ln\left(\frac{\widehat{p}\widehat{R}_{sST} - \widehat{p}\widehat{N}\widehat{E}_{sE}}{\widehat{p}\widehat{R}_{sST}(1 - \widehat{p}\widehat{P}_{sST}\widehat{p}\widehat{R}_{sST})^{1/\widehat{p}\widehat{N}\widehat{E}_{sE}} + \frac{\widehat{p}\widehat{N}\widehat{E}_{sE}}{\widehat{p}\widehat{R}_{sST}}}\right)} \quad \text{for } sE \neq 1
\end{aligned} \tag{3.178}$$

(stream sST aligned in series and the other stream in parallel), where the factors $\widehat{p}\widehat{R}_{sST}$ and $\widehat{p}\widehat{P}_{sST}$ are specified as:

$$\widehat{p}\widehat{R}_c = \frac{(\widehat{T}o_c - \widehat{T}i_c)}{(\widehat{T}i_h - \widehat{T}o_h)} \tag{3.179}$$

$$\widehat{pR}_h = \frac{(\widehat{T}_{i_h} - \widehat{T}_{o_h})}{(\widehat{T}_{o_c} - \widehat{T}_{i_c})} \quad (3.180)$$

$$\widehat{pP}_c = \frac{(\widehat{T}_{i_h} - \widehat{T}_{o_h})}{(\widehat{T}_{i_h} - \widehat{T}_{i_c})} \quad (3.181)$$

$$\widehat{pP}_h = \frac{(\widehat{T}_{o_c} - \widehat{T}_{i_c})}{(\widehat{T}_{i_h} - \widehat{T}_{i_c})} \quad (3.182)$$

In addition, the other parameters inserted for simplification purposes in Eq. (3.113) are shown below:

$$\widehat{pNut}_{sB,sE,sL,sST}^{Hau} = 3.66 + \frac{0.0668 \left(\frac{4 \widehat{Cp}_{sST} \widehat{m}_{sST}}{\pi \widehat{k}_{sST} \widehat{pNB}_{sB} \widehat{pNE}_{sE} \widehat{pL}_{sL}} \right)}{1 + 0.04 \left(\frac{4 \widehat{Cp}_{sST} \widehat{m}_{sST}}{\pi \widehat{k}_{sST} \widehat{pNB}_{sB} \widehat{pNE}_{sE} \widehat{pL}_{sL}} \right)^{2/3}} \quad (3.183)$$

$$\widehat{pNut}_{tran_{sd,sB,sE,sST}}^{Gni} = \frac{0.0061 \left(\frac{4 \widehat{m}_{sST}}{\pi \widehat{\mu}_{sST} \widehat{pd}t_{sd} \widehat{pNB}_{sB} \widehat{pNE}_{sE}} - 1000 \right) \left(\frac{\widehat{Cp}_{sST} \widehat{\mu}_{sST}}{\widehat{k}_{sST}} \right)}{1 + 12.7(0.0061)^{1/2} \left(\left(\frac{\widehat{Cp}_{sST} \widehat{\mu}_{sST}}{\widehat{k}_{sST}} \right)^{2/3} - 1 \right)} \quad (3.184)$$

$$\widehat{pNut}_{tur_{sd,sB,sE,sST}}^{Gni} = \frac{\left(0.00175 + 0.132 \left(\frac{\pi \widehat{\mu}_{sST} \widehat{pd}t_{sd} \widehat{pNB}_{sB} \widehat{pNE}_{sE}}{4 \widehat{m}_{sST}} \right)^{0.42} \right) \left(\frac{4 \widehat{m}_{sST}}{\pi \widehat{\mu}_{sST} \widehat{pd}t_{sd} \widehat{pNB}_{sB} \widehat{pNE}_{sE}} - 1000 \right) \left(\frac{\widehat{Cp}_{sST} \widehat{\mu}_{sST}}{\widehat{k}_{sST}} \right)}{1 + 12.7 \left(0.00175 + 0.132 \left(\frac{\pi \widehat{\mu}_{sST} \widehat{pd}t_{sd} \widehat{pNB}_{sB} \widehat{pNE}_{sE}}{4 \widehat{m}_{sST}} \right)^{0.42} \right)^{1/2} \left(\left(\frac{\widehat{Cp}_{sST} \widehat{\mu}_{sST}}{\widehat{k}_{sST}} \right)^{2/3} - 1 \right)} \quad (3.185)$$

$$\widehat{pNua}_{sd,sD,sB,sE,sL,sST}^{Hau} = 3.66 + \frac{0.0668 \frac{\widehat{Cp}_{sST} \widehat{m}_{sST} \widehat{pd}h_{sd,sD}^2}{\widehat{k}_{sST} \widehat{pAa}_{sd,sD} \widehat{pNB}_{sB} \widehat{pNE}_{sE} \widehat{pL}_{sL}}}{1 + 0.04 \left(\frac{\widehat{Cp}_{sST} \widehat{m}_{sST} \widehat{pd}h_{sd,sD}^2}{\widehat{k}_{sST} \widehat{pAa}_{sd,sD} \widehat{pNB}_{sB} \widehat{pNE}_{sE} \widehat{pL}_{sL}} \right)^{2/3}} \quad (3.186)$$

$$\widehat{pNua}_{tran_{sd,sD,sB,sE,sST}}^{Gni} = \frac{\left(0.00337 + 4.082 \left(\frac{\widehat{\mu}_{sST} \widehat{pAa}_{sd,sD} \widehat{pNB}_{sB} \widehat{pNE}_{sE}}{\widehat{m}_{sST} \widehat{pd}h_{sd,sD}} \right)^{0.93} \right) \left(\frac{\widehat{m}_{sST} \widehat{pd}h_{sd,sD}}{\widehat{\mu}_{sST} \widehat{pAa}_{sd,sD} \widehat{pNB}_{sB} \widehat{pNE}_{sE}} - 1000 \right) \frac{\widehat{Cp}_{sST} \widehat{\mu}_{sST}}{\widehat{k}_{sST}}}{1 + 12.7 \left(0.00337 + 4.082 \left(\frac{\widehat{\mu}_{sST} \widehat{pAa}_{sd,sD} \widehat{pNB}_{sB} \widehat{pNE}_{sE}}{\widehat{m}_{sST} \widehat{pd}h_{sd,sD}} \right)^{0.93} \right)^{1/2} \left(\left(\frac{\widehat{Cp}_{sST} \widehat{\mu}_{sST}}{\widehat{k}_{sST}} \right)^{2/3} - 1 \right)} \quad (3.187)$$

$$\widehat{pNu}_{curb_{sd,sB,sE,sT}}^{Gni} = \frac{\left(0.02225 \left(\frac{\widehat{\dot{m}}_{sNT} \widehat{pA}_{sd,sD} \widehat{pNB}_{sB} \widehat{pNE}_{sE}}{\widehat{m}_{sNT} \widehat{pd}h_{sd,sD}}\right)^{0.1965}\right) \left(\frac{\widehat{m}_{sNT} \widehat{pd}h_{sd,sD}}{\widehat{\dot{m}}_{sNT} \widehat{pA}_{sd,sD} \widehat{pNB}_{sB} \widehat{pNE}_{sE}} - 1000\right) \frac{\widehat{Cp}_{sNT} \widehat{\dot{m}}_{sNT}}{\widehat{k}_{sNT}}}{1 + 12.7 \left(0.02225 \left(\frac{\widehat{\dot{m}}_{sNT} \widehat{pA}_{sd,sD} \widehat{pNB}_{sB} \widehat{pNE}_{sE}}{\widehat{m}_{sNT} \widehat{pd}h_{sd,sD}}\right)^{0.1965}\right)^{\frac{1}{2}} \left(\left(\frac{\widehat{Cp}_{sNT} \widehat{\dot{m}}_{sNT}}{\widehat{k}_{sNT}}\right)^{\frac{2}{3}} - 1\right)} \quad (3.188)$$

where if $sST = h$, then $sST^* = c$ and vice-versa.

3.3.1.7 Pressure drop and velocity bounds

The lower and upper velocity bounds for tube-side and annulus-side flows are given by:

$$vt \geq \widehat{vt}_{min} \quad (3.189)$$

$$vt \leq \widehat{vt}_{max} \quad (3.190)$$

$$va \geq \widehat{va}_{min} \quad (3.191)$$

$$va \leq \widehat{va}_{max} \quad (3.192)$$

while the pressure drop bounds are represented by:

$$\Delta Pt \leq \widehat{\Delta P}_{c_{disp}} yT_c + \widehat{\Delta P}_{h_{disp}} yT_h \quad (3.193)$$

$$\Delta Pa \leq \widehat{\Delta P}_{c_{disp}} yT_h + \widehat{\Delta P}_{h_{disp}} yT_c \quad (3.194)$$

3.3.2 Objective function

The objective function is given by the minimization of the structure heat transfer area:

$$\min A \quad (3.195)$$

4 RESULTS

4.1 MINLP Results

In this section, we present the results of the application of the design optimization using both MINLP approaches. Four main aspects are here explored: (i) Numerical aspects such as initial estimates and variable bounds required for convergence achievement; (ii) Comparison of the mathematical programming solution in a broader search space with a result from the literature obtained using a traditional trial and error procedure; (iii) Analysis of the flexibility of the optimization formulation to describe different flow regimes; and (iv) Comparison between the proposed MINLP approaches. The numerical results were obtained using the GAMS software version 23.7.3. Because the DICOPT solver (an outer approximation algorithm) has presented severe convergence obstacles in the investigated problems, all of the solutions presented here were obtained using the SBB solver (a branch-and-bound algorithm).

4.1.1 Numerical aspects

Before starting the results discussion per say, two numerical aspects of the proposed formulations will be explored, the variables initial estimates and bounds.

4.1.1.1 Initial estimates

The convergence of the root node relaxation of the SBB solver was highly sensitive of the initial estimate; therefore, it was necessary to identify a suitable initial set of values for some of the problem variables.

The GAMS software has a default initial estimate for all variables (zero), but for all examples illustrated in this work that was not enough to attain convergence. As a beginning strategy, a feasible point was given as initial estimate; however, this procedure demanded a previous analysis of the problem with direct intervention of the user for each problem to be solved.

Therefore, aiming to simplify the process, a trial and error procedure was explored to identify which variables were more critical in relation to the initial estimate selection to

guarantee the optimization convergence, i.e. which variables demanded a nonzero initial estimate.

This way, we reached a set of sensitive variables, which must have nonzero estimates. In the sequence, we looked for an automatic estimate procedure for this set of variables, which could substitute the identification of a feasible point in an ad hoc basis.

The few binary variables belonging to the sensitive set showed a flexibility toward its initial estimate, needing only that one of the corresponding binaries of the set had the value equal to 1 (thus obeying the constraint where only one diameter or one Reynolds range is selected for example), no matter which one. In order to create a pattern and apply it to all examples approached in this work (and that could be useful for future problems), an arbitrary initial estimate for these variables was selected, according to Table 6.

Table 6. Initial estimates for key binary variables.

Variable	Initial Estimate
Inner tube diameter selection	$yd_3 = 1$
Stream allocation	$yT_c = 1$
Range of Reynolds identification	$yRet_4 = yRea_4 = 1$
Range of Nusselt identification	$yNut_2 = yNua_2 = 1$

Source: The autor.

For the continuous key variables, there was also a flexibility in relation to the specific value of the nonzero initial estimate that should be attributed to promote the convergence. Trying to generalize an automatic procedure, presented in Table 7, it is suggested the mean between the lower and upper bounds, with the exception of the Hausen Nusselt number, for which the theoretical Nusselt value worked.

Table 7. Initial estimates for key continuous variables.

Variable	Initial Estimate
Length of one unit	$L = \frac{L_{lo} + L_{up}}{2}$
Reynolds number*	$Re_x = \frac{Re_{x_{lo}} + Re_{x_{up}}}{2}$
Nusselt number*	$Nu_x = \frac{Nu_{x_{lo}} + Nu_{x_{up}}}{2}$
Seider &Tate Nusselt number*	$Nu_x^{S\&T} = \frac{Nu_{x_{lo}}^{S\&T} + Nu_{x_{up}}^{S\&T}}{2}$
Hausen Nusselt number	$Nu_t^{Hau} = 3.66$ $Nu_a^{Hau} = 3.66$

* x being t (tube side) or a (annulus side).

Source: The autor.

The subscripts lo and up represent, respectively, the lower and upper bounds of each variable, which will be further explored in the next subsection.

4.1.1.2 Variable bounds

In the optimization process all variables have their own search space. In GAMS one may define a variable as a free or a positive variable. A free variable is not bounded (meaning that it ranges from - infinite to + infinite). A positive variable has its lower bound at zero and it is unbounded from the upper side. In exception of the objective function (which needs to be unbounded for the search) and Nu_x^{Gni} (due to the subtraction term in its defining equation) all variables were defined as positive variables, since attributing negative values would not only hold no physical meaning but also be impossible to the formulation in hand.

In addition, it is possible to further restrict the variable bound in order to ameliorate convergence, since it would reduce the search domain. However, one must be careful in doing

so, not to discard any viable solution. So, the methodology applied to determine the variables bounds for the proposed formulation is here explained.

The starting point is that since all discrete options are known parameters, the minimum and maximum possible measurements for a single unit are also known, as well as the maximum number units that a given flow may be divided into. Therefore, it is possible to calculate, for example, the minimum flow area for the tube side:

$$At_{io} = \left(\frac{\pi dt_{io}^2}{4} \right) NB_{io} NPt_{io} \quad (4.1)$$

The same logic can be applied sequentially to several variables.

For allocation dependent variables it is also quite simple, the upper bound for mass flow on the tube side for example, would be the maximum value between the cold and hot stream mass flows.

For regimen dependent variables, for which the bounds are chosen among its possibilities:

$$ft_{io} = \min(ft_{io}^{lam}, ft_{io}^{tran}, ft_{io}^{turb}) \quad (4.2)$$

Furthermore, some variables, like velocities and pressure drop have imposed bounds in the formulation (e.g. $v_t \leq 3$). Finally, a few variables had their bounds manually inputted:

Table 8. Manually inputted bounds.

Variable	Lower bound / Upper bound
ht	10 / $1 \cdot 10^5$
ha	10 / $1 \cdot 10^5$
Nut^{Gni}	$-1 \cdot 10^5$ / $1 \cdot 10^5$
Nua^{Gni}	$-1 \cdot 10^5$ / $1 \cdot 10^5$

Source: The autor.

4.1.2 Comparison with the literature

Example 1 is a design problem given by Serth (2007) that consists in determining the number of required hairpins and its arrangement for the service shown in Table 9. The dimensions of the hairpin employed are shown in Table 10.

Table 9. Example 1 - Stream data

Parameter	Unit	Cold stream (benzene)	Hot stream (aniline)
Mass flow, \hat{m}_{sST}	kg/s	1.26	1.22
Inlet temperature, $\hat{T}_{i,sST}$	°C	15.55	65.55
Outlet temperature, $\hat{T}_{o,sST}$	°C	48.85	37.75
Density, $\hat{\rho}_{sST}$	kg/m ³	879	1022
Viscosity, $\hat{\mu}_{sST}$	Pa·s	$5.5 \cdot 10^{-4}$	$2 \cdot 10^{-3}$
Heat capacity, $\hat{C}_{p,sST}$	J/(kg·°C)	1758.46	2177.14
Thermal conductivity \hat{k}_{sST}	W/(m·°C)	0.159	0.173
Fouling resistance, $\hat{R}_{f,sST}$	m ² °C/W	$1.7 \cdot 10^{-4}$	$1.76 \cdot 10^{-4}$
Available pressure drop, $\hat{\Delta P}_{sST \text{ disp}}$	kPa	138	138

Source: The autor.

Table 10. Example 1 - Hairpin data (pipe schedule 40)

Parameter	Unit	Value
Total hairpin tube length, L	m	9.75
Inner tube NPS	in	1 ¼
Outer tube NPS	in	2
Tube thermal conductivity, \widehat{ktube}	W/(m·k)	16.27

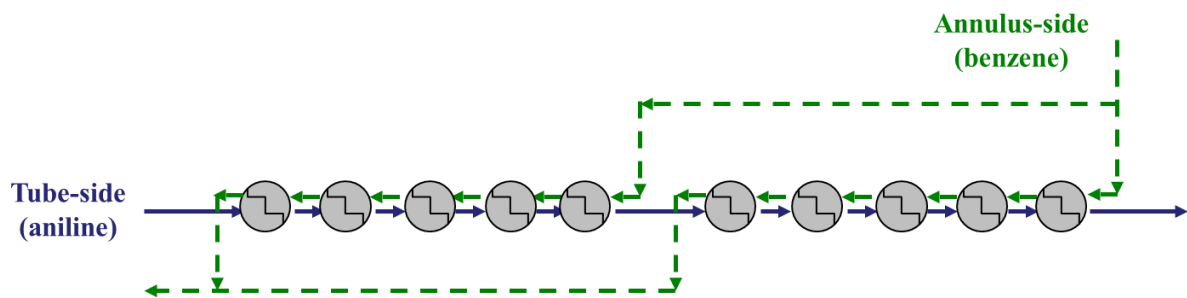
NPS = Nominal pipe size

Source: The autor.

The design methodology employed in Serth (2007) consists in a trial and error procedure, starting by assuming an arbitrary fluid allocation and arrangement (e.g. benzene flowing on the inner tube and both streams connected in series). Then, the number of required hairpins and the streams pressure drops are calculated and checked against the available limits. If the resultant heat exchanger is not fitting, a new configuration/fluid allocation may be proposed and the calculations are remade. When a heat exchanger attains the process requirements with an acceptable over-design, the procedure stops.

The solution obtained by Serth (2007) using the procedure previously presented is illustrated in Figure 20 and consists in 10 hairpins, with inner pipe stream connected in series and annulus-side stream organized in two parallel branches of five hairpins each.

Figure 20: Example 1 - Heat exchanger structure proposed by Serth (2007).



Source: The autor.

The goal of the current analysis is to verify if the utilization of the proposed mathematical programming approach using a broader search space can identify a better solution than the solution previously found by the trial and error procedure.

The thermo-fluid dynamic relations used by Serth (2007) are different from the model employed in this work, particularly the friction factor and the Nusselt number correlations. Therefore, before the optimization, the predictions between both sets of correlations were compared along a range of values of Reynolds number. The comparison indicated that the results from the correlations employed by Serth (2007) are associated to higher values of the friction factor and lower values of the Nusselt number.

However, aiming at providing a fair comparison through a conservative analysis, correction factors were calculated based on the maximum ratio of friction factor and the minimum ratio of the Nusselt number associated to the predictions from Serth (2007) and the current work, along the entire Reynolds number range.

Table 11. Structural discrete options (pipe schedule 40).

Parameter	Unit	Discrete options									
\widehat{pNB}_{sB}	--	1 to 20									
\widehat{pNE}_{sE}	--	1 to 20									
\widehat{pL}_{sL}	ft	5	10	15	20	25	160				
\widehat{pL}_{sL}	m	1.524	3.048	4.572	6.096	7.620	48.768				
Inner tube NPS	in	½	¾	1	1 ¼	1 ½	2	2 ½	3	3 ½	
Inner tube OD	m	0.021	0.027	0.033	0.042	0.048	0.060	0.073	0.089	0.102	
Outer tube NPS	in	1 ¼	1 ½	2	2 ½	3	3 ½	4	4 ½	5	
Outer tube OD	m	0.042	0.048	0.060	0.073	0.089	0.102	0.114	0.127	0.168	

NPS = Nominal pipe size, OD = Outer diameter

Source: The autor.

Table 12 contains the reported values by Serth (2007) of the performance of his solution for the design problem, the validation solution of the proposed model, and the optimal solution using the original MINLP formulation.

The validation solution presented in

Table 12 corresponds to the adoption of the heat exchanger reported by Serth (2007) to both mathematical models. The results indicate a description of Serth (2007) solution associated to higher pressure drops and lower convective heat transfer coefficients, as it was expected according to the conservative approach employed to consider the differences in the thermo-fluid dynamic correlations. The exception was the small decrease of the tube-side pressure drop due to the presence of a viscosity correction factor that is not contemplated in the proposed modelling.

The original optimization approach obtained the optimal result reported in

Table 12, where it is possible to observe a reduction of 11% in relation to the literature. The comparison of the optimal solution and the literature solution indicates that,

despite the similarity of the overall heat transfer coefficients, the area reduction is attained due to a higher logarithmic mean temperature difference (LMTD) resultant from the counter-current arrangement of the set of units of the proposed heat exchanger.

Table 12. Example 1 – Design results.

Variable	Unit	Serth (2007)	Validation solution	Optimal solution
Tube side stream	–	Aniline	Aniline	Aniline
Total heat exchanger area, A	m ²	12.91	12.92	11.49
Required heat exchanger area	m ²	11.68	11.70	9.79
Inner tube NPS – OD	in – m	1 ¼ – 0.042	1 ¼ – 0.042	¾ – 0.027
Outer tube NPS – OD	in – m	2 – 0.060	2 – 0.060	1 ¼ – 0.042
Unit length, L	ft (m)	160 (48.77)	160 (48.77)	25 (7.62)
Number of branches, NB	–	1	1	3
Tube side units in parallel / in series	–	1 / 2	1 / 2	1 / 6
Annular side units in parallel / in series	–	2 / 1	2 / 1	1 / 6
Tube side velocity, vt	m/s	1.24	1.24	1.157
Annulus side velocity, va	m/s	0.93	0.93	1.176
Tube side film coefficient, ht	W/(m ² °C)	999	961	935
Annulus side film coefficient, ha	W/(m ² °C)	1448	1330	1675
Overall heat transfer coefficient, U	W/(m ² °C)	391.8	380.2	390.8
Corrected LMTD	°C	16.14	16.59	19.31
Tube side pressure drop, dPt	kPa	82.0	79.0	62.2
Annulus side pressure drop, dPa	kPa	70.3	72.5	132.8

NPS = Nominal pipe size, OD = Outer diameter

Source: The autor.

4.1.3 Analysis of the modeling of different flow regimes

This analysis illustrates the modeling of different flow regimes by the proposed formulations. The discussions are based on two new examples where a hot stream must be cooled from

323.15 K to 313.15 K. Example 2 involves the utilization of a cooling water stream to fulfill this task and Example 3 employs an ethylene glycol stream. The data of the streams of these examples are shown in

Table 13, where must be noted that the viscosity of the ethylene glycol is about 25 times higher than that of the cooling water and its thermal conductivity is about 40% of the cooling water value.

Table 13. Examples 2 and 3 – Stream data.

Parameter	Unit	Hot stream (solvent)	Cold stream (cooling water)	Cold stream (ethylene glycol)
Mass flow, \widehat{m}_{sST}	kg/s	8	3.68	4.38
Inlet temperature, $\widehat{T}_{i_{sST}}$	°C	50	20	5
Outlet temperature, $\widehat{T}_{o_{sST}}$	°C	40	30	20
Density, $\widehat{\rho}_{sST}$	kg/m ³	90	997	1 010
Viscosity, $\widehat{\mu}_{sST}$	Pa·s	$9.5 \cdot 10^{-4}$	$9.0 \cdot 10^{-4}$	0.024
Heat capacity, $\widehat{C}_{p_{sST}}$	J/(kg·°C)	1922	4182	2340
Thermal conductivity \widehat{k}_{sST}	W/(m·°C)	0.187	0.610	0.264
Fouling resistance, $\widehat{R}_{f_{sST}}$	m ² °C /W	$3 \cdot 10^{-4}$	$3 \cdot 10^{-4}$	$3 \cdot 10^{-4}$
Available pressure drop, $\widehat{\Delta P}_{sST \text{ disp}}$	kPa	100	100	100

Source: The autor.

The discrete options employed in the optimization are the ones presented in Table 11, with exception of the elimination of the unit length of 160 ft, as it had only comparison purposes with the literature in the previous example. The correction factors applied in the model in Example 1 were also eliminated by the same reason. The velocity bounds applied in the optimization runs were 1 m/s to 3 m/s and a minimum excess area of 20% was applied.

The application of the original optimization approach yielded the results presented in Table 11. The higher viscosity of the ethylene glycol stream and its lower thermal conductivity contributed to reduce the overall heat transfer coefficient to 160 W/(m²°C) in Example 3 when compared to 820 W/(m²°C) in Example 2. Consequently, the heat transfer area increased to 35.75 m² from 11.49 m². The fluid dynamic aspects also modified the

design, since the need to accommodate the higher pressure drops associated to the ethylene glycol stream elevated the number of parallel branches in Example 3 to 10 branches (of 14 units each) from 6 branches (of 15 units each) in Example 2.

Table 14. Examples 2 and 3 – Design results.

Variable	Unit	Cooling water	Ethylene Glycol
Tube side stream	–	Cooling water	Ethylene Glycol
Total heat exchanger area, A	m ²	11.49	35.75
Required heat exchanger area	m ²	9.37	29.67
Inner tube NPS – OD	in – m	$\frac{3}{4}$ – 0.027	$\frac{3}{4}$ – 0.027
Outer tube NPS – OD	in – m	1 $\frac{1}{2}$ – 0.048	1 $\frac{1}{2}$ – 0.048
Unit length, L	ft (m)	5 (1.52)	10 (3.048)
Number of branches, NB	–	6	10
Tube side units in parallel / in series	–	1 - 15	1 - 14
Annular side units in parallel / in series	–	1 - 15	1 - 14
Tube side velocity, vt	m/s	1.786	1.260
Annulus side velocity, va	m/s	2.236	1.342
Tube side film coefficient, ht	W/(m ² °C)	8 744	256
Annulus side film coefficient, ha	W/(m ² °C)	3 010	1 868
Overall heat transfer coefficient, U	W/(m ² °C)	820	160
Corrected LMTD	°C	20	32.44
Tube side pressure drop, dPt	kPa	45.4	94.3
Annulus side pressure drop, dPa	kPa	84.6	62.5

NPS = Nominal pipe size, OD = Outer diameter

Source: The autor.

The behavior observed is directly linked to the flow regime in the optimal solution of each example. The solution of Example 2 was associated to a Reynolds number of 41 412, i.e. turbulent flow, that is associated to a convective heat transfer coefficient of 8 744 W/(m²°C). The equivalent Reynolds number in Example 3 was reduced to only 1 110, where the resultant laminar flow was associated to a low convective heat transfer coefficient of 256 W/(m²°C). It

is interesting to observe that an increase of the heat transfer coefficient in Example 3 is limited by the fluid dynamic constraints, since the pressure drop of the solution, 94.3 kPa, is near to the maximum value, 100 kPa (it does not match the upper limit exactly due to the discrete feature of the problem) .

These results illustrate that the proposed optimization formulations can model the behavior of the optimal heat exchangers considering different flow regimes.

4.1.4 Comparison of the MINLP approaches

The comparison of the MINLP approaches were based on a sample of 5 different problems, composed of Examples 1 to 3, already described, and additionally, Example 4 (Kakaç and Liu, 2002) and Example 5, described in Table 15 and Table 16.

Table 15. Example 4 – Stream data

Parameter	Unit	Cold stream (water)	Hot stream (water)
Mass flow, \hat{m}_{sST}	kg/s	1.39	1.36
Inlet temperature, $\hat{T}_{i,sST}$	°C	20	140
Outlet temperature, $\hat{T}_{o,sST}$	°C	35	125
Density, $\hat{\rho}_{sST}$	kg/m ³	996.4	932.5
Viscosity, $\hat{\mu}_{sST}$	Pa.s	$8.41 \cdot 10^{-4}$	$2.07 \cdot 10^{-4}$
Heat capacity, $\hat{C}_{p,sST}$	J/(kg. °C)	4 179	4268
Thermal conductivity \hat{k}_{sST}	W/(m. °C)	0609	0.687
Fouling resistance, $\hat{R}f_{sST}$	m ² °C /W	$3.52 \cdot 10^{-4}$	$1.76 \cdot 10^{-4}$
Available pressure drop, $\hat{\Delta P}_{sST \text{ disp}}$	kPa	10	10

Source: The autor.

Table 16. Example 5 – Stream data

Parameter	Unit	Cold stream	Hot stream
Mass flow, \widehat{m}_{sST}	kg/s	11.44	5.5
Inlet temperature, $\widehat{T}_{i_{sST}}$	°C	30.1	90
Outlet temperature, $\widehat{T}_{o_{sST}}$	°C	40	50
Density, $\widehat{\rho}_{sST}$	kg/m ³	995	786
Viscosity, $\widehat{\mu}_{sST}$	Pa·s	$7.2 \cdot 10^{-4}$	$1.89 \cdot 10^{-3}$
Heat capacity, $\widehat{C}_{p_{sST}}$	J/(kg·°C)	4187	2177
Thermal conductivity \widehat{k}_{sST}	W/(m·°C)	0.59	0.12
Fouling resistance, $\widehat{R}_{f_{sST}}$	m ² °C /W	$4 \cdot 10^{-4}$	$2 \cdot 10^{-4}$
Available press. Drop, $\widehat{\Delta P}_{sST \text{ disp}}$	kPa	100	100

Source: The autor.

These design tasks were solved using both proposed MINLP approaches, considering velocity bounds of 1 m/s to 3 m/s and a minimum excess area of 20%. The thermo-fluid dynamic model was employed without any correction factor, therefore the solution obtained for Example 1 will differ from the results reported in the comparison with the literature.

The complete solutions for all 5 examples are depicted from Table 17 to Table 21 and its respective heat exchangers structures are illustrated from Figure 22 to Figure 26.

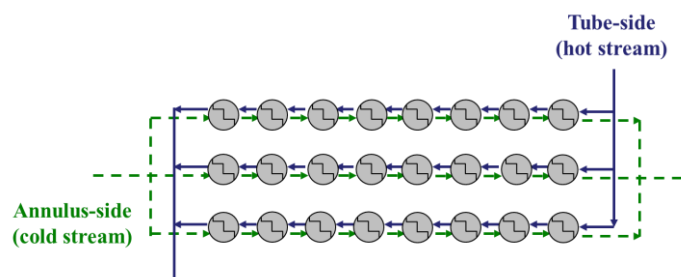
Example 1

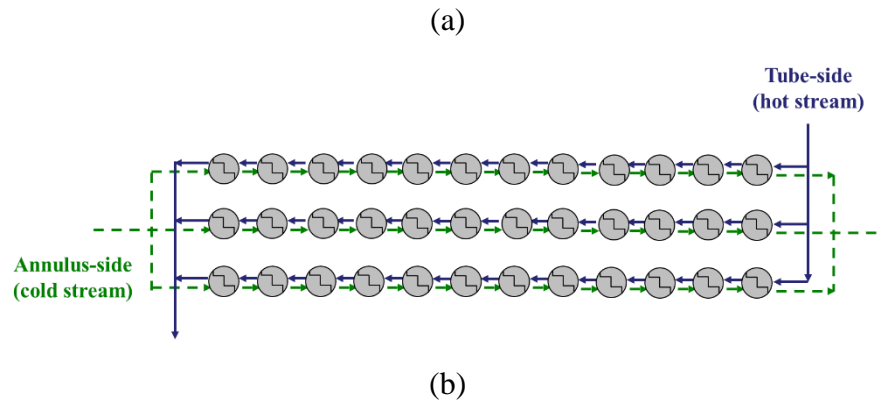
Table 17. Example 1 – Optimization results.

Variable	Unit	Original formulation	Modified formulation
Tube side stream	–	Hot stream	Hot stream
Total heat exchanger area, A	m ²	9.19	9.19
Required heat exchanger area	m ²	7.52	7.52
Inner tube NPS – OD	in – m	$\frac{3}{4}$ – 0.027	$\frac{3}{4}$ – 0.027
Outer tube NPS – OD	in – m	1 $\frac{1}{4}$ – 0.042	1 $\frac{1}{4}$ – 0.042
Unit length, L	ft (m)	15 (4.57)	10 (3.05)
Number of branches, NB	–	3	3
Tube side units in parallel / in series	–	1 / 8	1 / 12
Annular side units in parallel / in series	–	1 / 8	1 / 12
Tube side velocity, v_t	m/s	1.157	1.157
Annulus side velocity, v_a	m/s	1.176	1.176
Tube side film coefficient, h_t	W/(m ² °C)	1 384	1 384
Annulus side film coefficient, h_a	W/(m ² °C)	2 235	2 235
Overall heat transfer coefficient, U	W/(m ² °C)	508	508
Corrected LMTD	°C	19.31	19.31
Tube side pressure drop, dPt	kPa	40.8	40.8
Annulus side pressure drop, dPa	kPa	77.8	77.8

Source: The autor.

Figure 22: Example 1 – Optimal structures – Original MINLP (a) and Modified MINLP (b).





Source: The autor.

In this first example two solutions with the same total heat exchanger areas were found. They differ only in the number of units per branch and its respective lengths, while the total branch length remains the same (120 ft).

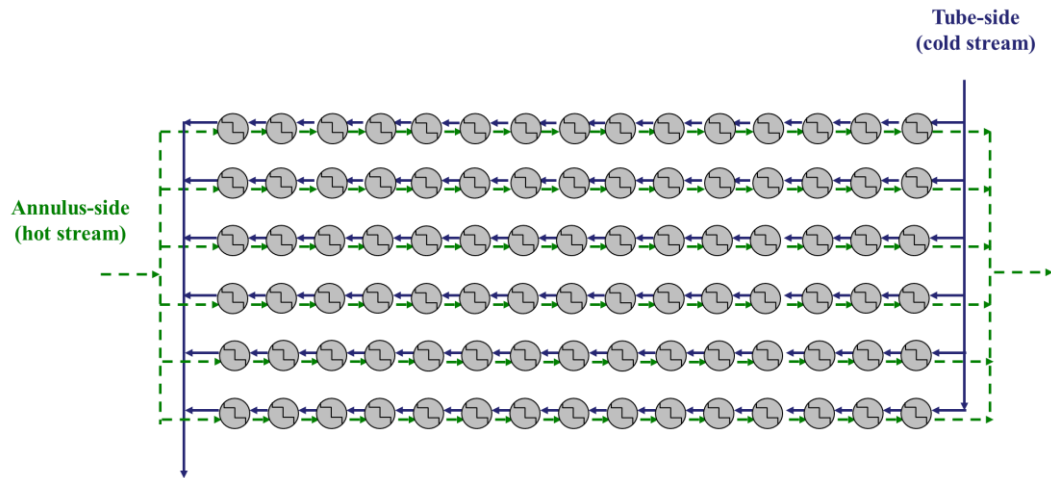
Example 2

Table 18. Example 2 – Optimization results.

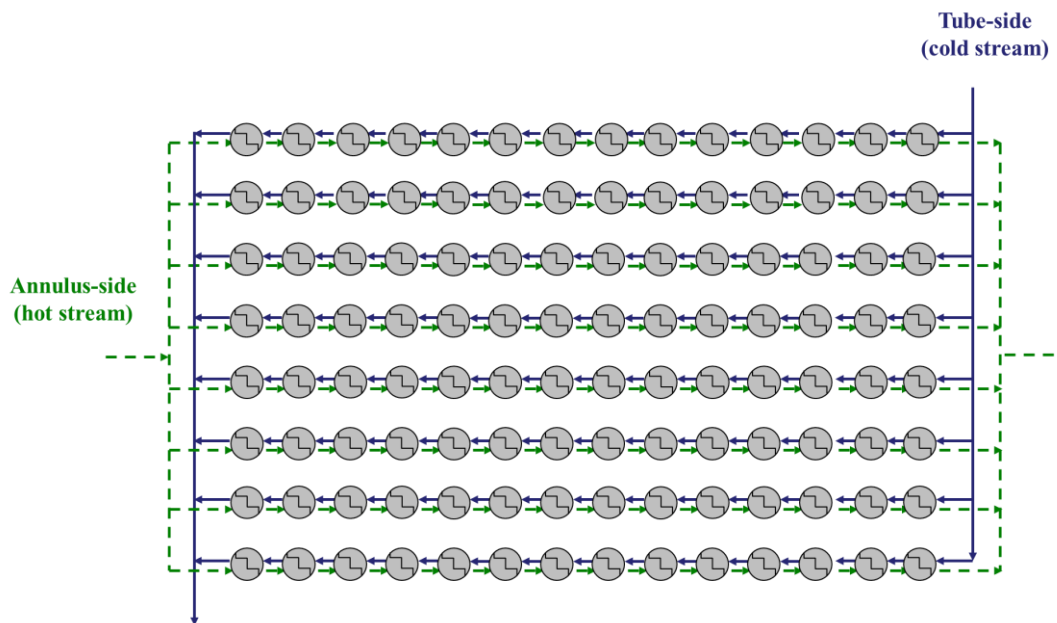
Variable	Unit	Original formulation	Modified formulation
Tube side stream	–	Cold stream	Cold stream
Total heat exchanger area, A	m ²	11.49	11.44
Required heat exchanger area	m ²	9.37	9.49
Inner tube NPS – OD	in – m	¾ – 0.027	½ – 0.021
Outer tube NPS – OD	in – m	1 ½ – 0.048	1 ¼ – 0.042
Unit length, L	ft (m)	5 (1.52)	5 (1.52)
Number of branches, NB	–	6	8
Tube side units in parallel / in series	–	1 / 15	1 / 14
Annular side units in parallel / in series	–	1 / 15	1 / 14
Tube side velocity, vt	m/s	1.786	2.351
Annulus side velocity, va	m/s	2.236	2.084
Tube side film coefficient, ht	W/(m ² °C)	8 744	11 517
Annulus side film coefficient, ha	W/(m ² °C)	3 010	2 828
Overall heat transfer coefficient, U	W/(m ² °C)	820	810
Corrected LMTD	°C	20.00	20
Tube side pressure drop, dPt	kPa	45.4	97.4
Annulus side pressure drop, dPa	kPa	84.6	72.5

Source: The autor.

Figure 23: Example 2 – Optimal structures – Original MINLP (a) and Modified MINLP (b).



(a)



(b)

Source: The autor.

Despite the proximity of the heat exchanger areas found, the modified model was able to find a better solution for the Example 2 (0.5% of area reduction), showing the existence of multiple local optima.

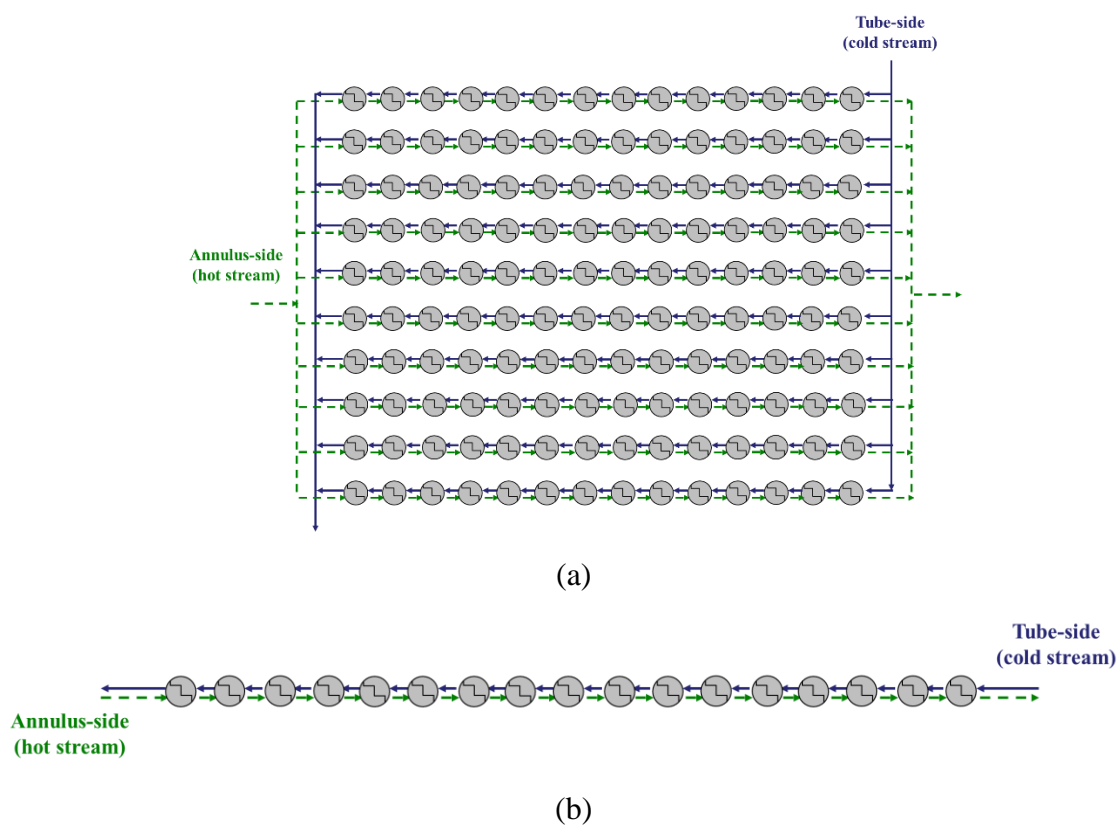
Example 3

Table 19. Example 3 – Optimization results.

Variable	Unit	Original formulation	Modified formulation
Tube side stream	–	Cold stream	Cold stream
Total heat exchanger area, A	m ²	35.75	23.77
Required heat exchanger area	m ²	29.67	19.23
Inner tube NPS – OD	in – m	$\frac{3}{4}$ – 0.027	2 $\frac{1}{2}$ – 0.073
Outer tube NPS – OD	in – m	1 $\frac{1}{2}$ – 0.048	4 $\frac{1}{2}$ – 0.127
Unit length, L	ft (m)	10 (3.05)	20 (6.10)
Number of branches, NB	–	10	1
Tube side units in parallel / in series	–	1 / 14	1 / 17
Annular side units in parallel / in series	–	1 / 14	1 / 17
Tube side velocity, vt	m/s	1.260	1.404
Annulus side velocity, va	m/s	1.342	1.660
Tube side film coefficient, ht	W/(m ² °C)	256	412
Annulus side film coefficient, ha	W/(m ² °C)	1 868	2 080
Overall heat transfer coefficient, U	W/(m ² °C)	160	246.5
Corrected LMTD	°C	32.44	32.44
Tube side pressure drop, dPt	kPa	94.3	78.1
Annulus side pressure drop, dPa	kPa	62.5	62.8

Source: The autor.

Figure 24: Example 3 – Optimal structures – Original MINLP (a) and Modified MINLP (b).



Source: The autor.

Example 3 showed a more significant difference between both approaches. The modified model was able to find a solution with a reduction of 33% in the heat exchanger area through very distinct structures, once again showing the appearance of local optima.

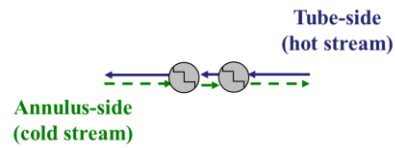
Example 4

Table 20. Example 4 – Optimization results.

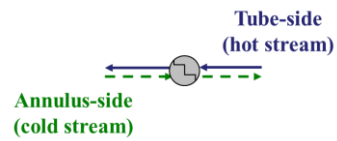
Variable	Unit	Original formulation	Modified formulation
Tube side stream	–	Hot stream	Hot stream
Total heat exchanger area, A	m ²	0.92	0.92
Required heat exchanger area	m ²	0.77	0.77
Inner tube NPS – OD	in – m	1 ½ – 0.048	1 ½ – 0.048
Outer tube NPS – OD	in – m	2 ½ – 0.073	2 ½ – 0.073
Unit length, L	ft (m)	10 (3.05)	20 (6.10)
Number of branches, NB	–	1	1
Tube side units in parallel / in series	–	1 / 2	1 / 1
Annular side units in parallel / in series	–	1 / 2	1 / 1
Tube side velocity, vt	m/s	1.110	1.110
Annulus side velocity, va	m/s	1.107	1.107
Tube side film coefficient, ht	W/(m ² °C)	9 950	9 950
Annulus side film coefficient, ha	W/(m ² °C)	5 780	5 780
Overall heat transfer coefficient, U	W/(m ² °C)	1 081	1 081
Corrected LMTD	°C	105.00	105.00
Tube side pressure drop, dPt	kPa	1.7	1.7
Annulus side pressure drop, dPa	kPa	7.3	7.3

Source: The autor.

Figure 25: Example 4 – Optimal structures – Original MINLP (a) and Modified MINLP (b).



(a)



(b)

Source: The autor.

Similarly to Example 1, both approaches achieved the same heat exchanger areas, through structures with different number of units per branch, however maintaining the same total branch length (20 ft in this case).

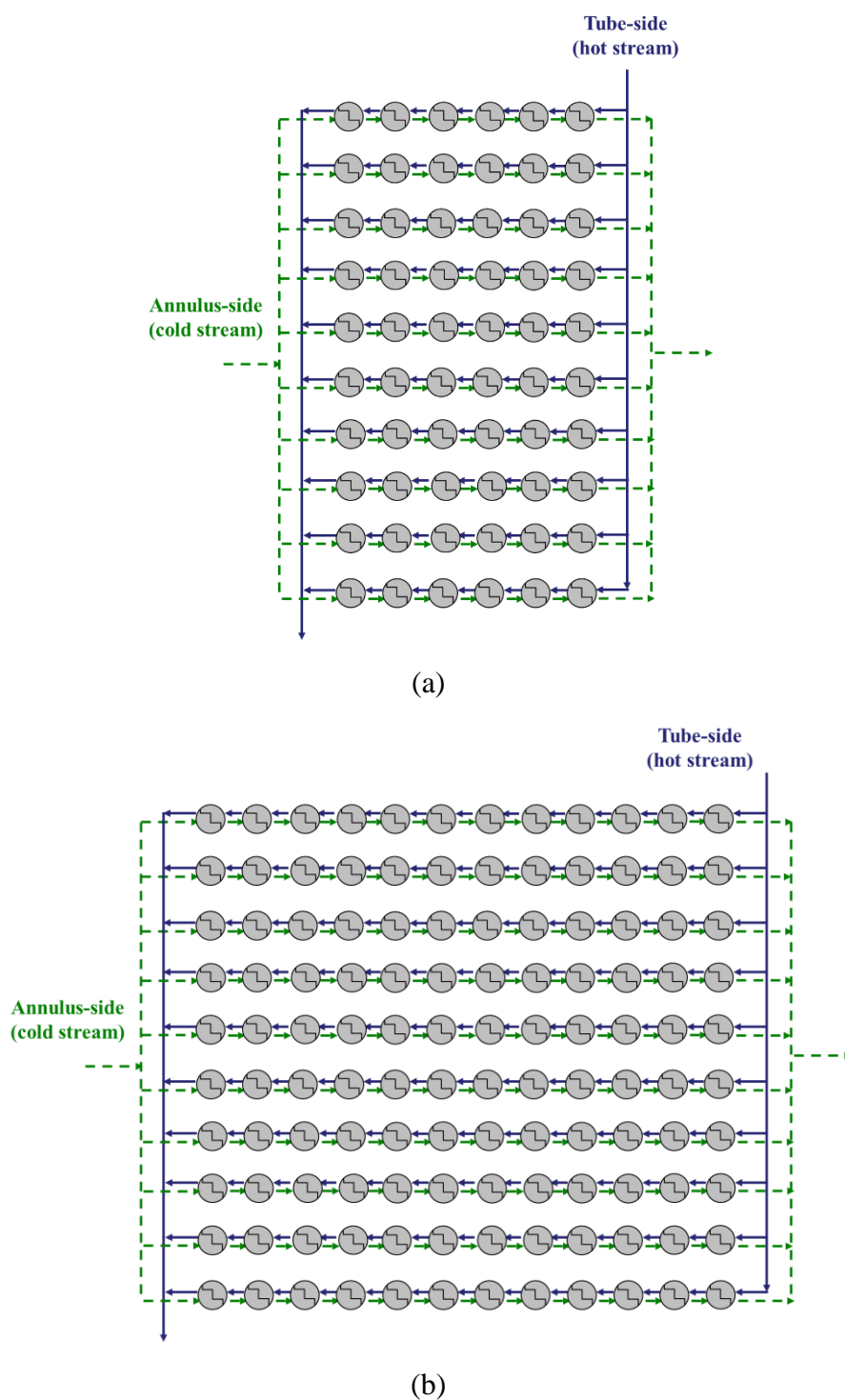
Example 5

Table 21. Example 5 – Optimization results.

Variable	Unit	Original formulation	Modified formulation
Tube side stream	–	Hot stream	Hot stream
Total heat exchanger area, A	m ²	30.64	30.64
Required heat exchanger area	m ²	24.47	24.47
Inner tube NPS – OD	in – m	$\frac{3}{4}$ – 0.027	$\frac{3}{4}$ – 0.027
Outer tube NPS – OD	in – m	1 $\frac{1}{2}$ – 0.048	1 $\frac{1}{2}$ – 0.048
Unit length, L	ft (m)	20 (6.10)	10 (3.05)
Number of branches, NB	–	10	10
Tube side units in parallel / in series	–	1 / 6	1 / 12
Annular side units in parallel / in series	–	1 / 6	1 / 12
Tube side velocity, vt	m/s	2.034	2.034
Annulus side velocity, va	m/s	1.523	1.523
Tube side film coefficient, ht	W/(m ² °C)	1 497	1 497
Annulus side film coefficient, ha	W/(m ² °C)	8 233	8 233
Overall heat transfer coefficient, U	W/(m ² °C)	593	593
Corrected LMTD	°C	32.67	32.67
Tube side pressure drop, dPt	kPa	89.1	89.1
Annulus side pressure drop, dPa	kPa	77.3	77.3

Source: The autor.

Figure 26: Example 5 – Optimal structures – Original MINLP (a) and Modified MINLP (b).



Source: The autor.

Similarly to Example 1 and Example 4, both approaches achieved the same heat exchanger areas, through structures with different number of units per branch, however maintaining the same total branch length (120 ft in this case).

To ease the comparisons the final heat exchangers areas and the elapsed time for each optimization run using a computer with CPU Intel Core i7-6700 (16GB RAM) are shown in Table 22.

Table 22. Examples 1 to 5 – Performance comparison of the different MINLP approaches

Example	Original MINLP		Modified MINLP	
	Area (m ²)	Time (s)	Area (m ²)	Time (s)
1	9.19	12.28	9.19	22.68
2	11.49	76.79	11.44	92.12
3	35.75	13.46	23.78	31.91
4	0.92	11.05	0.92	21.26
5	30.64	41.40	30.64	106.97

Source: The autor.

The analysis of the results in Table 22 indicates that the modified formulation demanded more computational time to solve all of the design problems. The analysis of the area of the solutions obtained by the two approaches indicated that the original and modified approaches obtained solutions with the same area in the Examples 1, 4, and 5 (the structures of the solutions are different, but they have the same area, as can be observed in Figure 22, Figure 25 Figure 26, respectively). In Examples 2 and 3, the modified approach identified a solution with a smaller area. The area reduction in the Example 2 is only 0.4%, but in Example 3, the area reduction is 33%. The considerable area reduction in the Example 3 was achieved using the modified formulation because the optimization could identify a solution without the presence of laminar flow for the ethylene glycol stream, thus increasing the overall heat transfer coefficient. The considerable difference between the objective functions of the local optimal solutions in Example 3 illustrates the importance of the utilization of a global optimization scheme to address the design problem, aspect explored in the third approach proposed by this work.

4.2 MILP Results

In this section, we present the results of the application of the design optimization using the MILP approach, exploring three main aspects of the problem: (i) numerical aspects;

(ii) the analysis of the global optimum of a given design task; and (iii) analysis of the structural flexibility of the design arrangement.

4.2.1 Numerical aspects

In subsection 4.1.1, numerical aspects of the MINLP approaches were discussed. It presented a strong sensibility to initial estimates. The MILP approach has the advantage of not being dependent on that factor. No matter the initial values, as long as there is at least one viable solution in the search domain, not only convergence is guaranteed but the global optima as well.

However, these advantages come at a cost. The size of the problem increases exponentially. For example, for a given problem with a finite number of discrete options (shown in Table 23) the number of restrictions, variables and computational effort for each approach are presented in Table 24.

Table 23. Number of discrete options for a given task.

Parameter	Number of discrete options
\widehat{pNB}_{sB}	6
\widehat{pNE}_{sE}	8
\widehat{pNL}_{sL}	2
\widehat{pdte}_{sd}	4
\widehat{pDte}_{sD}	4

Source: The autor.

Table 24. Comparison between the three approaches.

Approach	N° of restrictions	N° of variables	Processing time (s)
MINLP 1	106	135	12.5
MINLP 2	282	191	15.2
MILP	869 337	205 926	604.3

Source: The autor.

The same variable bounds applied to the MINLP were used here. Although it doesn't impact the final solution, it accelerates the process and diminish the problem dimension.

4.2.2 Trial and Error Procedure

Aiming to compare the performance of the proposed MILP approach with a trial and error design technique, a given design task was solved through a trial and error procedure, which will be detailed in this section. In the next section the same design task will be solved for with the MILP formulation to obtain the global optimum.

The data for this sixth example is presented in Table 25.

Table 25. Example 6 - Stream data

Parameter	Unit	Cold stream	Hot stream
Mass flow, \widehat{m}_{sST}	kg/s	2.52	2.11
Inlet temperature, \widehat{T}_{i_sST}	°C	20	60
Outlet temperature, \widehat{T}_{o_sST}	°C	30	50
Density, $\widehat{\rho}_{sST}$	kg/m ³	850	1000
Viscosity, $\widehat{\mu}_{sST}$	Pa·s	$5.5 \cdot 10^{-4}$	$2 \cdot 10^{-4}$
Heat capacity, \widehat{C}_{p_sST}	J/(kg·°C)	1 760	2 100
Thermal conductivity \widehat{k}_{sST}	W/(m·°C)	0.160	0.175
Fouling resistance, \widehat{R}_{f_sST}	m ² °C/W	$2 \cdot 10^{-4}$	$2 \cdot 10^{-4}$

Source: The autor.

The discrete options applied to this design problem are shown in Table 26, where the heat exchanger will be build using pipes with thermal conductivity of 55 W/(m°C). The additional design specifications include flow velocity in both sides between 1 m/s and 3 m/s, available pressure drop for the hot and cold streams equal to 50 kPa, and the final design must have a minimum excess area of 20%. In the numerical tests for the MILP approach, the set up of the search space was associated to some problems in relation to memory requirements, which can limit the extent of the number of mechanical alternatives explored in the analysis.

To level the comparison the same search space was applied to this trial and error procedure, which is shown in Table 26.

Table 26. Structural discrete options (pipe schedule 40).

Parameter	Unit	Discrete options			
\widehat{pNB}_{sB}	--	1 to 6			
\widehat{pNE}_{sE}	--	1 to 8			
\widehat{pL}_{sL}	ft	5	10		
\widehat{pL}_{sL}	m	1.524	3.048		
Inner tube NPS	in	¾	1	1 ¼	1 ½
Inner tube OD	m	0.027	0.033	0.042	0.048
Outer tube NPS	in	1 ¼	1 ½	2	2 ½
Outer tube OD	m	0.042	0.048	0.060	0.073

NPS = Nominal pipe size, OD = Outer diameter

Source: The autor.

This trial an error procedure is similar to the one presented by Serth (2007). For the given design task we first assume a starting structure and calculate the respective heat transfer coefficient, required area and pressure drops. If the results meet the design requirements with a reasonable excess area the procedure stops. Otherwise, a structure change is made and the calculations are repeated. In the example here presented 4 trials were necessary. Each selected structure is presented in Table 27, their respective results in Table 28 and the heat exchanger illustrations in Figure 27.

Table 27. Fixed design variables for each Trial.

Parameter	Unit	Trial 1	Trial 2	Trial 3	Trial 4
Tube side stream	–	Cold stream	Hot stream	Hot stream	Hot stream
Inner tube NPS – OD	in – m	1 – 0.033	1 – 0.033	1 – 0.033	1 – 0.033
Outer tube NPS – OD	in – m	2 – 0.060	2 – 0.060	2 – 0.060	2 – 0.060
Unit length, L	ft (m)	10 (3.05)	10 (3.05)	10 (3.05)	5 (1.52)
Hairpin area	m ²	0.32	0.32	0.32	0.16
Number of branches, NB	–	1	1	2	2
Tube side units in parallel, NPt	–	1	1	1	1
Annular side units in parallel, NPa	–	1	1	1	1

Source: The autor.

Table 28. Trials results.

Parameter	Unit	Trial 1	Trial 2	Trial 3	Trial 4
Total heat exchanger area, A	m ²	1.60	1.60	2.56	2.24
Required heat exchanger area	m ²	1.27	1.32	1.79	1.79
Tube side velocity, vt	m/s	5.32	3.79	1.90	1.89
Annulus side velocity, va	m/s	1.64	2.30	1.15	1.15
Tube side pressure drop, dPt	kPa	137.7	74.9	16.2	14.1
Annulus side pressure drop, dPa	kPa	20.5	40.1	9.1	8.0

Source: The autor.

Trial 1

We start by assuming the simplest structure: both streams aligned in series in only one branch. We also select arbitrary hairpin dimensions between our discrete options, as well as an arbitrary fluid allocation.

The required area for the first trial is of 1.27 m², which, for a minimum 20% excess area, would require a total of 5 units in the given branch. However, both velocity and pressure drop for the tube side are too elevated for the design bounds. Therefore, since the annular cross-section is larger than the tube-side's we attempt switching the allocation fluid for Trial 2.

Trial 2

The required area in this case is of 1.32 m² which also requires 5 units per branch. Although there is a significant reduction, the tube-side velocity and pressure drop are still above allowed limits. Thus, the third trial involves the addition of one branch, dividing the flow in two parallel branches.

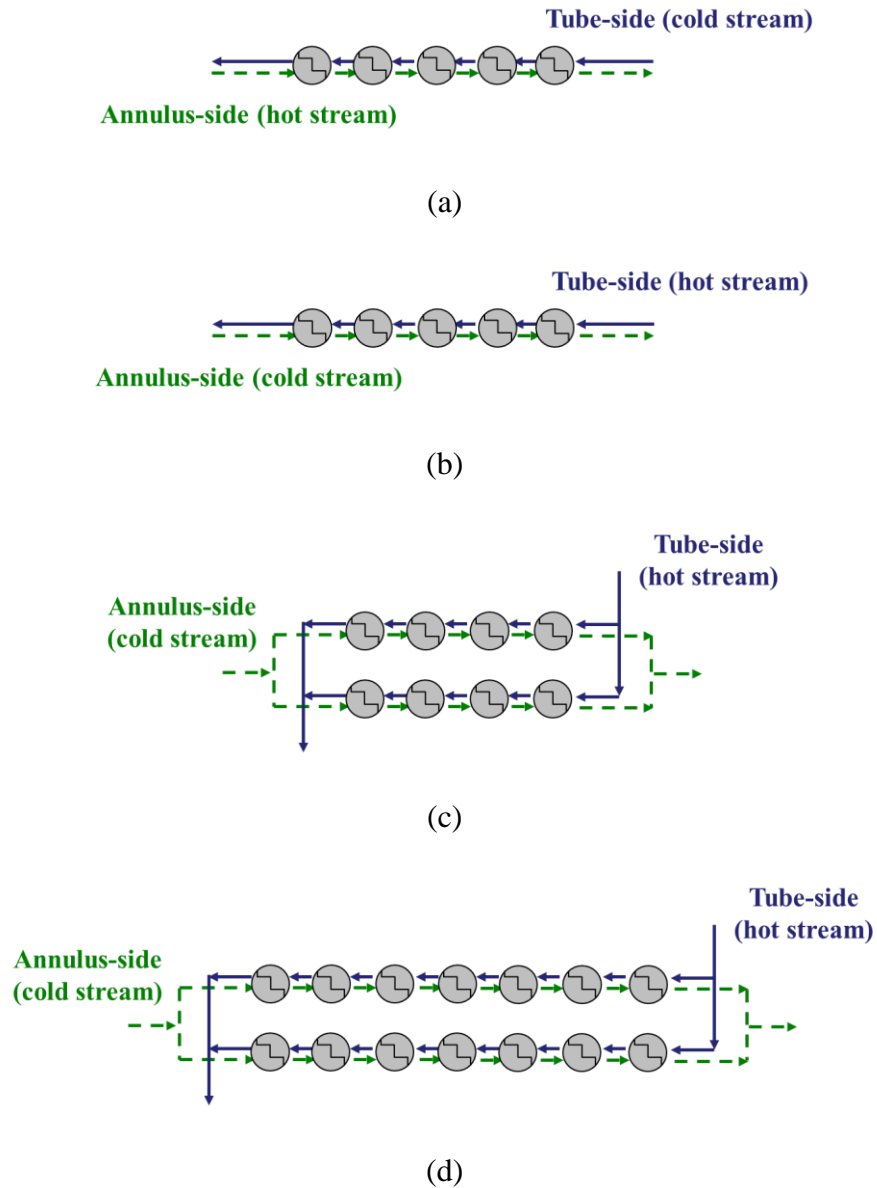
Trial 3

There is an augmentation of the required area to 1.79 m² (0.895 m² per branch), which, for the same minimum excess area, requires 4 units per branch. The heat exchanger found in the third trial meets all the requirements. However, the excess area is of 43%, which is a little high. In an attempt to ameliorate the obtained result, we switch from four 10ft units to seven 5ft unit, keeping all heat transfer coefficients the same (since none of the velocities or hairpin diameters were changed) and reducing the total branch length from 40ft to 35ft.

Trial 4

The heat exchanger from the last trial meets all the requirements and has only 25% of excess area. The procedure stops. The selected structure is illustrated in Figure 27(d), and a more detailed result is presented in the next section, alongside the global optimum, in Table 29.

Figure 27: Representation of the heat exchangers structures: Trial 1 (a), Trial 2 (b), Trial 3 (c) and Trial 4 (d).

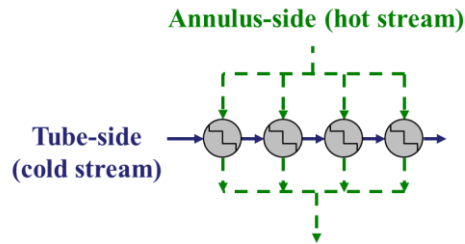


Source: The autor.

4.2.3 Global optimum analysis

The same design problem presented in the previous section is solved through the MILP proposed formulation, to obtain the global optimum. In doing so, we are able to find an area reduction of 17.4%, with the structure illustrated in Figure 28. The elapsed time of the optimization run using a computer with CPU Intel Core i7-6700 (16GB RAM) was of 239.5 seconds.

Figure 28: Example 6 – Globally optimal solution.



Source: The autor.

This area reduction was possible through the identification of an alternative solution associated to higher flow velocities and heat transfer coefficients, as can be seen in Table 2.

Table 29. Example 6 – Design results.

Variable	Unit	Trial and error solution	Globally optimal solution
Tube side stream	–	Hot stream	Cold stream
Total heat exchanger area, A	m ²	2.24	1.85
Required heat exchanger area	m ²	1.79	1.49
Inner tube NPS – OD	in – m	1 – 0.033	1 ½ – 0.048
Outer tube NPS – OD	in – m	2 – 0.060	2 – 0.060
Unit length, L	ft (m)	5 (1.52)	10 (3.05)
Number of branches, NB	–	2	1
Tube side units in parallel / in series	–	1 / 7	1 / 4
Annular side units in parallel / in series	–	1 / 7	4 / 1
Tube side velocity, vt	m/s	1.89	2.26
Annulus side velocity, va	m/s	1.15	1.57
Tube side film coefficient, ht	W/(m ² °C)	6 502	3 533
Annulus side film coefficient, ha	W/(m ² °C)	1 995	6 516
Overall heat transfer coefficient, U	W/(m ² °C)	824	1 004
Corrected LMTD	°C	30.0	29.6
Tube side pressure drop, dPt	kPa	14.1	13.7
Annulus side pressure drop, dPa	kPa	8.0	22.7

Source: The autor.

4.2.4 Structural flexibility

In this section, we approach design problems where the specifications of the modular unit available are fixed (pipe diameters and length), but the stream allocation and heat exchanger arrangement are completely free; i.e. the problem is the determination of the least cost arrangement of the modular units for a given design task. Two aspects are explored: the modification of the heat exchanger arrangement according to the different hydraulic bounds and the flexibility of the modular design to accommodate modifications in the process throughput. The dimensions of the modular units employed in the examples analyzed are depicted in Table 30. The hairpins will be built with a material with a thermal conductivity of 55 W/(m°C).

Table 30. Hairpin data (pipe schedule 40) for the structural flexibility analysis.

Parameter	Unit	Value
Total hairpin tube length, L	m	3.05
Inner tube NPS	in	1
Outer tube NPS	in	2
Hairpin area	m ²	0.32

Source: The autor.

4.2.4.1 Variation of the hydraulic bounds

The data of the streams of the examples explored in the hydraulic analysis are depicted in Table 31. These examples are associated to different sets of available pressured drops for the hot and cold streams, Example 7: 50.0 kPa/50 kPa; Example 8: 20.0 kPa/50 kPa; and Example 9: 20.0 kPa/20 kPa.

Table 31. Examples 7 to 9 – Stream data.

Parameter	Unit	Cold stream (cooling water)	Hot stream (solvent)
Mass flow, \hat{m}_{sST}	kg/s	2.21	4.80
Inlet temperature, $\hat{T}_{i_{sST}}$	°C	20	60
Outlet temperature, $\hat{T}_{o_{sST}}$	°C	25	55
Density, $\hat{\rho}_{sST}$	kg/m ³	997	790
Viscosity, $\hat{\mu}_{sST}$	Pa·s	$9 \cdot 10^{-4}$	$9.5 \cdot 10^{-4}$
Heat capacity, $\hat{C}_{p_{sST}}$	J/(kg°C)	4 182	1 922
Thermal conductivity \hat{k}_{sST}	W/(m°C)	0.610	0.187
Fouling resistance, $\hat{R}_{f_{sST}}$	m ² °C/W	$3 \cdot 10^{-4}$	$3 \cdot 10^{-4}$

Source: The autor.

The results of the application of the MILP optimization for each example are shown in Table 32.

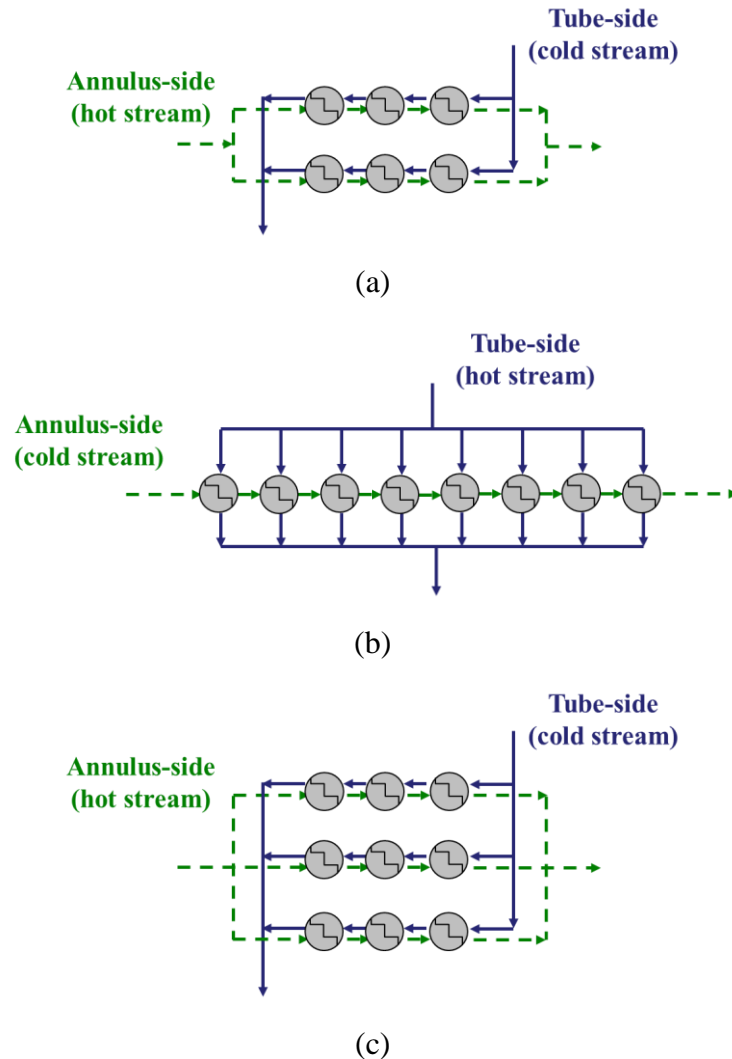
Table 32. Examples 7 to 9 – Design results.

Variable	Unit	Example 7	Example 8	Example 9
Tube side stream	–	Cold stream	Hot stream	Cold stream
Total heat exchanger area, A	m ²	1.92	2.56	2.88
Required heat exchanger area	m ²	1.59	2.02	1.86
Number of branches, NB	–	2	1	3
Tube side units in parallel / in series	–	1 / 3	8 / 1	1 / 3
Annular side units in parallel / in series	–	1 / 3	1 / 8	1 / 3
Tube side velocity, vt	m/s	1.986	1.362	1.324
Annulus side velocity, va	m/s	2.357	1.719	1.572
Tube side film coefficient, ht	W/(m ² °C)	9 365	1 896	6 522
Annulus side film coefficient, ha	W/(m ² °C)	3 079	8 155	2 125
Overall heat transfer coefficient, U	W/(m ² °C)	831	654	710
Corrected LMTD	°C	35.00	34.90	35.00
Tube side pressure drop, dPt	kPa	16.5	2.3	7.9
Annulus side pressure drop, dPa	kPa	26.2	47.2	12.6
Cold stream available pressure drop, $\widehat{\Delta P}_{c\ disp}$	kPa	50.0	50.0	20.0
Hot stream available pressure drop, $\widehat{\Delta P}_{h\ disp}$	kPa	50.0	20.0	20.0

Source: The autor.

An analysis of the results indicates that the sequence of solutions present a crescent area (a total increase of 50% from Example 7 to Example 9), illustrating a typical trade-off between available pressure drop and heat transfer area. The modification of the heat exchanger arrangement in each case according to the reduction of the available pressure drops can be observed in Figure 29, where the structure of each solution is displayed.

Figure 29: Arrangement of the design solutions (a) Example 7 ($\Delta\bar{P}_{h_disp} = 50$ kPa, $\Delta\bar{P}_{c_disp} = 50$ kPa); (b) Example 8 ($\Delta\bar{P}_{h_disp} = 20$ kPa, $\Delta\bar{P}_{c_disp} = 50$ kPa); (c) Example 9 ($\Delta\bar{P}_{h_disp} = 20$ kPa, $\Delta\bar{P}_{c_disp} = 20$ kPa).



Source: The autor.

The reduction of the hot stream available pressure drop from Example 7 to Example 8 modified the alignment of this stream in the heat exchanger. In the solution of Example 7, the hot stream was flowing in series along two parallel branches and, in Example 8, the hot stream was routed to a parallel flow along eight units. The reduction of the cold stream available pressure drop from Example 8 to Example 9 modified the cold stream alignment from flowing through a single path along eight units in series to a scheme involving three parallel branches.

4.2.4.2 Modifications in the process throughput

Process plants may be subject to several modifications during its lifetime. An increase of the market demand becomes an opportunity to increase the process throughput, which may impose equipment substitutions in debottlenecking projects. The modular nature of the double pipe heat exchanger allows increasing the heat exchanger capacity through the purchase of more units. Additionally, it is also possible to reorganize the arrangement of the existent units to accommodate the process modifications, therefore reducing the need of additional capital costs. The application of the proposed MILP optimization in this kind of problem is explored here in two examples, considering crescent throughput increases in relation to the original conditions of Example 7, as shown in Table 33.

Table 33. Examples 10 and 11 – Mass flow rates.

Parameter	Unit	Example 10		Example 11	
		Cold stream	Hot stream	Cold stream	Hot stream
Mass flow, \hat{m}_{sST}	kg/s	2.65	5.76	4.42	9.60

Source: The autor.

The optimal design of Example 10 and 11 are shown in Table 34 (the results of the Example 7 were also included to ease the comparison).

Table 34. Examples 10 and 11 (together with Example 7) – Optimization results.

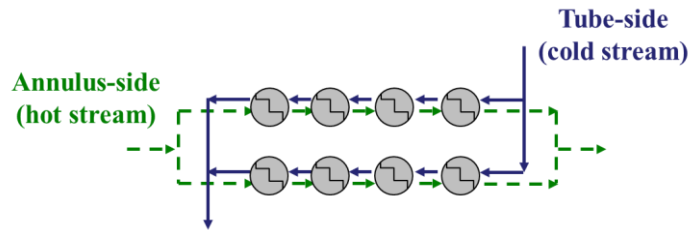
Variable	Unit	Example 7	Example 10	Example 11
Tube side stream	–	Cold stream	Cold stream	Cold stream
Total heat exchanger area, A	m ²	1.92	2.56	2.88
Required heat exchanger area	m ²	1.59	1.80	2.39
Number of branches, NB	–	2	2	3
Tube side units in parallel / in series	–	1 / 3	1 / 4	1 / 3
Annular side units in parallel / in series	–	1 / 3	1 / 4	1 / 3
Tube side velocity, vt	m/s	1.986	2.383	1.986
Annulus side velocity, va	m/s	2.357	2.829	2.357
Tube side film coefficient, ht	W/(m ² °C)	9 365	11 024	9 365
Annulus side film coefficient, ha	W/(m ² °C)	3 079	3 632	3 079
Overall heat transfer coefficient, U	W/(m ² °C)	831	882	831
Corrected LMTD	°C	35.00	35.00	35.00
Tube side pressure drop, dPt	kPa	16.5	30.7	16.5
Annulus side pressure drop, dPa	kPa	26.2	48.7	26.2

Source: The autor.

The analysis of Table 34 indicates that the crescent increase of the throughput from Example 7 to Examples 10 and 11 brings larger heat transfer areas. The heat transfer area of the optimal heat exchangers in Examples 10 and 11 are 33% and 50% higher than the solution of the Example 7.

The arrangement of Example 10 is shown in Figure 30 , where it is possible to observe that to answer an increase of 20% of the heat load, one unit was added in each branch (i.e. instead of buying an entire new heat exchanger it is only necessary to purchase two hairpin units).

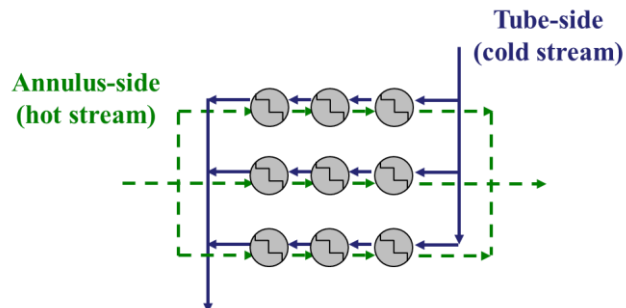
Figure 30: Example 10 – Arrangement of the design solution.



Source: The autor.

In Example 11, the increase of the mass flow rates was higher, 50%, therefore, simply adding more units to the existent branches would entail too elevated flow velocities and pressure drops. Thus, the optimization solution encloses three branches instead of two, as illustrated in Figure 31, thus indicating that the existent units must be reorganized and three more units must be bought.

Figure 31: Example 11 – Arrangement of the design solution.



Source: The autor.

CONCLUSIONS AND SUGGESTIONS

This chapter presents conclusions and observations for improvement around the work that was presented and discussed in this dissertation.

Conclusions

This work revolves around the solution of the design problem of double pipe heat exchangers using mathematical programming. The design variables are selected among discrete values, due to their physical nature or available commercial alternatives. Three formulations are developed, the first in the form of a MINLP problem, which is based on the original nonlinear equations, a second MINLP approach involves mathematical transformations that eliminate the nonlinearities in the binary variables and in a third approach those transformations are applied to all nonlinearities involved, yielding a MILP problem.

A comparison with the literature has shown that the proposed formulation was able to reduce the heat transfer area of the design solution. The application of the original and modified MINLP formulations to a sample of five design problems indicated that the later approach demands more computational time.

The analysis of the heat transfer area of the solutions indicated that the modified formulation obtained a better solution in two examples. The difference is lower than 0.5% in one of the examples, but it is 33% in the other example. This large difference between the objective functions in these pair of local optima, resultant of the nonconvexity of the MINLP, illustrates the importance of the investigation of alternatives that can identify rigorously the global optimum, as the third formulation proposed, the MILP approach.

The linear nature of the MILP approach eliminates any convergence problems and provide conditions to identify the global optimum with conventional optimization algorithms (e.g. branch and bound). A comparison with the results using a traditional trial and error procedure indicates that the proposed procedure can bring considerable reduction costs.

A set of design problems explored the trade-off between available pressure drop and heat transfer area and showed the proposed structure flexibility before modifications in the process throughput, showing a benefit of double pipe heat exchangers in situations where it becomes possible to rearrange the hairpins or purchase a few extra units instead of an entire new heat exchanger being bought.

Suggestions

The proposed formulations assume constant physical properties (representing average values), which is a very usual assumption in heat exchangers design problems without phase changing. However, in scenarios where at least one stream has a large fluctuation of its properties in the temperature range of the exchanger or when there is phase change, this approach may bring significant errors. In those events, formulations that were able to evaluate the properties variation in different positions along the equipment through discretization techniques would increase the problem complexity, but should bring much superior results.

Another modification to the proposed formulation that could be further studied is the possibility of adding other types of nonrectangular arrangement superstructures.

In addition, for the MILP formulation, some computational drawbacks associated to the definition of the search space were observed in relation to memory requirements necessary to solve the design problem. Future work on this issue may explore alternative representations of the discrete variables (Gonçalves et al., 2017) or resort to a supercomputer.

Another interesting discussion that may be added is the use of a stochastic generation of initial estimates to run multiple times both MINLP formulation and verify if the second approach statistically has a better performance.

REFERÊNCIAS

BAADACHE, K.,BOUGRIOU, C. Optimisation of the design of shell and double concentric tubes heat exchanger using the Genetic Algorithm. *Heat Mass Transfer*, v.51, p. 1371-1381, 2015.

BUTTERWORTH, D., GUY, A., WELKEY, J. Design and application of twisted tube exchangers. *Advances in Industrial Heat Transfer*, 2008.

COLBURN, A. A Method of correlating forced convection heat transfer data and a comparison with fluid Friction. *Trans. AIChE*, v. 29, p. 174, 1933.

DASTMALCHI, M., SHEIKHZADEH, G., AREFMANESH, A. Optimization of micro-finned tubes in double pipe heat exchangers using particle swarm algorithm. *Applied Thermal Engineering*, v. 119, p. 1-9, 2017.

DURAN, M., & GROSSMAN, I. An outer-approximation algorithm for a class of mixed-integer nonlinear programs. *Mathematical Programming*, v. 36, p. 307-339, 1986.

GENEMCO: Disponível em: GENEMCO Food Processing Equipment: <<http://www.genemco.com/aoe/tripletube.html>> Acesso em: 15 nov. 2017

GNIELINSKI, V. New Equations for heat and mass transfer in turbulent pipe and channel flow. *Int. Chem. Eng.*, v.16, p. 359-368, sd..

GONÇALVES, C. C. Alternative MILP formulations for shell and tube heat exchanger optimal design. *I&EC Research*, 2017.

HAN, H.-Z., LI, B.-X., WU, H., SHAO, W. Multi-objective shape optimization of double pipe heat exchanger with inner corrugated tube using RSM method. *International Journal of Thermal Sciences*,v. 90, p. 173-186, 2015.

HAUSEN, H. Darstellung des Wärmeüberganges in Rohren durch Verallgemeinert Potenzbeziehungen. *Z. VDI Beith Verfahrenstech*, v. 4, p. 91-98, 1943 apud INCROPERA, F. P., DEWITT, D. P., BERGMAN, T. L., LAVINE, A. S. Fundamentos de transferência de calor e de massa . 6th ed.. LTC, 2009.

INCROPERA, F. P., DEWITT, D. P., BERGMAN, T. L., LAVINE, A. S. *Fundamentos de transferência de calor e de massa* . 6th ed.. LTC, 2009.

INDHE, M. J., & BHATKAR, V. W. Optimization of Longitudinal Fin Profile for Double Pipe Heat Exchanger. *International Research Journal of Engineering and Technology*, v. 2, p. 517-529, 2015.

IQBAL, Z., SYED, K. S., ISHAQ, M. Optimal convective heat transfer in double pipe with parabolic fins. *International Journal of Heat and Mass Transfer*, v. 54, p.5415-5426, 2011.

IQBAL, Z., SYED, K. S., ISHAQ, M. Optimal fin shape in finned double pipe with fully developed laminar flow. *Applied Thermal Engineering*, v.51, p. 1202-1223, 2003.

KAKAÇ, S., LIU, H. *Heat exchangers - Selection, Rating and Thermal Design*. 2nd ed.. CRC Press, 2002.

KAREEM, R. Optimisation of double pipe helical tube heat exchanger and its comparison with straight double tube heat exchanger. *Journal of The Institution of Engineers (India) Series C*, 2016.

KAYS, W., CRAWFORD, M. *Convective heat and mass transfer*. 3rd ed.. New York: McGraw-Hill, 1993.

KOCH Heat Transter. Disponível em: <<http://www.kochheattransfer.com/products/alco-hairpin-heat-exchangers>> Acesso em: 15 nov. de 2017.

OMIDI, M., FARHADI, M., JAFARI, M. A comprehensive review on double pipe heat exchangers. *Applied Thermal Engineering*, v. 110, p. 1075-1090, 2017.

RENNIE, T. J., RAGHAVAN, V. G. Numerical studies of a double-pipe helical heat exchanger. *Applied thermal Engineering*, v. 26, p. 1266-1273, 2006.

SAHITI, N., KRASNIQI, F., FEJZULLAHU, X., BUNJAKU, J., MURIQI, A. Entropy generation minimization of a double-pipe pin fin heat exchanger. *Applied Thermal Engineering*, v. 28, p. 2337-2344, 2008.

SAUNDERS, E. *Heat exchangers: selection, design & construction*. Longman Scientific & Technical, 1988.

SERTH, R. W. *Process heat transfer principles and applications*. Kingsville, Texas, US: Elsevier, 2007.

SIEDER, E., TATE, G. Heat Transfer and pressure drop of liquids in tubes. *Ind. Eng. Chem.*, v.28, p. 1429 – 1435, 1936.

SORSAK, A., KRAVANJA, Z. MINLP retrofit of heat exchanger networks comprising different exchanger types. *Computers & Chemical Engineering*, v. 28, p. 235-251, 2004.

SÖYLEMEZ, M. S. Thermoeconomical optimization of double-pipe heat exchanger for waste heat recovery. *Thermophysics*, v. 18, p. 559-563, 2004.

SWAMEE, P. K., AGGARWAL, N., AGGARWAL, V. Optimum design of double pipe heat exchanger. *International Journal of Heat and Mass Transfer*, v. 51, p. 2260-2266, 2008.

SYED, K. S., IQBAL, Z., ISHAQ, M. Optimal configuration of finned annulus in a double pipe with fully developed laminar flow. *Applied Thermal Engineering*, v. 31, 1435-1446, 2011.

TAGHILOU, M., GHADIMI, B., SEYYEDVALILU, M. H. Optimization of double pipe fin-pin heat exchanger using entropy generation minimization. *International Journal of Engineering*, v. 27, p. 1431-1438, 2014.

TOWLER, G., & SINNOT, R. *Chemical engineering design - principles, practice and economics of plant and process design* . 2nd ed.. BH, 2008.

WILLIAMS, H. *Model building in mathematical programming*. 5th ed.. Wiley, 2013.

WINTERTON. Where did ditus and boelter equation come from? *Int. J. Heat Mass Transfer*, v. 41, p. 809-810, 1998.

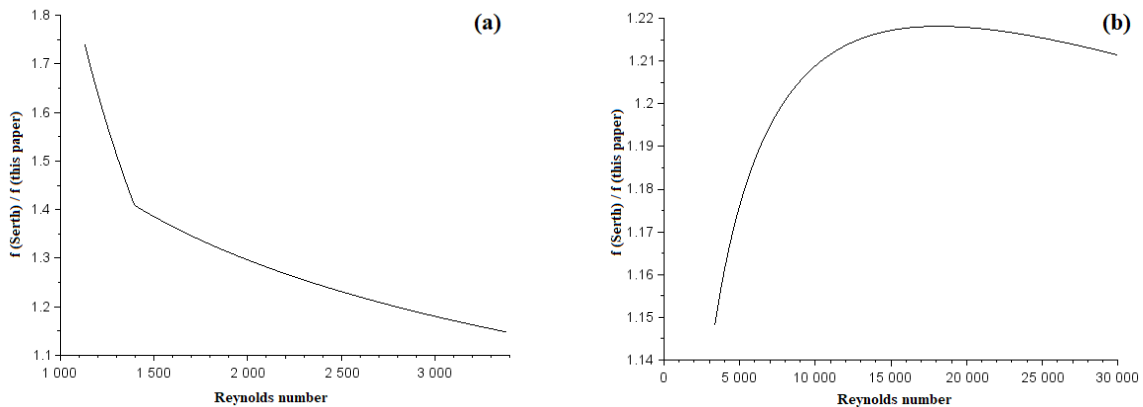
APPENDIX A – Description of correlations correction factor

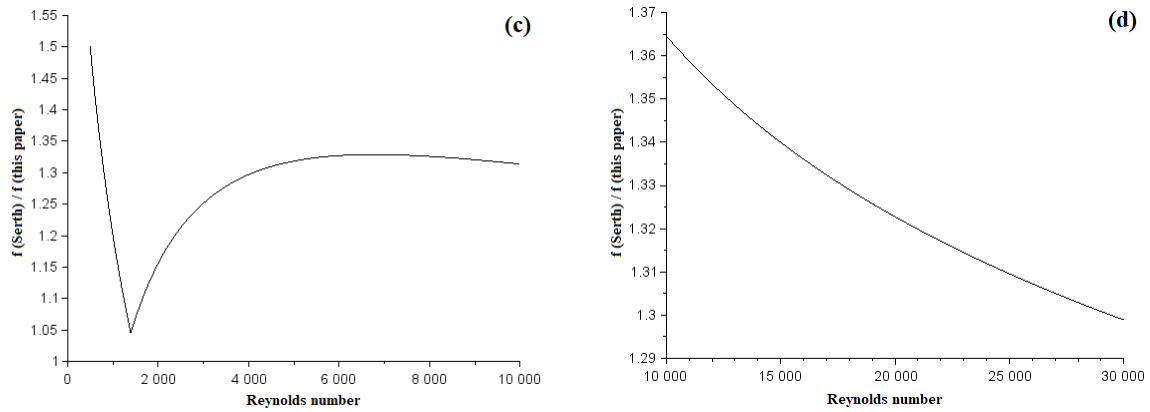
This section gives a more detailed description of the calculation of the correction factors, which were included for mean of comparison with the example presented by Serth. They were applied only on the transitional and turbulent regions, which were the regimes explored in the Serth procedure, for both tube (K_{ft}^{tran} and K_{ft}^{turb}) and annulus-side (K_{fa}^{tran} and K_{fa}^{turb}).

Determination of the correction factors:

For the determination of the correction factors the first step was to analyze the ratios between the friction factor calculated by Serth and by this work and check, if for the respective Reynolds ranges there was a reasonable variation. Those ratios are shown in Figure A1:

Figure A1: Ratio between the friction factors calculated by Serth and by this work. (a) Inner tube with transitional flow, (b) Inner tube with turbulent flow, (c) Annulus side with transitional flow and (d) Annulus side with turbulent flow.





Source: The autor.

Then, the highest ratio value was selected for each range, maintaining a conservative approach. The correction factors obtained are presented in Table A1.

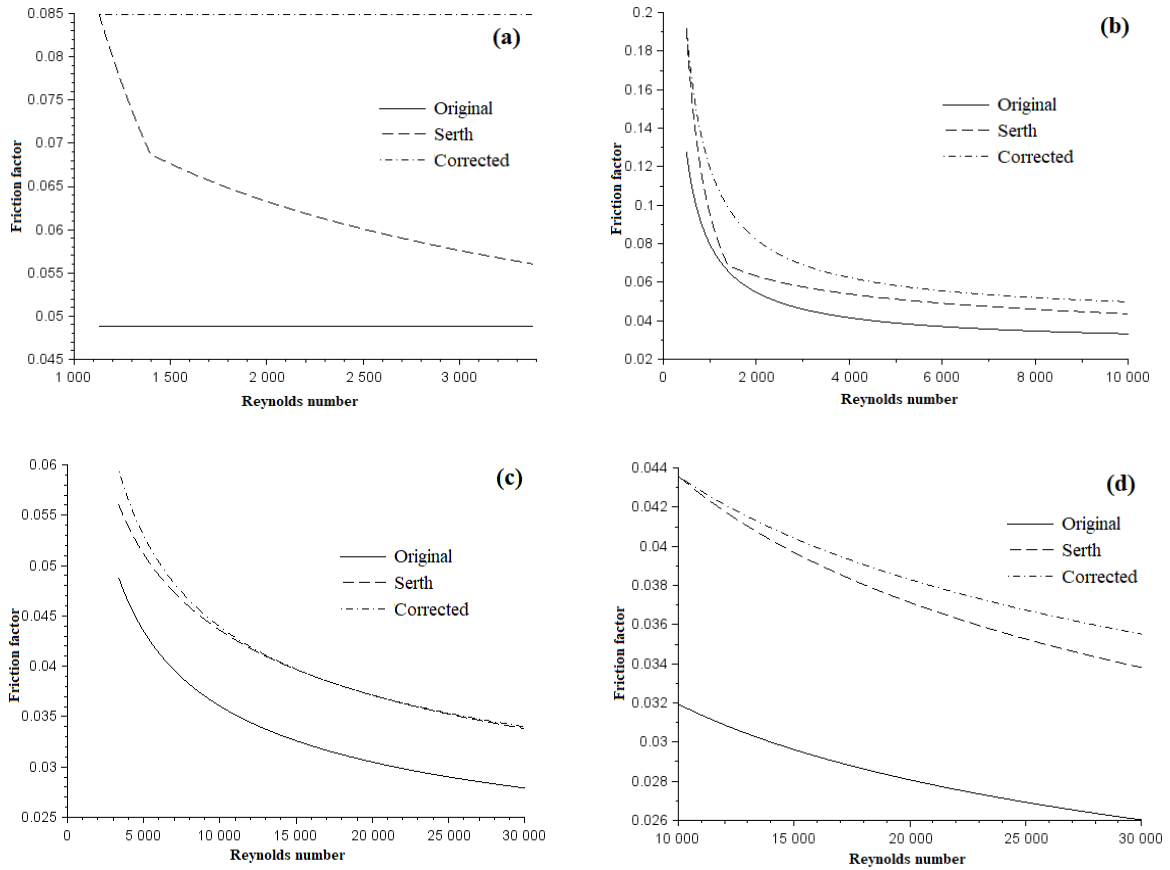
Table A1. Friction factor correction factors

Correction factor	Value
K_{ft}^{tran}	1.7393
K_{ft}^{turb}	1.2181
K_{fa}^{tran}	1.5016
K_{fa}^{turb}	1.3646

Source: The autor.

After applying the correction factors, due to the conservative approach adopted, the corrected friction factors calculated in this work becomes equal or higher than the ones calculated by Serth in the entire Reynolds range, as shown in Figure A2.

Figure A2: Friction factors calculated by Serth and by this work. (a) Inner tube with transitional flow, (b) Inner tube with turbulent flow, (c) Annulus side with transitional flow and (d) Annulus side with turbulent flow.



Source: The autor.

The correlations applied in this work for each Reynolds range remain unchanged, however, when calculating the resultant friction factor the correction factors are applied to its corresponding terms:

Tube-side friction factor 'corrected' calculation

$$f_t^{lam} = \frac{64}{Ret} \quad \text{for } Ret \leq 1311 \quad (A1)$$

$$f_t^{tran} = 0.0488 \quad \text{for } 1311 < Ret \leq 3380 \quad (A2)$$

$$f_t^{turb} = 0.014 + \frac{1.056}{Ret^{0.42}} \quad \text{for } Ret > 3380 \quad (A3)$$

$$f_t = f_t^{lam} yRet_1 + f_t^{tran} (yRet_2 + yRet_3) K_{ft}^{tran} + f_t^{turb} yRet_4 K_{ft}^{turb} \quad (A4)$$

Annulus-side friction factor ‘corrected’ correlations

$$fa^{lam} = \frac{64}{Rea} \quad \text{for } Rea \leq 500 \quad (A5)$$

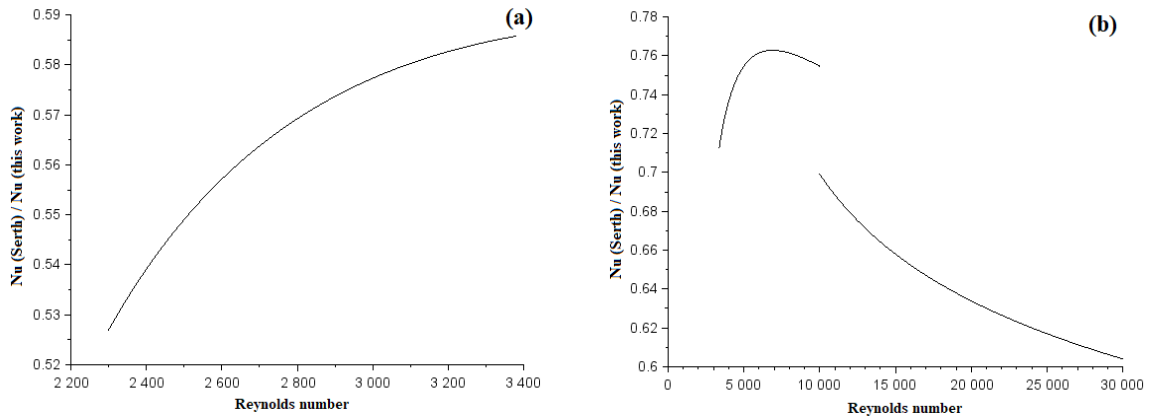
$$fa^{tran} = 0.02696 + \frac{32.656}{Rea^{0.93}} \quad \text{for } 500 < Rea \leq 10000 \quad (A6)$$

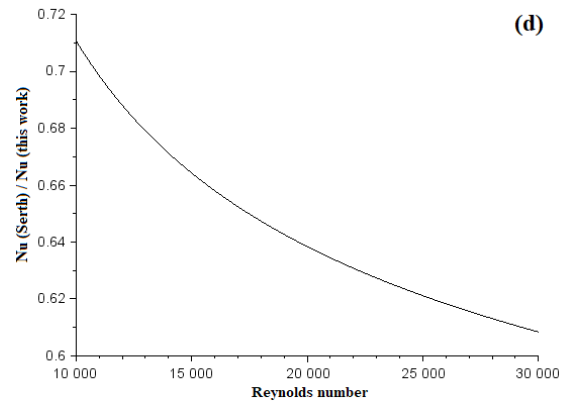
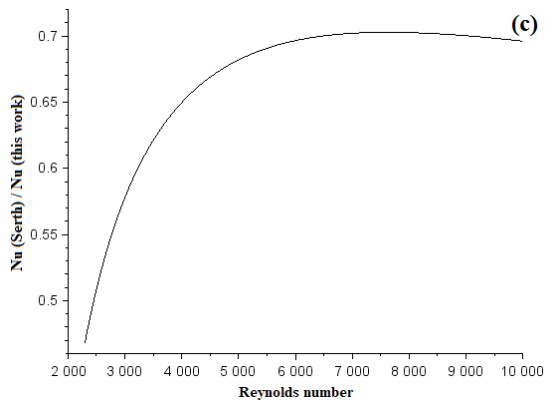
$$fa^{turb} = \frac{0.178}{Rea^{0.1865}} \quad \text{for } Rea > 10000 \quad (A7)$$

$$fa = fa^{lam} yRea_1 + fa^{tran} (yRea_2 + yRea_3) K_{fa}^{tran} + fa^{turb} yRea_4 K_{fa}^{turb} \quad (A8)$$

In the sequence, the Nusselt number calculation is subjected to the same analysis. The ratios for the Nusselt number are presented in Figure A3.

Figure A3: Ratio between the Nusselt numbers calculated by Serth and by this work. (a) Inner tube with transitional flow, (b) Inner tube with turbulent flow, (c) Annulus side with transitional flow and (d) Annulus side with turbulent flow.





Source: The autor.

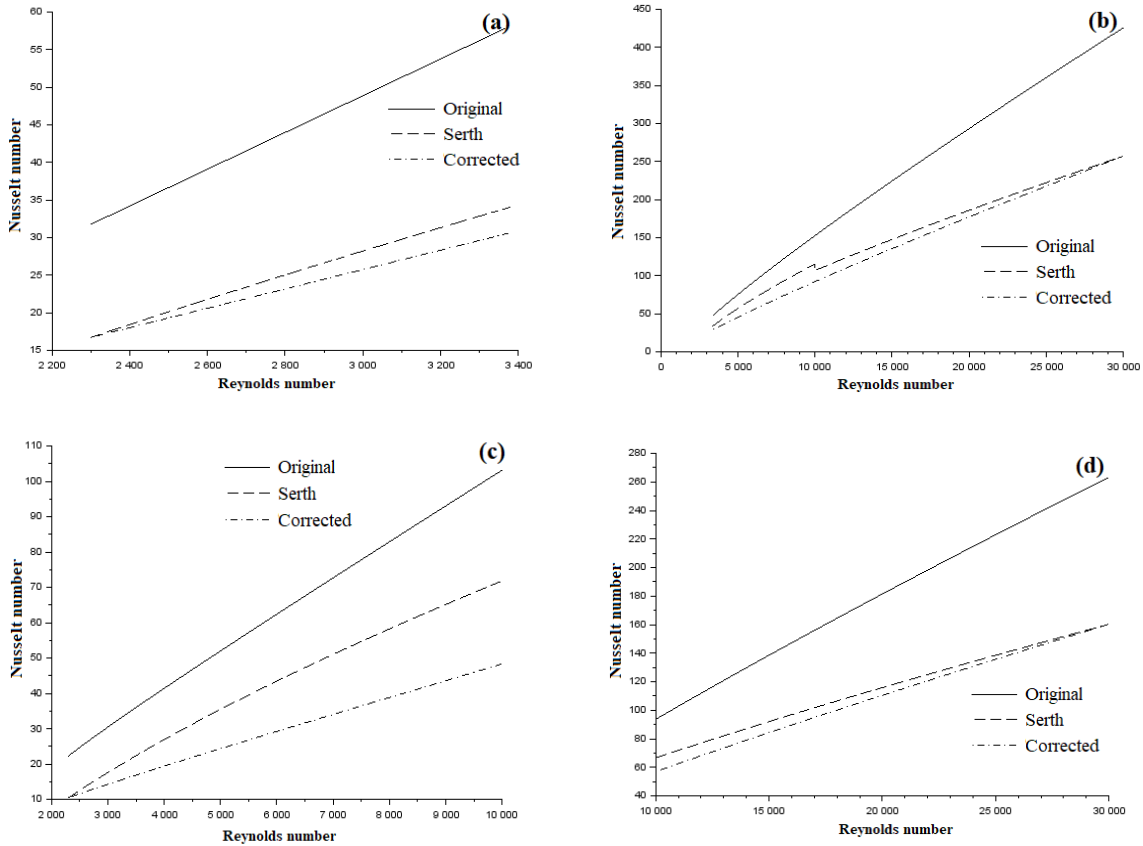
This time, the conservative approach was to select the smallest ratios as correction factors (Table A2), yielding lower heat transfer coefficients, as shown in Figure A4:

Table A2. Friction factor correction factors

Correction factor	Value
K_{Nut}^{tran}	1.7393
K_{Nut}^{turb}	1.2181
K_{Nuaa}^{tran}	1.5016
K_{Nuaa}^{turb}	1.3646

Source: The autor.

Figure A4: Nusselt numbers calculated by Serth and by this work. (a) Inner tube with transitional flow, (b) Inner tube with turbulent flow, (c) Annulus side with transitional flow and (d) Annulus side with turbulent flow.



Source: The autor.

Once again, the correlations remain unchanged, with the application of the correction factors in the Nusselt number final calculation, yielding:

Tube-side Nusselt 'corrected' calculation

$$Nut^{theo} = 3.66 \quad \text{for } Ret \leq 2300, Prt \leq 5, Nut^{S\&T} < 3.66 \quad (A9)$$

$$Nut^{S\&T} = 1.86 \left(\frac{Ret Prt dti}{L} \right)^{\frac{1}{3}} \quad \text{for } Ret \leq 2300, Prt \leq 5, Nut^{S\&T} \geq 3.66 \quad (A10)$$

$$Nut^{Hau} = 3.66 + \frac{0,0668 (dti/L) Ret Prt}{1 + 0,04((dti/L)Ret Prt)^{2/3}} \quad \text{for } Ret \leq 2300 \text{ and } Prt > 5 \quad (A11)$$

$$Nut^{Gni} = \frac{(ft/8) (Ret - 1000) Prt}{1 + 12.7 (ft/8)^{1/2} (Prt^{2/3} - 1)} \quad \text{for } Ret > 2300 \quad (A12)$$

$$\begin{aligned} Nut &= Nut^{theo} (yRet_1 + yRet_2) yPrt_1 yNut_1 + Nut^{S\&T} (yRet_1 + yRet_2) yPrt_1 yNut_2 \\ &\quad + Nut^{Hau} (yRet_1 + yRet_2) yPrt_2 + Nut^{Gni} K_{Nut}^{tran} yRet_3 \\ &\quad + Nut^{Gni} K_{Nut}^{turb} yRet_4 \end{aligned} \quad (A13)$$

Annulus-side Nusselt 'corrected' calculation

$$Nua^{theo} = 3.66 \quad \text{for } Rea \leq 2300, Pra \leq 5 \text{ and } Nua^{S\&T} < 3.66 \quad (A14)$$

$$Nua^{S\&T} = 1.86 \left(\frac{Rea Pra dh}{L} \right)^{\frac{1}{3}} \quad \text{for } Rea \leq 2300, Pra \leq 5 \text{ and } Nua^{S\&T} \geq 3.66 \quad (A15)$$

$$Nua^{Hau} = 3.66 + \frac{0.0668 (dh/L) Rea Pra}{1 + 0.04 ((dh/L) Rea Pra)^{\frac{2}{3}}} \quad \text{for } Rea \leq 2300 \text{ and } Pra > 5 \quad (A16)$$

$$Nua^{Gni} = \frac{(fa/8) (Rea - 1000) Pra}{1 + 12.7 (fa/8)^{\frac{1}{2}} (Pra^{\frac{2}{3}} - 1)} \quad \text{for } Rea > 2300 \quad (A17)$$

$$\begin{aligned} Nua &= Nua^{theo} (yRea_1 + yRea_2) yPra_1 yNua_1 + Nua^{S\&T} (yRea_1 + yRea_2) yPra_1 yNua_2 \\ &\quad + Nua^{Hau} (yRea_1 + yRea_2) yPra_2 + Nua^{Gni} K_{Nua}^{tran} yRea_3 \\ &\quad + Nua^{Gni} K_{Nua}^{turb} yRea_3 \end{aligned} \quad (A18)$$

APPENDIX B – List of symbols in alphabetic order divided by type

Parameters

$\widehat{\Delta P}_{sST\ disp}$	Stream <i>sST</i> available pressure drop (Pa)
$\widehat{\Delta T}_{lm}$	Logarithmic mean temperature (°C)
$\hat{\mu}_{sST}$	Stream <i>sST</i> viscosity (Pa·s)
$\hat{\rho}_{sST}$	Stream <i>sST</i> density (kg/m ³)
$\widehat{\Phi}$	Nonlinear continuous functions upper limit
\hat{A}_{exc}	Minimum area excess (%)
\widehat{Cp}_{sST}	Stream <i>sST</i> heat capacity (J/(kg °C))
\widehat{k}_{sST}	Stream <i>sST</i> thermal conductivity (W/(m °C))
\widehat{k}_{tube}	Tube material's thermal conductivity (W/m °C)
\hat{m}_{sST}	Stream <i>sST</i> mass flow (kg/s)
$\widehat{pA}_{sd,sB,sE,sL,sE'}$	Auxiliary parameter area calculation
\widehat{pdte}_{sd}	Available inside tube external diameters (m)
\widehat{pDte}_{sD}	Available outside tube external diameters (m)
\widehat{pdti}_{sd}	Available inside tube internal diameters (m)
\widehat{pDti}_{sD}	Available outside tube internal diameters (m)
$\widehat{pdPa1}_{sd,sD,sB,sE,sL,sE',sST}$	Auxiliary parameter pressure drop calculation
$\widehat{pdPa23}_{sd,sD,sB,sE,sL,sE',sST}$	Auxiliary parameter pressure drop calculation
$\widehat{pdPa4}_{sd,sD,sB,sE,sL,sE',sST}$	Auxiliary parameter pressure drop calculation
$\widehat{pdPt1}_{sd,sB,sE,sL,sE',sST}$	Auxiliary parameter pressure drop calculation
$\widehat{pdPt23}_{sd,sB,sE,sL,sE',sST}$	Auxiliary parameter pressure drop calculation
$\widehat{pdPt4}_{sd,sB,sE,sL,sE',sST}$	Auxiliary parameter pressure drop calculation
$\widehat{pF}_{sST,sE}$	F factor in case <i>sST</i> stream is in series, for <i>sE</i> ≠ 1

\widehat{pL}_{sL}	Heat exchanger length (m)
\widehat{pNB}_{sB}	Number of available branches
\widehat{pNE}_{sE}	Number of available heat exchangers in series by branch
$\widehat{pNu}a_{sd,sD,sB,sE,sL,sST}^{S\&T}$	Auxiliary parameter S&T correlation
$\widehat{pNu}t_{sB,sE,sL,sST}^{S\&T}$	Auxiliary parameter S&T correlation
\widehat{pP}_{sST}	P parameter for the calculation of F factor if sST stream is in series
\widehat{pR}_{sST}	R parameter for the calculation of F factor if sST stream is in series
\widehat{Q}	Heat-transfer rate (W)
\widehat{Rf}_{sST}	Stream sST fouling resistance (m ² °C /W)
\widehat{T}_i_{sST}	Stream sST inlet temperature (°C)
\widehat{T}_o_{sST}	Stream sST outlet temperature (°C)
\widehat{UNu}	Nusselt number upper limit
\widehat{UPr}	Prandtl number upper limit
\widehat{URe}	Reynolds number upper limit
$\widehat{v}a_{max}$	Annulus-side maximum velocity (m/s)
$\widehat{v}a_{min}$	Annulus-side minimum velocity (m/s)
$\widehat{v}t_{max}$	Tube-side maximum velocity (m/s)
$\widehat{v}t_{min}$	Tube-side minimum velocity (m/s)

Continuous Variables

ΔPa	Annulus-side pressure drop (Pa)
ΔPt	Tube-side pressure drop (Pa)
μa	Annulus-side stream viscosity (Pa·s)
μt	Tube-side stream viscosity (Pa·s)

ρ_a	Annulus-side stream density (kg/m ³)
ρ_t	Tube-side stream density (kg/m ³)
A	Heat transfer area (m ²)
A_a	Annulus-side flow area (m ²)
A_t	Tube-side flow area (m ²)
C_{pa}	Annulus-side stream heat capacity (J/(kg °C))
C_{pt}	Tube-side stream heat capacity (J/(kg °C))
dh	Hydraulic diameter (m)
d_{te}	Inner tube external diameter (m)
D_{te}	Outside tube external diameter (m)
d_{ti}	Inner tube internal diameter (m)
D_{ti}	Outside tube internal diameter (m)
F	Correction factor
f_a	Annulus-side friction factor
f_a^{lam}	Annulus-side friction factor for laminar flow
f_a^{tran}	Annulus-side friction factor for transitional flow
f_a^{turb}	Annulus-side friction factor for turbulent flow
f_t	Tube-side friction factor
f_t^{lam}	Tube-side friction factor for laminar flow
f_t^{tran}	Tube-side friction factor for transitional flow
f_t^{turb}	Tube-side friction factor for turbulent flow
h_a	Annulus-side convective heat transfer coefficient (W/(m ² °C))
h_t	Tube-side convective heat transfer coefficient (W/(m ² °C))
k_a	Annulus-side stream thermal conductivity (W/(m °C))

kt	Tube-side stream thermal conductivity (W/(m °C))
L	Length of a double pipe unit (m)
La	Annulus-side hydraulic length (m)
Lt	Tube-side hydraulic length (m)
ma	Annular region mass flow (kg/s)
mt	Inside tube mass flow (kg/s)
NB	Number of parallel branches
NP_a	Annulus-side units in parallel per branch
NP_t	Tube-side units in parallel per branch
NS_a	Annulus-side units in series per branch
NS_t	Tube-side units in series per branch
Nua	Annulus-side Nusselt number
Nua^{Gni}	Annulus-side Gnielinski Nusselt number
Nua^{Hau}	Annulus-side Hausen Nusselt number
$Nua^{S\&T}$	Annulus-side Seider & Tate Nusselt number
Nua^{theo}	Annulus-side theoretical Nusselt number
Nut	Tube-side Nusselt number
Nut^{Gni}	Tube-side Gnielinski Nusselt number
Nut^{Hau}	Tube-side Hausen Nusselt number
$Nut^{S\&T}$	Tube-side Seider & Tate Nusselt number
Nut^{theo}	Tube-side theoretical Nusselt number
Pra	Annulus-side stream Prandtl number
Prt	Tube-side stream Prandtl number
Rea	Annulus-side Reynolds number

Ret	Inner tube Reynolds number
Rfa	Annulus-side stream fouling resistance ($m^2 \text{ } ^\circ\text{C} / \text{W}$)
Rft	Tube-side stream fouling resistance ($m^2 \text{ } ^\circ\text{C} / \text{W}$)
U	Overall heat transfer coefficient ($\text{W}/(\text{m}^2 \text{ } ^\circ\text{C})$)
va	Annulus-side velocity (m/s)
vt	Tube-side velocity (m/s)
$wA_{sd,sB,sE,sL,sE'}$	Replacement for $yd_{sd}yB_{sB}yPt_{sE}yL_{sL}ySt_{sE'}$
$wAF1_{sd,sB,sE,sL,sE'',sST}$	Replacement for $wA_{sd,sB,sE,sL,sE''}yT_{sST}$
$wAF2_{sd,sB,sE,sE',sL,sE'',sST}$	Replacement for $wAF1_{sd,sB,sE,sL,sE'',sST}yPa_{sE'}$
$wdPa_{sd,sD,sB,sE,sL,sE',sST,sRea}$	Replacement for $yd_{sd}yD_{sD}yB_{sB}yPa_{sE}yL_{sL}ySa_{sE'}yT_{sST}yRea_{sRea}$
$wdPt_{sd,sB,sE,sL,sE',sST,sRet}$	Replacement for $yd_{sd}yB_{sB}yPt_{sE}yL_{sL}ySt_{sE'}yT_{sST}yRet_{sRet}$
wfa_1	Replacement for the product $fa^{lam}yRea_1$
wfa_2	Replacement for the product $fa^{tran}yRea_2$
wfa_3	Replacement for the product $fa^{tran}yRea_3$
wfa_4	Replacement for the product $fa^{turb}yRea_4$
wft_1	Replacement for the product $ft^{lam}yRet_1$
wft_2	Replacement for the product $ft^{tran}yRet_2$
wft_3	Replacement for the product $ft^{tran}yRet_3$
wft_4	Replacement for the product $ft^{turb}yRet_4$
$wha^{Gni}_{sd,sD,sB,sE',sL,sST,sRea}$	Replacement for $yd_{sd}yD_{sD}yB_{sB}yPa_{sE}yL_{sL}yT_{sST}yRea_{sRea}$
$wha^{Hau}_{sd,sD,sB,sE',sL,sST,sRea,sPra}$	Replacement for $yd_{sd}yD_{sD}yB_{sB}yPa_{sE}yL_{sL}yT_{sST}yRea_{sRea}yPra_{sPra}$
$wha^{S\&T}_{sd,sD,sB,sE',sL,sST,sRea,sPra,sNua}$	Replacement for $yd_{sd}yD_{sD}yB_{sB}yPa_{sE}yL_{sL}yT_{sST}yRea_{sRea}yPra_{sPra}yNua_{sNua}$
$wha^{theo}_{sd,sD,sST,sRea,sPra,sNua}$	Replacement for $yd_{sd}yD_{sD}yT_{sST}yRea_{sRea}yPra_{sPra}yNua_{sNua}$

$wht_{sd,sB,sE,sST,sRet}^{Gni}$	Replacement for $yd_{sd}yB_{sB}yPt_{sE}yT_{sST}yRet_{sRet}$
$wht_{sd,sB,sE,sL,sST,sRet,sPrt}^{Hau}$	Replacement for $yd_{sd}yB_{sB}yPt_{sE}yL_{sL}yT_{sST}yRet_{sRet}yPrt_{sPrt}$
$wht_{sd,sB,sE,sL,sST,sRet,sPrt,sNut}^{S\&T}$	Replacement for $yd_{sd}yB_{sB}yPt_{sE}yL_{sL}yT_{sST}yRet_{sRet}yPrt_{sPrt}yNut_{sNut}$
$wht_{sd,sST,sRet,sPrt,sNut}^{theo}$	Replacement for $yd_{sd}yT_{sST}yRet_{sRet}yPrt_{sPrt}yNut_{sNut}$
$wNua_{sd,sD,sB,sE,sL,sST}$	Replacement for $yd_{sd}yD_{sD}yB_{sB}yPa_{sE}yL_{sL}yT_{sST}$
$wNua^{Gni}$	Replacement for the product $Nua^{Gni} (yRea_3 + yRea_4)$
$wNua_1^{Hau}$	Replacement for the product $yRea_1yPra_2$
$wNua_2^{Hau}$	Replacement for the product $yRea_2yPra_2$
$wNua_1^{S\&T}$	Replacement for the product $yRea_1yPra_1yNua_2$
$wNua_2^{S\&T}$	Replacement for the product $yRea_2yPra_1yNua_2$
$wNua_1^{theo}$	Replacement for the product $yRea_1yPra_1yNua_1$
$wNua_2^{theo}$	Replacement for the product $yRea_2yPra_1yNua$
$wNut_{sB,sE,sL,sST}$	Replacement for $yB_{sB}yPt_{sE}yL_{sL}yT_{sST}$
$wNut^{Gni}$	Replacement for the product $Nut^{Gni} (yRet_3 + yRet_4)$
$wNut_1^{Hau}$	Replacement for the product $yRet_1yPrt_2$
$wNut_2^{Hau}$	Replacement for the product $yRet_2yPrt_2$
$wNut_1^{S\&T}$	Replacement for the product $yRet_1yPrt_1yNut_2$
$wNut_2^{S\&T}$	Replacement for the product $yRet_2yPrt_1yNut_2$
$wNut_1^{theo}$	Replacement for the product $yRet_1yPrt_1yNut_1$
$wNut_2^{theo}$	Replacement for the product $yRet_2yPrt_1yNut_1$
$wPaT_{sE,sST}$	Replacement for the product $yPa_{sE}yT_{sST}$
$wPtT_{sE,sST}$	Replacement for the product $yPt_{sE}yT_{sST}$
$wVa_{sd,sD,sB,sE,sST}$	Replacement for $yd_{sd}yD_{sD}yB_{sB}yPa_{sE}yT_{sST}$
$wvt_{sd,sB,sE,sST}$	Replacement for $yd_{sd}yB_{sB}yPt_{sE}yT_{sST}$

$wydT_{sd,sST}$	Replacement for $yd_{sd}yT_{sST}$
$wyPtSt_{sE,sE'}$	Replacement for $yPt_{sE}ySt_{sE'}$
$wyPaSa_{sE,sE'}$	Replacement for $yPa_{sE}ySa_{sE'}$

Binary Variables

yB_{sB}	Number of branches selection
yd_{sd}	Inner tube diameter selection
yD_{sD}	Outer tube diameter selection
yL_{sL}	Tube length selection
$yNua_{sNua}$	Range of annular region Seider and Tate Nusselt number selection
$yNut_{sNut}$	Range of inner tube Seider and Tate Nusselt number selection
yPa_{sE}	Annulus -side number of units in parallel per branch selection
$yPra_{sPra}$	Range of annular region Prandtl number selection
$yPrt_{sPrt}$	Range of inner tube Prandtl number selection
yPt_{sE}	Tube-side number of units in parallel per branch selection
$yRea_{sRea}$	Range of annular region Reynolds number selection
$yRet_{sRet}$	Range of inner tube Reynolds number selection
ySa_{sE}	Annulus-side number of units in series per branch selection
ySt_{sE}	Tube-side number of units in series per branch selection
yT_{sST}	Stream sST allocation (1 = tube-side; 0 = annulus-side)

Subscripts

sB	Index of number of branches
sd	Index of inner tube diameters
sD	Index of outer tube diameters

<i>sE</i>	Index of number of units per branch
<i>sL</i>	Index of tube length
<i>sNua</i>	Index of ranges of annular region Seider and Tate Nusselt number
<i>sNut</i>	Index of ranges of inner tube Seider and Tate Nusselt number
<i>sPra</i>	Index of ranges of annular region Prandtl number
<i>sPrt</i>	Index of ranges of inner tube Prandtl number
<i>sRea</i>	Index of ranges of annular region Reynolds number
<i>sRet</i>	Index of ranges of inner tube Reynolds number
<i>sST</i>	Index of streams

APPENDIX C – Scientific production

In this appendix the scientific production, developed throughout the master, is presented. Both associated or not with this work. With the exception of the two scientific articles, which are still in finalization stage, the first page of each work is shown here.

C.1 Scientific paper I: Optimal Design of Double Pipe Heat Exchanger Modular Units.
Part I: Mixed-Integer Nonlinear Programming Approach.

C.2 Scientific paper I: Optimal Design of Double Pipe Heat Exchanger Modular Units.
Part II: Mixed-Integer Linear Programming Approach.

C.3 Conference paper I: Otimização de Paradas e Distribuição de Vazões em Redes de Trocadores de Calor. Conference: XXI Congresso Brasileiro de Engenharia Química – COBEQ 2016. Autores: Melo, A.; Hemerly, A.; Chacon R.



XXI Congresso Brasileiro
de Engenharia Química
Fortaleza/CE
25 a 29 de setembro



XVI Encontro Brasileiro sobre o
Ensino de Engenharia Química
Fortaleza/CE
25 a 29 de setembro

OTIMIZAÇÃO DE PARADAS E DISTRIBUIÇÃO DE VAZÕES EM REDES DE TROCADORES DE CALOR

A. P. MELO, R. CHACON e A. L. H. COSTA

¹Universidade do Estado do Rio de Janeiro, Programa de Pós-Graduação em Engenharia Química
E-mail para contato: andrehc@uerj.br

RESUMO – No setor industrial, onde a competitividade é elevada, a busca por redução de custos é de extrema importância. Na indústria química, esta pressão se destaca em relação à redução do consumo de energia, onde redes de trocadores de calor assumem especial importância. Entretanto, estas estruturas sofrem com o acúmulo de depósitos, implicando no aumento do consumo de utilidades. No contexto de mitigação desses efeitos, a otimização do cronograma de paradas é frequentemente utilizada. Todavia, outro fator que pode não só alterar o cronograma ótimo, mas também intensificar a redução dos efeitos indesejados é a distribuição das vazões entre os equipamentos. Desta forma este trabalho aplica técnicas de programação matemática para minimização de custos em redes de trocadores envolvendo o cronograma de paradas e a distribuição das vazões simultaneamente, sendo as restrições dadas pelos balanços de massa e energia. As vantagens da metodologia proposta são ilustradas com um exemplo da literatura.

1. INTRODUÇÃO

Com a elevada competitividade do setor industrial, a busca por elevado desempenho, eficiência e retorno financeiro são fatores constantes, de modo que a otimização, seja esta de projeto ou operacional, ganha força. No contexto da engenharia de processos, a redução de custos está fortemente associada à redução no consumo de energia, responsável por parcela significativa do custo operacional de uma planta. As redes de trocadores de calor, por sua vez, assumem especial importância nesse quesito.

Trocadores de calor são equipamentos que sofrem acúmulos de depósitos, que reduzem a eficiência da rede e geram um aumento no consumo de utilidades. Quando um trocador de calor se encontra sujo, há uma queda no coeficiente global de transferência de calor do mesmo, e consequentemente de sua eficiência energética. Em redes extensas de trocadores de calor, a distribuição das vazões entre os equipamentos pode trazer ganhos significativos, aumentando a troca térmica na rede (Oliveira Filho et al., 2009; Assis et al., 2013).

No entanto, apesar da distribuição das vazões trazer ganhos, é preciso ainda que esses

C.4 Conference paper II: Reforma a Vapor de Gás Natural: A que distância estamos da cinética ótima em reatores industriais? Conference: XXI Congresso Brasileiro de Engenharia Química – COBEQ 2016. Autors: Chacon R.; Melo A.; Alberton, A.L.; Lima, E.; Paredes, M.



XXI Congresso Brasileiro
de Engenharia Química
Fortaleza/CE
25 a 29 de setembro



XVI Encontro Brasileiro sobre o
Ensino de Engenharia Química
Fortaleza/CE
25 a 29 de setembro

REFORMA A VAPOR DE GÁS NATURAL: A QUE DISTÂNCIA ESTAMOS DA CINÉTICA ÓTIMA EM REATORES INDUSTRIAIS?

R. CHACON¹, A. MELO¹, E. LIMA¹, M. PAREDES¹, A. L. ALBERTON¹

¹Instituto de Química, Universidade do Estado do Rio de Janeiro

E-mail para contato: andre.alberton@uerj.br

RESUMO – *A reforma a vapor de gás natural constitui o principal processo de produção de gás de síntese, com grande interesse na melhoria dos sistemas catalíticos pelo impacto econômico esperado. No reformador, o catalisador é distribuído em tubos na zona de radiação do forno, havendo queimadores que fornecem a energia necessária para o sistema reacional. O presente trabalho avalia a influência máxima esperada na melhoria de reformadores industriais atuais, admitindo cinética das reações suficientemente rápida e taxas limitadas por transferência de massa. Os resultados dos perfis e da dimensão do reator para atingir conversões equivalentes foram obtidos e comparados com valores reportados na literatura.*

1. INTRODUÇÃO

A reforma a vapor do metano é uma das mais importantes rotas industriais para a produção de gás de síntese e hidrogênio (Quinta Ferreira *et al.*, 1992), sendo tipicamente o processo mais econômico para a produção comercial de hidrogênio (Balat M., 2008 *apud* Rout, *et al.*, 2015). Esses produtos são largamente utilizados como, por exemplo, na produção de metanol e seus derivados, produção de amônia, etc.

No processo de reforma a vapor, o forno opera a pressões e temperaturas nas faixas de 10-30 bar e 675-1000 K, sendo o gás natural convertido em gás de síntese em um leito catalítico de Ni/MgAl₂O₄ (Xu & Froment, 1989 a). Devido à importância deste sistema na indústria, este se tornou um foco frequente de estudo, e diversos modelos para descrever o reformador foram propostos na literatura (Schwaab, *et al.*, 2009).

Embora haja divergências na literatura sobre mecanismos catalíticos, etapas limitantes, e expressões cinéticas resultantes, um dos conjuntos mais aceitos de trabalhos consideram para

C.5 Conference paper III: Avaliação de Competitividade do Gás Natural na Cadeia Química: Casos de Países como Japão, Coreia do Sul e Alemanha e Sugestão para o Brasil. Conference: Rio Oil & Gas 2016. Autores: Gaya, M.A., Hemerly, A., Melo, A.; Belizario, A., Bittencourt, E., Santos, R.T., Barbosa, F.S.



IBP1962_16
**AVALIAÇÃO DE COMPETITIVIDADE DO GÁS NATURAL
 NA CADEIA QUÍMICA: CASOS DE PAÍSES
 COMO JAPÃO, COREIA DO SUL E ALEMANHA E
 SUGESTÃO PARA O BRASIL.**

Marco Antonio Gaya de Figueiredo¹, André Luiz Hemerly Costa², Alice Peccini de Melo³, Ana Carlota Belizario dos Santos⁴, Eduardo F. Bittencourt⁵, Rafael Thomaz P. Santos⁶, Flávia de Souza R. Barbosa⁷

Copyright 2016, Instituto Brasileiro de Petróleo, Gás e Biocombustíveis - IBP

Este Trabalho Técnico foi preparado para apresentação na Rio Oil & Gas Expo and Conference 2016, realizado no período de 24 a 27 de outubro de 2016, no Rio de Janeiro. Este Trabalho Técnico foi selecionado para apresentação pelo Comitê Técnico do evento, seguindo as informações contidas no trabalho completo submetido pelo(s) autor(es). Os organizadores não irão traduzir ou corrigir os textos recebidos. O material conforme, apresentado, não necessariamente reflete as opiniões do Instituto Brasileiro de Petróleo, Gás e Biocombustíveis, Sócios e Representantes. É de conhecimento e aprovação do(s) autor(es) que este Trabalho Técnico seja publicado nos Anais da Rio Oil & Gas Expo and Conference 2016.

Resumo

Neste trabalho, um dos principais objetivos foi estudar a cadeia do gás natural no setor não energético, mais especificamente como matéria-prima para indústria química, para então poder compreender como países como Alemanha, Japão e Coreia do Sul, ao contrário do Brasil, são capazes de gerar produtos de alto valor agregado a partir desta matéria-prima. Diferentemente do Brasil, estes países não são produtores de gás natural, verificando-se que Coreia do Sul e Japão importam todo o gás natural consumido internamente, enquanto a Alemanha vem mostrando um decréscimo na sua produção, importando hoje aproximadamente 90% do volume consumido no país. Entretanto, ao se investigar as principais aplicações do gás natural, ainda que se verifique uma utilização majoritária para fins energéticos, como na maioria dos demais países no mundo, estes três países parecem possuir a capacidade de agregar valor ao longo de sua cadeia produtiva de produtos químicos, obtendo-se derivados usualmente provenientes de uma cadeia gasquímica.

Abstract

In this work, a key objective was to study the chain of natural gas in the non-energy sector, more specifically as raw materials for chemical industry, to then be able to understand how countries like Germany, Japan and South Korea, unlike Brazil, are capable of generating products along the chain of products with high added value from this raw material. Japan, South Korea and Germany are not natural gas producing countries, and so are importers of this product and pay a cost considered high worldwide, for the natural gas. Although there is a use of majority natural gas for energy purposes, as in most other countries in the world, these three countries appear to have the ability to add value throughout the production chain of chemicals, resulting in derivatives products usually from a Gas to chemicals chain.

1. Introdução

O gás natural no mundo é utilizado em dois grandes setores, o de uso energético e o não energético, este último representando uma parcela muito menos significativa, se comparado ao anterior. O uso energético está principalmente relacionado ao mercado de combustíveis, enquanto o uso não energético refere-se no mercado de bens de consumo finais, por exemplo, uso como matéria-prima para a indústria química.

Se considerada a matriz energética mundial, atualmente a participação do gás natural é grande (Figura 1), e segundo a literatura há expectativa de que esta continue em expansão nos próximos anos. De acordo com a IEA (2011),

¹ D.Sc., UERJ

² D.Sc., UERJ

³ Engenheira Química, UERJ

⁴ Doutora, Consultora Sênior – PETROBRAS SA

⁵ B. Sc., MBA, PETROBRAS SA

⁶ M. Sc., PETROBRAS SA

⁷ D. Sc., Consultora

C.6 Conference paper IV: Assessment of Crude Oil Fouling Behavior Using Empirical and Semi-Empirical Models. Conference: Heat Exchanger Fouling and Cleaning XII – 2017. Autors: Melo, A.; Souza, A.R.; Andrade W.M., Costa A.L.H., Queiroz, E.M.m Assis, B.C.G.; Oliveira, A.G., Liporace, F.S.

ASSESSMENT OF CRUDE OIL FOULING BEHAVIOR USING EMPIRICAL AND SEMI-EMPIRICAL MODELS

A.P. Mello¹, A.R. Souza¹, Andrade, W. M.¹, A.L.H. Costa,¹ E.M. Queiroz²,
B.C.G. Assis³, S.G. de Oliveira³ and F.S. Liporace³

¹ Rio de Janeiro State University (UERJ), Rua São Francisco Xavier, 524, Rio de Janeiro, RJ, Brazil - andrehc@uerj.br

² Federal University of Rio de Janeiro (UFRJ), Centro de Tecnologia, Cidade Universitária, Rio de Janeiro, RJ, Brazil

³ Petróleo Brasileiro S.A. (PETROBRAS), Research and Development Center Leopoldo Américo Miguez de Mello (CENPES), Av. Horácio Macedo, 950, Cidade Universitária. Rio de Janeiro, RJ, Brazil

ABSTRACT

Crude preheat trains have a large impact on the energy efficiency of refinery distillation units, with a direct relation with the fuel consumption in the fired heater. As fouling problems can significantly impair the crude preheat train performance, it has become a major concern for the Oil & Gas industry. Several papers present industrial crude oil fouling data, but the discussions are usually limited to isolated data sets of individual refineries. Due to the complexity of fouling phenomena, there is a lack of analysis involving broader databanks. Aiming to fill this gap, this paper presents the results of the application of empirical and semi-empirical models to describe the fouling behavior in crude preheat trains encompassing a considerable number of different heat exchangers located in several Brazilian refineries. The discussion is organized in three topics: (i) analysis of the maximum fouling in heat exchangers; (ii) analysis of the fouling dynamic using empirical models; (iii) analysis of semi-empirical threshold model parameters. The analysis of the maximum fouling discusses the values of fouling resistances registered in the databank when compared to TEMA values. The analysis of the fouling dynamic using empirical models presents an overview of how fast fouling affects heat exchangers performance during crude preheat trains campaigns. Finally, the analysis of Ebert-Panchal parameters intends to identify a range of typical values of the activation energy. The results allow an assessment of how intense crude oil fouling is and, also, serve as benchmarks for further investigations.

INTRODUCTION

In heat exchangers, fouling is the undesired accumulation of deposits over the equipment thermal surface. It is a complex phenomenon that can be caused by different factors: crystallization, sedimentation, chemical reaction, corrosion, biological growth, and freezing. Because of this complexity, despite the intense research effort, the prediction of the fouling behavior using theoretical models has reached limited results. Therefore, fouling is usually handled in the design or operational problems using information strongly based on empirical data. Examples of this reality encompass traditional fouling factors employed in the heat exchanger design (TEMA,

1999), empirical models that describe typical profiles of fouling growth (Speight, 2015), and semi-empirical fouling rate models that can relate the temperature and velocity to the fouling rate (Wilson et al., 2005).

This dependency of empirical data is even more pronounced in the analysis of fouling involving crude oil. Crude oil is a natural raw material, originated from the exposition of organic matter to certain conditions of temperature and pressure during a large time span inside the Earth's crust. This formation process implies that a crude oil stream is composed by a mixture of a large number of different hydrocarbon molecules. Additionally, there are several other components that, despite its presence in smaller quantities, may assume an important role in different fouling processes, such as, asphaltenes, sulphur compounds, oxygenated molecules, etc. The compositional complexity of crude oils implies that the analysis of fouling in these streams based on laboratory data may provide results considerably different from the industrial reality (Asomaning et al., 2000).

Due to the experimental laboratory limitations, the analysis of crude oil fouling using industrial data can be an interesting alternative. The literature contains several papers of fouling investigation in crude oil streams using industrial data (Polley et al., 2007; Mozdianfard and Behranvand, 2013; Harche et al., 2014; Mozdianfard and Behranvand, 2015). However, the reported data in these papers are limited to isolated units or, at the best, set of heat exchangers belonging to the same refinery.

Aiming to offer to the fouling investigation community industrial data about crude oil fouling in refineries, this paper presents results involving a considerable number of heat exchangers operating in Brazilian refineries. The discussion involves three approaches: (i) analysis of the maximum fouling in the heat exchangers; (ii) analysis of the fouling dynamic using empirical models; (iii) analysis of semi-empirical threshold model parameters.

COMPUTATIONAL TOOLS

The data reported in this paper were collected using the software Fouling^{TR} (Liporace and Oliveira, 2007), developed by Petrobras R&D Center (Cenpes). This software receives real time process measurements of